



**Universität für Bodenkultur Wien**  
University of Natural Resources  
and Life Sciences, Vienna

# Master Thesis

## **Quantifying forest net primary production at high spatial resolution: possibilities and limitations**

Submitted by

**Aleksandar DUJAKOVIĆ**

in the framework of the Master programme

**Mountain Forestry**

in partial fulfilment of the requirements for the academic degree

**Master of Science**

Vienna, August 2022

Supervisor:

Univ.Prof. Dr.rer.nat. Clement Atzberger

Institute of Geomatics

Department of Landscape, Spatial and Infrastructure Sciences

## Affidavit

I hereby declare that I have authored this master thesis independently, and that I have not used any assistance other than that which is permitted. The work contained herein is my own except where explicitly stated otherwise. All ideas taken in wording or in basic content from unpublished sources or from published literature are duly identified and cited, and the precise references included.

I further declare that this master thesis has not been submitted, in whole or in part, in the same or a similar form, to any other educational institution as part of the requirements for an academic degree.

I hereby confirm that I am familiar with the standards of Scientific Integrity and with the guidelines of Good Scientific Practice, and that this work fully complies with these standards and guidelines.

Vienna, 09.08.2022

Aleksandar DUJAKOVIĆ (*manu propria*)

## Preface

The research presented in this master thesis was funded by the European Union's Horizon 2020 Framework Programme for Research and Innovation (grant agreement No. 774234 - Landsupport project).



## Acknowledgements

First and foremost, I am extremely grateful to my thesis supervisor Dr. Francesco Vuolo for giving me the opportunity to enter the field of remote sensing and great help and guidance that goes beyond this thesis. I received complete support from the beginning of the work on the thesis and the additional opportunity to advance in my career.

I would also like to thank my other supervisors Markus Immitzer, for his advice, support and great organization, and Professor Clement Atzberger for constructive and fruitful discussions at the seminars and for the first lectures on the topics in remote sensing I attended which raised my interest for this field.

I would also like to thank my colleagues from the Institute of Geomatics for their help in obtaining data and Jernej Jevšenak from Slovenian Forestry Institute for providing me with the Slovenian forest inventory data and support in the use of the data. I would also like to thank the European Union's Horizon 2020 Framework Programme for Research and Innovation under which this research was funded (grant agreement No. 774234 - Landsupport project).

Finally, I am extremely grateful to my family for their unconditional love and all their support. Without them, my studies and this thesis would not be possible.

## Table of content

Affidavit.....	i
Preface .....	ii
Acknowledgements.....	iii
Table of content .....	iv
List of figures.....	v
List of tables.....	vii
Abstract.....	viii
Kurzfassung .....	ix
1. Introduction.....	1
1.1. Carbon pools and Vegetation carbon sink .....	1
1.2. Carbon cycle and climate change.....	2
1.3. Net Primary Production .....	2
1.4. Factors governing the level of carbon storage .....	4
1.5. Net Primary Production estimation methods .....	4
1.6. Global NPP estimates .....	6
1.7. MOD17 NPP product.....	8
1.7.1. Limitations of coarse data and possible improvements with higher spatial resolution... 8	
1.7.2. Improvements of MODIS NPP/GPP model.....	9
2. Objectives .....	11
3. Materials and Methods.....	12
3.1. Description of MODIS NPP algorithm .....	12
3.2. High spatial resolution model input datasets .....	15
3.2.1. Land cover map.....	15
3.2.2. Climate dataset.....	15
3.2.3. Harmonized Landsat and Sentinel-2 dataset .....	15
3.3. Study area.....	16
3.4. Reference data.....	17
3.5. Input data processing .....	20
3.6. FPAR/LAI estimation .....	22
3.7. HLS NPP estimation .....	27
4. Results.....	29
4.1. Model parameters – sensitivity analysis .....	29
4.2. Slovenia.....	32
4.3. Austria.....	35
4.4. HLS NPP and MODIS NPP comparison .....	38
5. Discussion and conclusion.....	50
5.1. Future work.....	54
References.....	56

## List of figures

Figure 1: Schematic representation of the global carbon cycle, averaged globally for the decade 2010–2019 (Friedlingstein et al., 2020).....	1
Figure 2: Conceptual diagram of the biological forest carbon cycle. Abbreviation for fluxes: net primary production (NPP), gross primary production (GPP), autotrophic respiration ( $R_A$ ), root respiration (RR), heterotrophic respiration (RH), decomposition of detritus (D) and herbivory (H). The forest carbon cycle is characterized by the presented biological (forest ecosystem) cycle with addition of an industrial (forest products) cycle. Adapted from Gower (2003).....	3
Figure 3: Global mean terrestrial net primary production (NPP) for 2000 – 2010 (Running and Zhao, 2019).....	7
Figure 4: MODIS NPP on 0.5-km resolution representing annual NPP for 2020. NPP data derived from the MOD17A3HGFv006 (AppEEARS, <a href="https://lpdaacsvc.cr.usgs.gov/appeears/">https://lpdaacsvc.cr.usgs.gov/appeears/</a> ).....	7
Figure 5: Flowchart showing the logic behind the MOD17 algorithm in calculating the 8-day average GPP and annual NPP (Running and Zhao, 2019; MOD17 user guide).....	12
Figure 6: Increase of spatial resolution of model inputs when introducing new datasets.....	16
Figure 7: Sampling plots of the Slovenian National Forest Inventory. The green dots represent plots categorized as forests in 2018.....	17
Figure 8: NFI plots and polygons in Slovenia for which the NPP is estimated. This map represents part of the NFI plots with the shapefile of polygons for NPP estimation and land cover classification.....	18
Figure 9: Selected area (marked in yellow) of the tree core samples taken in 2020.....	19
Figure 10: The TMIN and VPD attenuation scalars are simple linear ramp functions of daily TMIN and VPD (Running and Zhao, 2019).....	21
Figure 11: Sentinel-2 LAI vs. MODIS LAI for a large and uniform forest area obtained on 01.05.2019. Scale: 0.1.....	23
Figure 12: S2-derived NPP vs MODIS MOD17 NPP for a large and uniform forest area for 2019....	24
Figure 13: S2-derived NPP vs MODIS MOD17 NPP aggregated at the MODIS spatial resolution (500 m).....	24
Figure 14: Regression of mean FPAR/LAI (MODIS) as a function of mean NDVI (HLS) for uniform forest stands. FPAR is logarithmic function, LAI is exponential function.....	26
Figure 15: Example of one polygon for NPP estimation. Square polygon is a shapefile in which the NPP is calculated. Mean annual NPP was extracted for the forest stands which are located within this polygon (09095A, 09096A and 09096B). Pixels represent NPP values [ $\text{kgC}/\text{m}^2/\text{year}$ ]. The background RGB image was obtained from “Map data ©2021 Google”.....	27
Figure 16: Daily GPP (a) and respiration (b) values. Orange vertical lines represent beginning and end of a period in which share of GPP and respiration is the highest, and for which mean parameter values are analysed.....	29
Figure 17: Correlation between FPAR(a)/LAI(b) and PAI (NFI data). Mean LAI/FPAR values between 1st May and 31st August are considered for correlation analysis.....	30
Figure 18: Sensitivity analysis of annual NPP to model parameters for conifers. Impact of change of parameters values in a range -25% to 25% on a change of NPP were calculated. Sensitivity of NPP to SWrad and $\epsilon$ is the same as to FPAR. Therefore, FPAR is the only shown on the graphs.....	31
Figure 19: Sensitivity analysis of annual NPP to model parameters for broadleaf. Impact of change of parameters values in a range -25% to 25% on a change of NPP were calculated. Sensitivity of NPP to SWrad and $\epsilon$ is the same as to FPAR. Therefore, FPAR is the only shown on the graphs.....	32
Figure 20: 6-years periodic annual increment (2012-2018) vs. 3-years annual average NPP (2016-2018).....	33
Figure 21: 6-years periodic annual increment (2012-2018) and 3-years annual average NPP (2016-2018) of 60% of the plots with highest timber volume.....	34
Figure 22: Examples of NFI plots with low stem density (a,b,c) and high stem density (d,e,f). The green point is the centre of a plot. Plots a, b and c have low PAI. Plots d, e and f have above average PAI. The background RGB imagery is obtained from “Map data ©2021 Google”.....	35

Figure 23: Annual HLS NPP for the period 2016-2020 for the 5 districts in the southern part of Austria. .....	36
Figure 24: Growth ring width (1/100 mm) versus NPP .....	36
Figure 25: Change of year ring width versus NPP-change .....	37
Figure 26: Boxplots of NPP (2016-2019) (a) and growth ring width (2016-2019) (b).....	38
Figure 27: Comparison of HLS NPP and MOD17 NPP for forest stands in Slovenia: The boxes represent the median and the 25th and 75th percentile, the symbol x represents the arithmetic mean. ....	39
Figure 28: Scatter plot which shows the correlation between HLS NPP and MOD17 NPP. Solid line is identity line. ....	40
Figure 29: (a) Correlation between HLS NPP and MOD17 NPP for homogeneous 1 km <sup>2</sup> forest polygons of all forest types and (b) for coniferous and broadleaf forests separately in the year 2018 .....	41
Figure 30: Comparison of HLS NPP and MOD17 NPP for homogeneous 1 km <sup>2</sup> forest polygons in Slovenia: The boxes represent the median and the 25th and 75th percentile, the symbol x represents the arithmetic mean.....	42
Figure 31: Distribution of aggregated NPP values for HLS NPP and MOD17 NPP products for the period 2016-2018 for the study areas in Slovenia. Two datasets differ in size and spatial resolution. Vertical axis shows frequency of the two NPP datasets relative to the total forest area of the analysed polygons. HLS NPP values for conifers and broadleaves have two peaks in distribution showing bimodal distribution. ....	43
Figure 32: Correlation between HLS NPP and MOD17 NPP for homogeneous 1 km <sup>2</sup> forest polygons. .....	44
Figure 33: Comparison of HLS NPP and MOD17 NPP for homogeneous 1 km <sup>2</sup> forest polygons in Austria: The boxes represent the median and the 25th and 75th percentile, the symbol x represents the arithmetic mean.....	45
Figure 34: HLS NPP on 10-m resolution representing average NPP for the period 2016–2020 for the southern part of Austria. Estimated NPP was obtained with S2GLC map, meteorological reanalysis data from ERA5 and E-OBS datasets and reflectance data from HLS.....	47
Figure 35: MOD17 NPP on 500-m resolution representing average NPP for the period 2016–2020 for the southern part of Austria. NPP data derived from the MOD17A3HGFv006 (AppEEARS, <a href="https://lpdaacsvc.cr.usgs.gov/appeears/">https://lpdaacsvc.cr.usgs.gov/appeears/</a> ) .....	48
Figure 36: Distribution of aggregated NPP values for HLS NPP and MOD17 NPP products for the period 2016-2020 for the study region in the southern part of Austria. Two datasets differ in size and spatial resolution. Vertical axis shows frequency of the two NPP datasets relative to the total forest area. .....	49

## List of tables

Table 1. Biome-Property-Look-Up-Table (BPLUT) for MODIS GPP/NPP algorithm (Running and Zhao, 2019).....	20
Table 2: Description of the bits in the one-byte Quality Assessment layer. Bits are listed from the MSB (bit 7) to the LSB (bit 0) .....	25
Table 3: Mean values of NPP estimation and forest inventory data. Relative standard deviation is used to show the difference of two sets of data with different units (gC/m <sup>2</sup> /year and m <sup>3</sup> /ha).....	32
Table 4: HLS NPP for each region separately and for each year.....	35
Table 5: Statistics for two modelled NPP for forest stands 2016. NPP [gC/m <sup>2</sup> /year]. RSD – relative standard deviation [%].....	38
Table 6: Statistics for two modelled NPP for forest stands 2017. NPP [gC/m <sup>2</sup> /year]. RSD – relative standard deviation [%].....	38
Table 7: Statistics for two modelled NPP for forest stands 2018. NPP [gC/m <sup>2</sup> /year]. RSD – relative standard deviation [%].....	39
Table 8: Statistics for two modelled NPP for forest stands for 2016-2018. NPP [gC/m <sup>2</sup> /year].....	39
Table 9: Statistics for two modelled NPP for 1 km <sup>2</sup> homogeneous polygons for 2016-2018. NPP [gC/m <sup>2</sup> /year].....	42
Table 10: Statistics for two modelled NPP for 1 km <sup>2</sup> homogeneous polygons for 2018. Data for conifers and broadleaves are given separately. NPP [gC/m <sup>2</sup> /year]. RSD – relative standard deviation [%].....	43
Table 11: Statistics for two modelled NPP for 2016-2020 for 1 km <sup>2</sup> homogeneous polygons. NPP [gC/m <sup>2</sup> /year].....	45
Table 12: Forest area according to two satellite-derived land cover maps (MODIS and Copernicus) and official Austrian forest inventory (BFW). $\Delta$ Area and Rel. $\Delta$ Area are the differences between the forest areas of satellite-derived LC maps (MCD12Q1 and S2GLC) and forest area obtained from NFI dataset. ....	46

## Abstract

Quantifying the rate of carbon uptake in forest ecosystems is essential for understanding how forest ecosystems impact the carbon cycle, to analyse the connection between the global carbon cycle and vegetation and to study factors which regulate spatial and temporal distribution of carbon dioxide (CO<sub>2</sub>). The MOD17 MODERate Resolution Imaging Spectroradiometer (MODIS) satellite product provides estimations of net primary production (NPP) of vegetation at 500 m spatial resolution. However, the coarse spatial resolution of MODIS NPP has limitations in capturing heterogeneity and fragmentation of forest areas and scaling issues in validation against forest inventory data. The aim of this thesis was to adapt the MOD17 NPP algorithm to generate high spatial resolution (10-30 m) NPP estimates using high spatial resolution input parameters derived from the Harmonized Landsat Sentinel-2 (HLS) project and other Copernicus datasets (climate data).

The new high spatial resolution HLS NPP product was compared to MODIS MOD17 NPP data and the connection between NPP and forest inventory data was explored. Moderate consistency was found between MOD17 and HLS NPP product for the area dominated by coniferous forest with a moderate correlation ( $R^2=0.53$ ,  $p<0.01$ ). For mixed forest areas correlation was weak for the years 2016 and 2018 ( $R^2=0.19$  and  $R^2=0.22$ ,  $p<0.01$ ) and there was no correlation for the year 2017. HLS NPP was lower than MOD17 NPP by 18.67% for the study area in Slovenia and by 23.24% for the southern part of Austria. Correlation analysis between periodic annual timber increment and HLS NPP for inventory plots in Slovenia showed that NPP algorithm cannot represent variation in timber volume increment, which was particularly the case for the plots with low stand density and low timber volume. The 10 m resolution NPP is feasible to obtain for forest areas in Europe and it is useful in estimation of NPP for forest stands and polygons of irregular shape. Variation in growing conditions due to effects of different forest site parameters cannot be fully represented by HLS NPP. Main limitations were the availability of ground data for validation and satellite Leaf Area Index (LAI) and Fraction of Photosynthetically Active Radiation (FPAR) data for forest. Therefore, for future work, it is significant to develop LAI and FPAR products for forest at high spatial and temporal resolution and to have ground-based estimates of NPP for validation.

## Kurzfassung

Die Ermittlung der Kohlenstoffaufnahme von Waldökosystemen ist von entscheidender Bedeutung die Auswirkungen von Waldökosystemen auf den Kohlenstoffkreislauf zu verstehen, Zusammenhänge zwischen dem globalen Kohlenstoffkreislauf und der Vegetation zu analysieren und Faktoren, welche die räumliche und zeitliche Verteilung von Kohlendioxid (CO<sub>2</sub>) regeln zu untersuchen. Das Satellitenprodukt MOD17 MODERate Resolution Imaging Spectroradiometer (MODIS) liefert Schätzungen der Nettoprimärproduktion (NPP) der Vegetation mit einer räumlichen Auflösung von 500 m. Diese relativ grobe räumliche Auflösung des MODIS-NPP Produktes stößt bezüglich der Erfassung von Heterogenität und Fragmentierung von Waldgebieten an seine Grenzen und es bestehen Skalierungsprobleme bei der Validierung mittels Waldinventurdaten. Ziel dieser Arbeit war es, den MOD17 NPP-Algorithmus so anzupassen, dass NPP-Schätzungen mit hoher räumlicher Auflösung (10-30 m) generiert werden können, wobei die Eingangsparameter mit hoher räumlicher Auflösung aus dem Harmonized Landsat Sentinel-2 (HLS Daten) Projekt und anderen Copernicus-Datensätzen (Klimadaten) abgeleitet wurden.

Das erstellte HLS-NPP-Produkt mit hoher räumlicher Auflösung wurde mit MODIS-MOD17-NPP-Daten verglichen bzw. der Zusammenhang zwischen NPP und Waldinventurdaten untersucht. In Gebieten mit hoher Nadelwalddominanz wurde eine moderate Übereinstimmung ( $R^2=0.53$ ,  $p<0.01$ ) zwischen MOD17- und HLS-NPP-Produkten festgestellt. Für Mischwaldflächen wurden geringe Korrelationen für die Jahre 2016 und 2018 ( $R=0.19$  bzw.  $R^2=0.22$ ,  $p<0,01$ ) gefunden und wurde für das Jahr 2017 kein Zusammenhang vorhanden. Die berechnete HLS-NPP war im Untersuchungsgebiet Slowenien um 18.67% und im Untersuchungsgebiet südliches Österreich um 23.24% niedriger als MOD17-NPP. Die Korrelationsanalyse zwischen dem periodischen jährlichen Holzzuwachs und der HLS-NPP für die Inventurflächen in Slowenien zeigte, dass der NPP-Algorithmus die Variation des Holzzuwachses nicht korrekt darstellen kann, insbesondere für die Flächen mit geringer Bestandsdichte und geringem Holzvorrat. Die Ermittlung der NPP mit einer Auflösung von 10 m ist für Waldgebiete in Europa durchführbar und auch für die Schätzung der NPP von Waldbeständen bzw. Polygonen mit unregelmäßiger Form nützlich. Variationen in den Wachstumsbedingungen aufgrund verschiedener Standortparameter können jedoch mit dem HLS-NPP-Produkt nicht vollständig dargestellt werden. Dies liegt vor allem an der begrenzten Verfügbarkeit von Bodendaten für die Validierung und von verlässlichen Satelliten-Leaf Area Index (LAI)- und Fraction of Photosynthetically Active Radiation (FAPAR)-Produkten für Waldflächen. Daher ist es für künftige Arbeiten essentiell, die vorhanden FAPAR- und LAI-Datensätze für Wälder mit hoher räumlicher und zeitlicher Auflösung zu verbessern und für die Validierung bodengestützte Schätzungen der NPP zu erhalten.

# 1. Introduction

## 1.1. Carbon pools and Vegetation carbon sink

Carbon is a chemical element which is essential component of life, and the carbon content of dry biomass is assumed to be 50% (Lewis et al., 2009; Chave et al., 2005). In the atmosphere it is found in the form of carbon dioxide (CO<sub>2</sub>).

Carbon is cycling between biosphere, atmosphere, geosphere, and hydrosphere through processes such as photosynthesis, decomposition, respiration, and mineralization (Pulselli and Marchi, 2015), which defines a process of the carbon cycle (Figure 1).

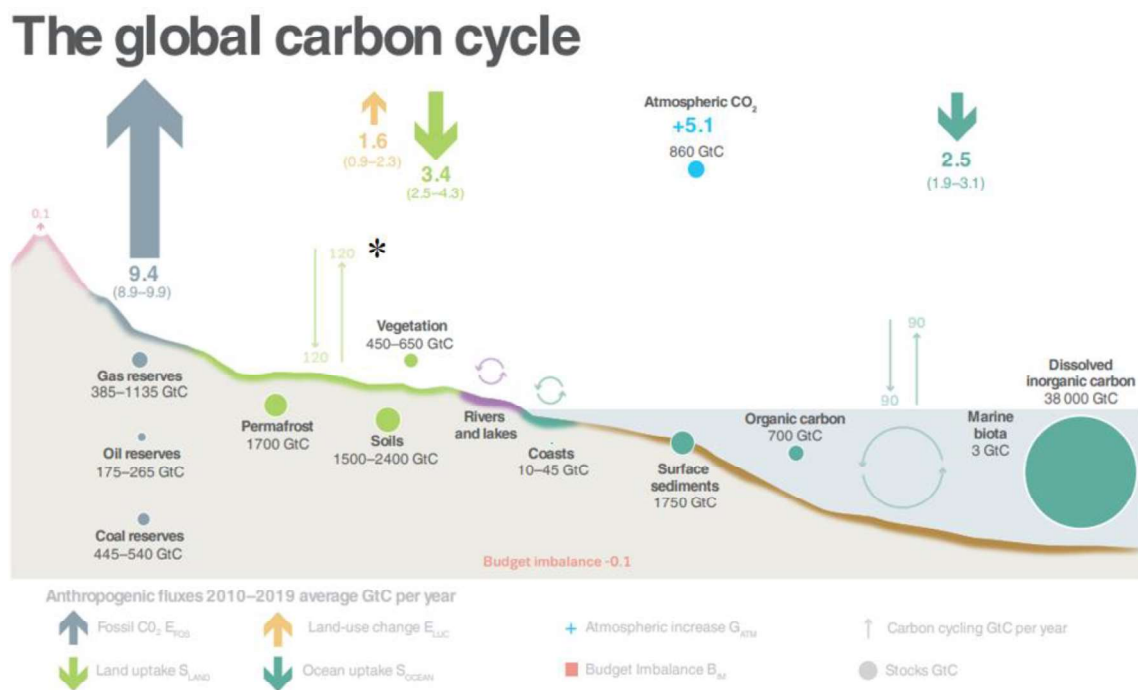


Figure 1: Schematic representation of the global carbon cycle, averaged globally for the decade 2010–2019 (Friedlingstein et al., 2020).

\*Total earth's biosphere's carbon sink absorbs approximately 3.61 GtC annually according to Keenan and Williams (2018) and  $3.4 \pm 0.9 \text{ GtC yr}^{-1}$  according to Friedlingstein et al. (2020).

Since the pre-industrial age, carbon dioxide (CO<sub>2</sub>) content in the atmosphere has been increasing, reaching concentration of  $404 \text{ cm}^3 \text{ m}^{-3}$  in 2016 (Tum, 2016) and  $409.9 \text{ cm}^3 \text{ m}^{-3}$  in 2019 (Friedlingstein et al., 2020).

Approximately half of the anthropogenic CO<sub>2</sub> emissions (Tum et al., 2016) remain in the atmosphere, reaching 5.4 Gigatons (Gt) of Carbon in 2019 (Friedlingstein et al., 2020).

Plants have important role in carbon cycle in Earth environment by capturing and storing carbon dioxide from the air through photosynthesis and putting out carbon dioxide back into the air through respiration and litter decomposition.

According to Dixon et al. (1994) 1146 Gt of carbon is stored in forest vegetation and soils. Total area of forest is approximately 4 billion hectares, which is 31% of the total land area

(FAO and UNEP, 2020) and contains over 86% of the global vegetation carbon pool (Dixon et al., 1994). As such, it is one of the most important parts of terrestrial ecosystems and has the highest production and important role in global matter and energy cycle, carbon balance and climate change (Yuan et al., 2006).

Through the process of photosynthesis, approximately 16% of the atmospheric CO<sub>2</sub> (121.6 Gt C) is absorbed by vegetation annually (Apps et al., 2005). A little less amount of carbon is released back into the atmosphere through respiration, degradation of organic matter, heterotrophs feeding on that vegetation (Goel and Agarwal, 2014; Gower, S. T., 2003), which results in increase of carbon sink in terrestrial ecosystems. Pan et al. (2011) estimated total forest sink of  $2.4 \pm 0.4$  Gt C y<sup>-1</sup> for 1990 to 2007 and after subtracting carbon emission losses from tropical deforestation and degradation the mean global net forest carbon sink was 1.0 and 1.2 Gt C y<sup>-1</sup> for 1990 to 1999 and 2000 to 2007, respectively. Pugh et al. (2019) observed global forest carbon sink increase from 1.74 Gt C year<sup>-1</sup> over 1981–1990 to 2.15 Gt C y<sup>-1</sup> over 2001–2010. For the last decade (2010-2019), total earth's biosphere's carbon sink absorbed  $3.4 \pm 0.9$  GtC yr<sup>-1</sup> according (Friedlingstein et al., 2020).

## 1.2. Carbon cycle and climate change

As the carbon cycle is out of equilibrium and atmospheric concentration of carbon dioxide is rising continuously, the global warming is increasing. The biosphere has important role in regulating Earth's climate (Apps et al., 2005) and the focus of numerous studies are on the role of terrestrial carbon cycle, with the highlight on forest, in mitigating the effects of climate change (Apps et al., 2005; Xu et al., 2018; Pugh et al., 2019; FAO and UNEP, 2020) and understanding how forest ecosystems impact the carbon cycle (Govind and Kumari, 2014).

It is expected that the rise of CO<sub>2</sub> content in the atmosphere has fertilizing effect on vegetation and growth through photosynthetic rate increase and longer growing seasons (Bacastow and Keeling, 1973; Alexandrov et al., 2003). Tum et al. (2016) showed the increase of forest carbon sink by 1% (0.5 Gt) over the 15 years, between 2000 and 2014 while Nemani et al. (2003) found a linearly increasing Net Primary Production trend of 0.19 Gt y<sup>-1</sup> for the period of 1982 – 1999.

However, although Gross Primary Production may increase with increased temperature, some authors suggest that heterotrophic decomposition rate may release additional quantities of CO<sub>2</sub> in the atmosphere and that the terrestrial biosphere may become carbon source instead of carbon sink (Cramer et al., 1999; Govind and Kumari, 2014).

Considering the complexity of global carbon cycle and its interconnection with the vegetation, it is important to quantify the response of ecosystems to changes in global biogeochemical cycles (Apps et al., 2005; Cramer et al., 1999). Moreover, for understanding the processes and factors that regulate the terrestrial carbon sink and response of terrestrial ecosystem to future climate warming, it is essential to assess the rate of carbon uptake in terrestrial vegetation (Tum, 2016).

## 1.3. Net Primary Production

Terrestrial Net Primary Production (NPP) is the rate of atmospheric carbon uptake by vegetation through process of photosynthesis minus carbon released by autotrophic respiration

and, as such, it is one of the important biophysical variables of vegetation activity and it is a beginning link of biogeochemical carbon cycle (Yuan et al., 2006).

Atmospheric carbon uptake is expressed as Gross Primary Production (GPP) which quantifies the “organic matter produced by all the individual plants in a defined area per unit time” (Yuan et al., 2006). After the amount of carbon released during autotrophic respiration is subtracted from GPP, NPP is obtained. The forest carbon cycle is presented in the Figure 2. There are other carbon losses caused by heterotrophic respiration and, in this case, the term “net ecosystem production” (NEP) is used. It is defined by Woodwell and Whittaker (1968) and it expresses the difference between GPP and total ecosystem respiration  $R_e$  (the sum of autotrophic and heterotrophic respiration).

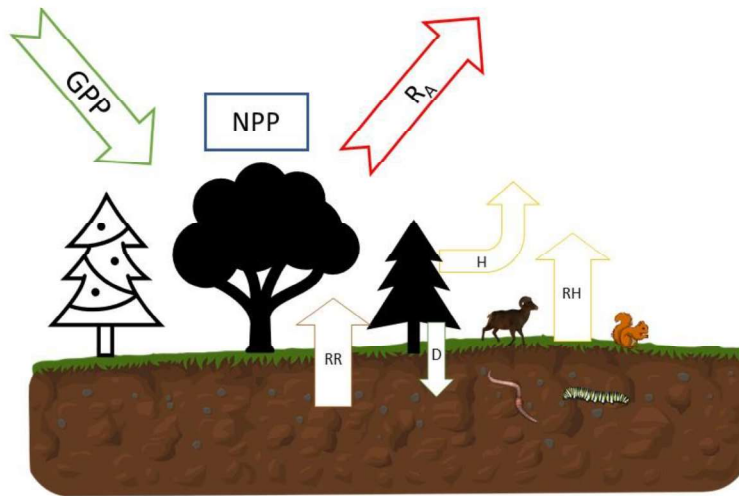


Figure 2: Conceptual diagram of the biological forest carbon cycle. Abbreviation for fluxes: net primary production (NPP), gross primary production (GPP), autotrophic respiration ( $R_A$ ), root respiration (RR), heterotrophic respiration (RH), decomposition of detritus (D) and herbivory (H). The forest carbon cycle is characterized by the presented biological (forest ecosystem) cycle with addition of an industrial (forest products) cycle. Adapted from Gower (2003).

Various large-scale disturbances that affect terrestrial vegetation, such as drought, flood, wind disaster, insect pests and human activities (land use change or deforestation) are also contributing to the carbon cycle. NEP minus the carbon release due to various disturbances is net biome production (NBP) (Yuan et al., 2006).

Running et al. (2000) argues that the change in terrestrial biological production is the most important “measure of global change” to humankind. Various authors (Yuan et al., 2006; Running et al., 2000; Cramer et al., 1999) pointed out that NPP is used commonly in carbon cycle models for studying global carbon cycle, carbon source and sink of ecosystem, and spatial and temporal distribution of  $CO_2$ , and as an “index of ecological change” (Liu et al. 2015).

With increased atmospheric carbon dioxide and global climate change, NPP over large areas is also changing (Cramer et al., 1999; Zhao and Running, 2010; Azhdari et al., 2020, Zhang et al., 2020).

According to Running et al. (2000), “the GPP and NPP products are designed to provide an accurate, regular measure of the production activity or growth of terrestrial vegetation.” This author presented potential usage of NPP models in both, theoretical and practical aspects.

Running et al. (2000) points out that the spatial and seasonal dynamics of CO<sub>2</sub> fluxes are important for global climate modelling, and they represent the dynamic interaction between the atmosphere, biosphere, and oceans, as well as relation of seasonal fluxes of net photosynthesis and respiration to seasonal variations of atmospheric CO<sub>2</sub>. This study highlights the practical utility of NPP models in measurement of economically and socially significant products of vegetation growth (crop yield, range forage and forest production).

Cramer et al. (1999) also emphasizes the importance of NPP for studying the response of the ecosystems to climate change.

Estimation of NPP is used to predict and assess the biomass potential related to food and energy production (Tum, 2016).

#### 1.4. Factors governing the level of carbon storage

Anthropogenic influence through net release of CO<sub>2</sub> to the atmosphere and forest conversion is the most important factor impacting the carbon pools (Cramer et al., 1999).

Climate change is causing changes in the rate of carbon storage because of changes in atmospheric CO<sub>2</sub> (Cramer et al., 1999), disturbances (Yuan et al., 2006), temperature, soil and atmospheric moisture (Field et al., 1995).

Quantity of carbon that is captured by plants depends on processes like photosynthesis and respiration. Environmental factors, which impact these processes, modify plant's ability to capture carbon. According to Ruimy et al. (1994) these factors are following: natural or cultivated vegetation; water availability; metabolic type of plants (C3 and C4 carbon fixation pathways).

Other factors include the solar irradiance, humidity, nutrient availability, forest age (Govind and Kumari, 2014), topography, physical and chemical characteristics of the soil and impact of animals through regulating plant community composition (Field et al., 1995).

Plant characteristics have effects on NPP due to their genetics, capability of access to resources, susceptibility to pests and pathogens, development of species composition (Field et al., 1995).

#### 1.5. Net Primary Production estimation methods

Ruimy et al. (1994) categorized the models into three groups: (1) statistical, (2) parametric and (3) process models.

Ground-based monitoring of terrestrial primary production (e.g. biomass measurement with forest inventories) enables direct measurement and serves as a basis for accurately estimating NPP (Pan et al., 2014). Repeated observations of tree carbon stocks are used to measure many of the basic components of a tree needed to estimate a volume, which is converted into biomass or carbon estimates (Neumann et al., 2016).

Another method of ground-based monitoring of terrestrial NPP is flux measurement of exchanges of carbon dioxide, water vapor, and energy between the biosphere and atmosphere using eddy covariance technique (Baldocchi et al., 2001, Pan et al., 2014).

As these fluxes or NPP obtained from forest inventory data (NFI) cannot be observed directly at the regional or global scale (Cramer et al., 1999), there was a necessity to estimate global carbon fluxes and establish global consistent database of NPP (Scurlock et al., 1999). To do

this, available local observations are scaled to the global level, using “physiological and physical principles for the development of global terrestrial ecosystem models” (Cramer et al., 1999). Therefore, these small-scale observations are used to calibrate, parameterize, evaluate (Zhao et al., 2005, Turner et al., 2006, Pan et al., 2006) and validate (Cramer et al., 1999, Neumann et al., 2016) terrestrial biosphere models.

As already mentioned, NPP is sensitive to many controlling factors, but climate plays a major role in NPP variability (Zhao et al. 2006). First NPP model (MIAMI, Lieth 1975), which is used as a baseline for other models (Cramer et al., 1999), relate annual NPP to the annual average temperature and precipitation without considering solar radiation and CO<sub>2</sub> concentration. More advanced models use different input data sets to represent global climate, vegetation and soils (Cramer et al., 1999).

Various process-based model (GLO PEM by Prince 1991; CASA by Potter et al., 1993; MOD17 by Running et al. 2000) use the concept of “radiation use efficiency” which was proposed by Monteith (Monteith 1972; Monteith 1977). This logic linearly relates the NPP of well-watered and fertilized annual crop plants to the amount of absorbed photosynthetically active solar radiation (APAR). Absorbed photosynthetically active radiation (APAR) is determined by the amount and geometry of displayed leaf material (LAI) and the geographic and seasonal variability of daylength and potential incident radiation, as modified by cloud cover and aerosols (Running et al. 2000). The conversion efficiency,  $\epsilon$  (gC/MJ), is the fraction of APAR converted into organic dry matter (NPP) (Ruimy et al., 1994). Therefore, NPP for a location (x) and time (t) is represented as:

$$\text{NPP}(x,t) = \text{APAR}(x,t) * \epsilon (x,t) \quad \text{Equation 1}$$

This equation presents the simplified calculation for CASA (Carnegie-Ames-Stanford Approach) model (Field et al., 1995) and uses  $\epsilon$  derived empirically which is applied to NPP.

Other models, like MOD17 (Running et al. 2000), have  $\epsilon$  applied to GPP and they model gross primary production and autotrophic respiration separately:

$$\text{NPP} = \text{GPP} - \text{Respiration} \quad \text{Equation 2}$$

Vegetation Indices (VIs), obtained from global satellite data sets, are utilized for photosynthetically active radiation (FPAR) estimation (Myneni et al., 2015), and thus the absorbed photosynthetically active radiation (APAR). That methodology connects satellite observations to biological production on large scales (Maisongrande et al., 1995) and provides opportunity for the “global monitoring of the temporal variation of terrestrial ecosystems” (Cramer et al., 1999).

The conversion efficiency of absorbed radiation into dry matter,  $\epsilon$ , is controlled by vegetation types (Ruimy et al., 1994) and climatic conditions (Running et al., 2004). For some early models (Ruimy et al., 1994), the maximum conversion efficiency ( $\epsilon_{\text{max}}$ ) is assumed to be constant inside each vegetation type. Environmental stress factors are affecting  $\epsilon$  and therefore, limiting daily GPP (Running et al., 2004). Consequently, maximum light use efficiency  $\epsilon_{\text{max}}$  is adjusted by temperature stress factors and moisture stress (CASA model, (Potter et al., 1993)) or minimum temperature and water pressure deficit (MOD17 model, (Running et al., 2004)).

To obtain the maximum conversion efficiency ( $\epsilon_{\max}$ ), these models require a land cover classification which are also derived from satellite data (Hilker et al., 2008).

Evolution of satellite sensors is followed by increasing capability in observation the Earth's vegetation in a spatially continuous mode and with high temporal resolution. Availability of continuous vegetation indices products (such as NDVI) which are used for modelling photosynthetically active radiation (FPAR) (Myneni et al., 2015), respiration (Running and Zhao, 2019) and land cover classification or vegetation type maps on which biome-parameters and the conversion efficiency are based (Running et al., 2000), gives opportunity for continuous monitoring of global vegetation production (Running et al., 2004).

## 1.6. Global NPP estimates

Approximately, 550 Gt of carbon exists in terrestrial vegetation (Bar-On et al., 2018). Ruimy et al. (1994) estimated from the literature that NPP value is about 60 Gt of carbon (GtC) per year for the whole of the continental surfaces, with rather large discrepancies between the estimates.

Tum et al. (2016) calculated, using BETHY/DLR model, global average of 60.2 Gt C per year for a period of fifteen years (2000–2014), with the main contribution from the Tropics. Cramer et al. (1999) compared seventeen global models of terrestrial biogeochemistry which resulted in a range from 44.4 to 66.3 Gt C year<sup>-1</sup>.

Mean global GPP and NPP estimates from MODIS (Zhao et al., 2005) from 2001 to 2003 are 109.29 Gt C y<sup>-1</sup> and 56.02 Gt C year<sup>-1</sup>, respectively. Mean global and European terrestrial NPP showed in Figure 3 and Figure 4 are products from MODIS NPP model (read more in the chapter 1.7).

Ito (2011) analysed the literature from 1862 to 2011 and extracted 251 estimates of total terrestrial NPP finding the mean value of 56.2 Gt C yr<sup>-1</sup> with the standard deviation of  $\pm 14.3$ .

Many authors showed a constant increase in annual NPP (Matsushita et al., 2004, Cao et al., 2004, Li et al., 2017). From 1961 to 2010, total global terrestrial NPP increased by 10.14 Gt C with an annual increase of 0.23 Gt C (Li et al., 2017).

This shows that even that the terrestrial net primary production is influenced by, and sensitive to many factors, models based on different types and parameters give similar results on a global scale (Field et al., 1995).

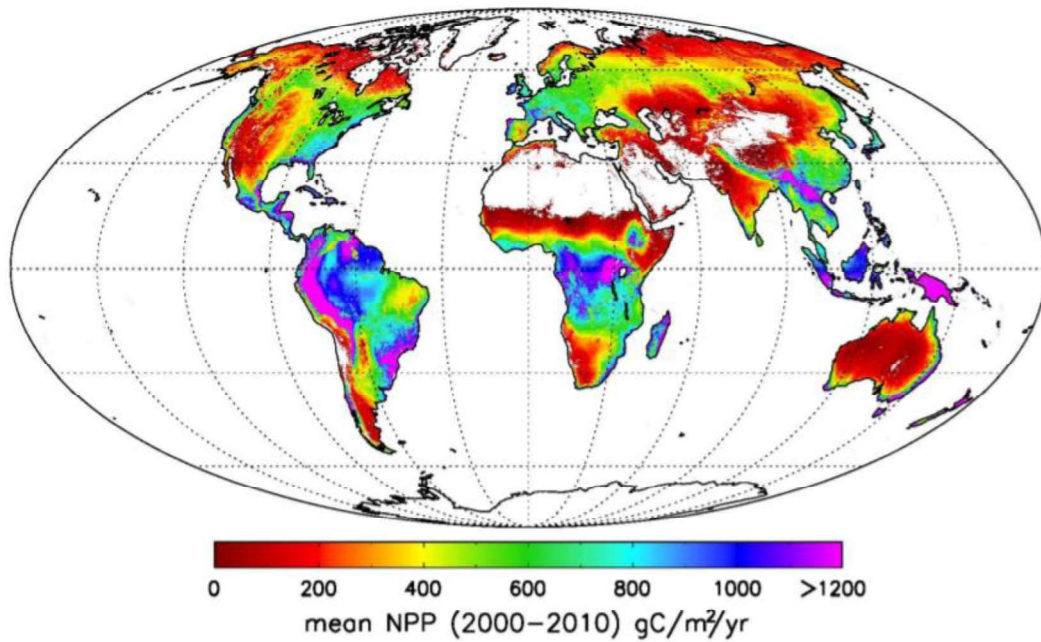


Figure 3: Global mean terrestrial net primary production (NPP) for 2000 – 2010 (Running and Zhao, 2019).

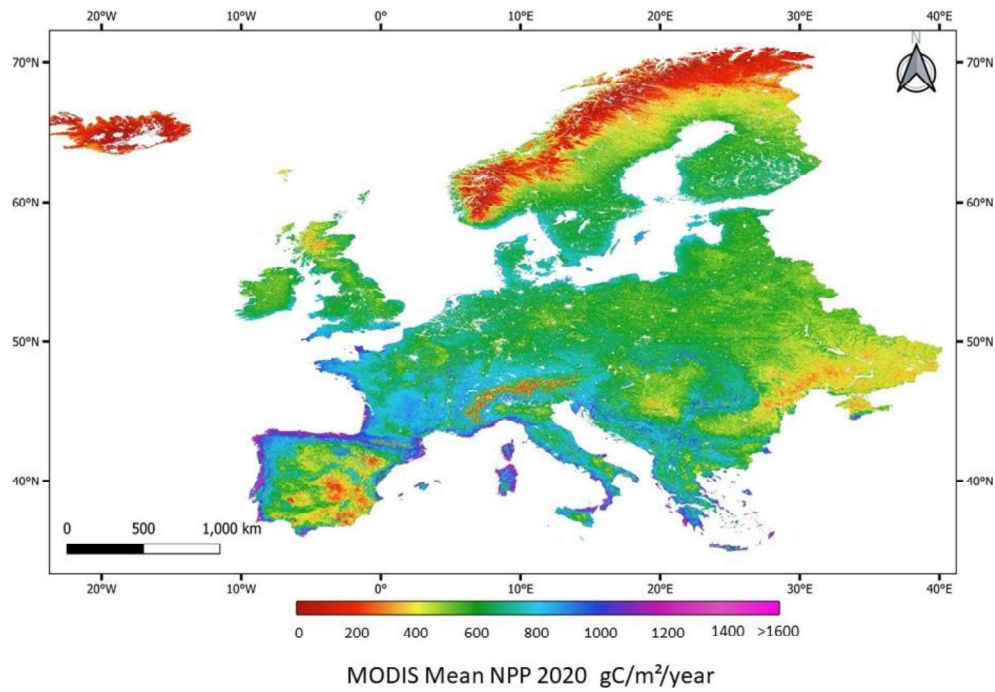


Figure 4: MODIS NPP on 0.5-km resolution representing annual NPP for 2020. NPP data derived from the MOD17A3HGFv006 (AppEEARS, <https://lpdaacsvc.cr.usgs.gov/appeears/>)

## 1.7. MOD17 NPP product

The MODerate Resolution Imaging Spectroradiometer (MODIS) is one of the primary global monitoring sensors on NASA Earth Observing System (EOS) satellites. The TERRA, EOS-AM platform was launched on December 19, 1999, and since the year 2000, the MOD17 product provides spatially and temporally continuous NPP estimates across the globe (Zhao et al., 2005).

The latest released MODIS NPP product, MOD17A3H collection 6, is an annual composite at 500 m spatial resolution delivered as a gridded Level-4 product in Sinusoidal projection (Running and Zhao, 2019). MODIS sensor was partly designed for the purpose of monitoring critical components of the biosphere carbon cycle at regional and global scales (Turner et al., 2003), and it has significantly improved vegetation observation capacities (Hasenauer et al., 2012). Consequently, NPP and GPP estimates obtained with MODIS algorithm has been widely used for or cited in quantifying the carbon fluxes and stocks of the world's forests (Park et al., 2021).

500 m and 1000 m spatial resolution are useful for regional level application if random errors in the NPP predictions are not too large and if the landscape is not too fragmented (Lang et al., 2013).

### 1.7.1. Limitations of coarse data and possible improvements with higher spatial resolution

Most of the remote sensing-based models use spatial resolution of 1 km (C-Fix model – Veroustraete et al., 1994; BEPS - Liu et al., 1997) and 0.5 km (MODIS - Running et al., 2004). Even though this spatial resolution is feasible for monitoring of growth for single forest stands with 25 – 100 ha sampling units (Lang et al., 2017), pixels for these spatial scales on European continent represent mixed vegetation (Veroustraete et al., 2002), and hence, have errors in model parameters (Zhao et al., 2005) and may miss finer scaled variations (Scurlock., et al. 1999). More authors (Running et al., 2004; Pan et al., 2014; Neumann et al., 2016; Lang et al., 2017) advocated that finer spatial resolution would be able to better represent specific local conditions.

Moreover, errors in land cover maps may cause large uncertainties (Quaife et al., 2008; Lang et al., 2013). Satellite-based model assume a constant land cover type within each pixel (Jay et al., 2016) and when landscape is fragmented or not homogeneous, scale patterns such as clear-cuts, thinning operations or disturbance events are not detectable (Neumann et al., 2016). It greatly simplifies the existing spatial and temporal variability in  $\epsilon$  (light use efficiency) and therefore, land cover classification is causing the largest error (Hilker et al., 2008). Biome-specific parameters extracted from the Biome Properties Look-Up Table (BPLUT) distinguish only between 11 different vegetation types (Turner et al., 2003) and 5 for forest.

Turner et al. (2003) showed that light use efficiency is highest on overcast days and decreases on clear sky days, while  $\epsilon_{\max}$  in MOD17 do not vary in time and it has values which are adjusted to clear sky conditions. He suggested that different values of  $\epsilon_{\max}$  should be specified for clear sky and overcast conditions and that final value is ranged between those values depending on the degree of cloudiness.

Running et al. (2004) and Lang et al. (2014) argued that MODIS data alone is insufficient for regional level planning and decision-making.

Calibration of the BPLUT tables used in the MOD17 algorithm most likely represents average forest conditions and may not capture heterogeneous, very open or very dense forests adequately (Neumann et al., 2016). Therefore, temporal variability (Hilker et al., 2008), plant's genetics, capability of access to resources and physical and chemical characteristics of the soil (Field et al., 1995) are not considered.

As models require field measurements of NPP for parameterization, calibration, and validation (Zheng et al., 2018), the plot measurements or field scales may not represent the NPP at the 500 m grid. Since most measurements are conducted in the small areas ranging from less than 1 to several hectares (Running et al., 2004), direct comparison of these results with coarse resolution models can be misleading (Pan et al., 2014, Ruimy et al., 1994, Kwon and Baker, 2017).

According to Hasenauer et al. (2012), MOD17 algorithm assumes a fully stocked forest. Hence, as forest management impacts the stand density and allocation of carbon, satellite driven NPP model does not detect these effects. To overcome this issue, authors proposed integration of stand density effect in the model to enhance NPP predictions.

The quality of the input climate data to ecosystem models is also critical to the modelled results (Matsushita et al., 2004). The current version of GMAO/NASA (used in the MOD17) is hourly time step dataset with about half-degree spatial resolution (0.5 Latitude degree by 0.625 Longitude degree) and the problem of coarse spatial resolution is to some extent solved with spatial interpolation. However, the accuracy of final NPP depends on the accuracy of GMAO data, properties of local environmental conditions (Running and Zhao, 2019) and on number and distribution of weather stations (Matsushita et al., 2004). Regions with low density of weather stations and lack of observations as well as with high productivity, such as tropics, result in large uncertainties in GPP and NPP (Zhao et al., 2006).

### 1.7.2. Improvements of MODIS NPP/GPP model

Since MODIS was placed in orbit in 1999 there have been multiple updates or “Collections” of the MODIS land products (Turner et al., 2006). Coarse resolution meteorological data input was improved by spatial interpolation and temporal filling of cloud-contaminated LAI/FPAR data and the Biome Parameter Look-Up Table (BPLUT) was modified (Zhao et al., 2005) for Collection 5 (C5). The latest Collection 6 (C6) has the higher spatial resolution of 500 m, which makes the data more useful at local scale (Running and Zhao, 2019).

To reduce biases from meteorological inputs, Zhao et al. (2006) proposed adjustment of reanalyses based on station observations and modification of parameters in the MOD17 BPLUT to compensate for the biases from different meteorological reanalyses.

Some studies were focused on model adjustment to local and regional conditions. Pan et al. (2006) incorporated other factors which are expressed at the local scales by developing the “available soil water index”, which significantly improved NPP estimates for coniferous forests in mid-Atlantic region of the United States. Wang et al. (2013) incorporated the time lagged serial correlation analysis to study the relationship between NPP and climatic factors in Wuhan in China, and thus, to improve FPAR, PAR and LUE. The authors stated that this accurate and operational model can be modified and applied to other regions to map vegetation NPP.

Neuman et al. (2016) created the NPP product for Europe (MODIS EURO) by running the original MOD17 algorithm in which the climate dataset used in MOD17 (NCEP2) (approximately 1.875° spatial resolution) was replaced with local European climate data (1-km resolution). MODIS EURO decreased the differences with NFI NPP from 26% to 7%.

Yu et al. (2018a) achieved higher NPP/GPP precision for most vegetation types with LAI and FPAR products based on Global Land Surface Satellite (GLASS). After validation of estimated data against the BigFoot NPP, RMSE for MODIS NPP on BigFoot sites was 219.26  $\text{gCm}^{-2} \text{yr}^{-1}$ , while with the RMSE for improved GLASS NPP was 160.16  $\text{gCm}^{-2} \text{yr}^{-1}$ .

High spatial resolution (30 m) GPP and NPP products were developed based on multi-scale remote sensing data and with a downscaling method where LAI/FPAR was obtained. Spatial and temporal adaptive reflectance fusion model (STARFM) (Yu et al., 2018b) was used, and it showed applicability and reliability.

Validation scaling issues were addressed by the BigFoot project (Turner et al., 2005) in which digital maps (25  $\text{km}^2$ ) of land cover, LAI, daily GPP, and annual NPP were developed from the Landsat data and ground measurements (Turner et al., 2006).

Increasing spatial resolution methods were already preformed using fine resolution climate data (Matsushita et al., 2004; Neumann et al., 2016), local and regional land cover maps with higher spatial resolution (Nilson et al., 2012; Kimball et al., 2017) or improved spatial resolution of land cover maps through an image fusion of Landsat and MODIS satellite data products (Jay et al., 2016).

High spatial resolution and reliable climate datasets provide improved quality of GPP/NPP products both spatially and temporally (Matsushita et al., 2004; Zhao et al., 2006; Neumann et al., 2016).

In essence, possible benefits of using high spatial resolution data are:

- Using high spatial resolution GPP/NPP (10 to 30 m) would provide the opportunity to match the scales of inventory data and modelled NPP, and therefore, improve validation and calibration activities;
- Finer spatial resolution would be able to better represent specific local conditions (Running et al., 2004; Pan et al., 2014; Neumann et al., 2016; Lang et al., 2017);
- Fragmented or heterogeneous areas such as clear-cuts, thinning operations or disturbance events are better detectable;
- Higher spatial resolution of land cover map would possibly provide more spatial variation of light use efficiency ( $\epsilon_{\text{max}}$ ) and other biome-parameters (Scurlock et al., 1999);
- Assess potential effects of different forest management practices on the allocation patterns of carbon;
- High spatial resolution NPP maps would be able to separate different forest stands, to distinguish ownership boundaries and they would be sufficient for regional level planning and decision-making.

## 2. Objectives

The goal of this thesis is to study the feasibility and to provide a roadmap to estimate forest production at high spatial resolution (10-30 m pixel size) using satellite and other data from the Copernicus programmes.

The study is focusing on the assessment of the MOD17 NPP algorithm, and its adaptation with USGS Landsat, Copernicus Sentinel-2 and other Copernicus weather data. The model is executed on different sites and the results are compared to native MOD17 data and to forest inventory data obtained with ground-based monitoring in Slovenia and Austria.

Benefits of 10-30 m spatial resolution NPP are analysed on a plot level (500 m<sup>2</sup>) and on a stand level.

A second objective is to assess the relationship between high spatial resolution NPP and annual increment at the plot scale (500 m<sup>2</sup>).

Furthermore, analysing this model at high spatial resolution would provide better understanding of input parameters on a smaller scale (on a stand and on a plot level). Potential improvements and directions of further research are presented.

### 3. Materials and Methods

#### 3.1. Description of MODIS NPP algorithm

The MODIS algorithm MOD17 is based on an ecophysiological modelling approach and it uses remotely sensed satellite-data and climate data to predict spatially and temporally continuous NPP and GPP (Gross Primary Production or carbon assimilation) (Running et al., 2004).

The basis is a “radiation use efficiency” which was proposed by Monteith (Monteith 1972; Monteith 1977). This logic linearly relates the NPP of well-watered and fertilized annual crop plants to the amount of absorbed photosynthetically active solar radiation (APAR).

The MOD17 algorithm (Figure 5) requires FPAR and LAI (leaf area index) data as well as land cover data, which is derived from MODIS reflectance data. The algorithm is combined with climatic controls on NPP (Running et al., 2000). For any given pixel within the global set of 500 m land pixels, estimates of both GPP (on an eight-day time-step) and annual NPP are calculated.

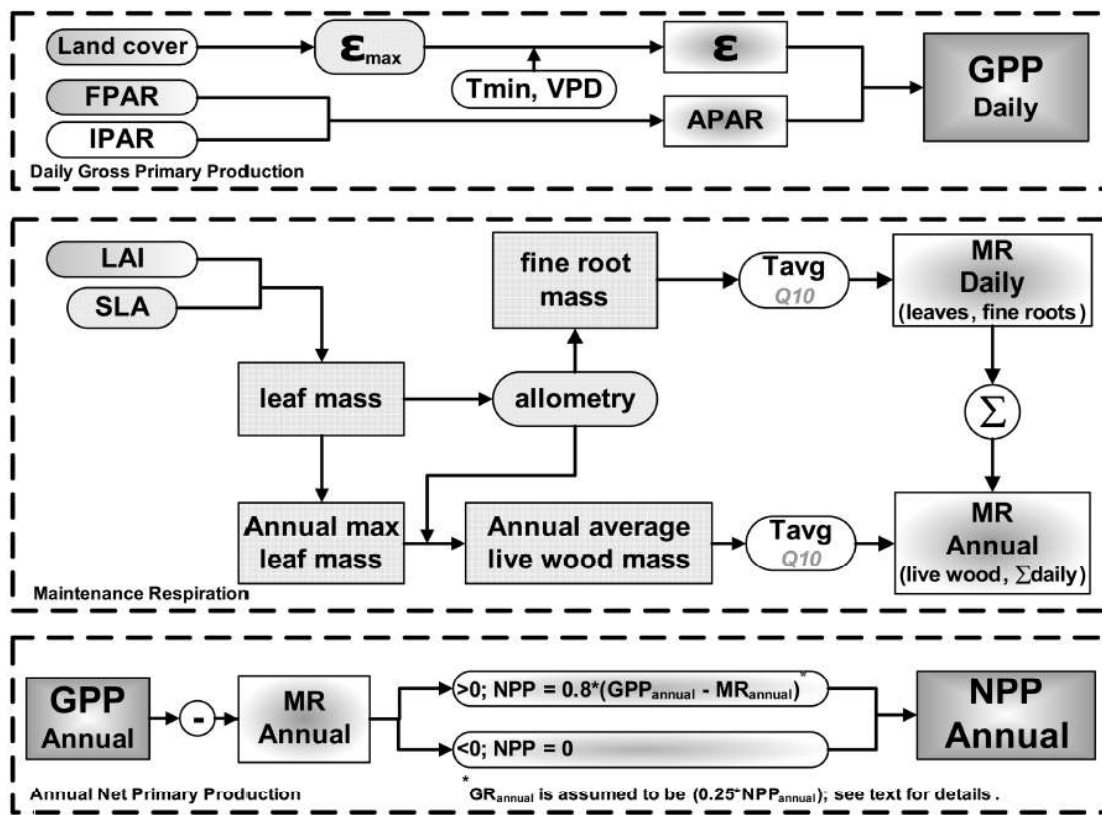


Figure 5: Flowchart showing the logic behind the MOD17 algorithm in calculating the 8-day average GPP and annual NPP (Running and Zhao, 2019; MOD17 user guide).

The annual growth respiration and net primary production are calculated as follows (Running and Zhao, 2019):

$$\text{NPP} = \text{GPP} - \text{Rm} - \text{Rg} \quad \text{Equation 3}$$

where:

**Rm** (annual maintenance respiration) and **Rg** are obtained as follows:

$$\text{Rm} = \sum \text{Leaf\_MR} + \sum \text{Froot\_MR} + \sum \text{Livewood\_MR} \quad \text{Equation 4}$$

$$\text{Rg} = 0.25 * \text{NPP} \quad \text{Equation 5}$$

Then:

$$\begin{aligned} \text{NPP} &= 0.8 * (\text{GPP} - \text{Rm}) && \text{when } \text{GPP} - \text{Rm} \geq 0 \\ \text{NPP} &= 0 && \text{when } \text{GPP} - \text{Rm} < 0 \end{aligned} \quad \text{Equation 6}$$

The calculation of the GPP is based on the following equations:

$$\text{GPP} = \text{PAR} \times \text{fPAR} \times \epsilon \quad \text{Equation 7}$$

where:

PAR represents the photosynthetically active radiation which is estimated from incident shortwave solar radiation load at the surface (SWRad, provided in the GMAO/NASA dataset) of which 45% is photosynthetically active as:

$$\text{PAR} = (\text{incident short wave radiation} * 0.45) \quad \text{Equation 8}$$

fPAR represents the fraction of PAR absorbed by the canopy. It is calculated in the MODIS product MOD15 (MOD15A2H) at 500 m pixel size.

$\epsilon$  (gC MJ<sup>-1</sup>) represents the photosynthetic efficiency term obtained as:

$$\epsilon = \epsilon_{\text{max}} * T_{\text{min\_scalar}} * \text{VPD\_scalar} \quad \text{Equation 9}$$

$\epsilon_{\text{max}}$  represents the maximum radiation conversion efficiency for a given vegetation type and  $\text{VPD\_scalar}$  and  $T_{\text{min\_scalar}}$ , which are multipliers between 0 and 1, are addressing water stress due to vapor pressure deficit (VPD) and low temperature limits ( $T_{\text{min}}$ , daily minimum temperature).  $\text{VPD\_scalar}$  and  $T_{\text{min\_scalar}}$  are calculated with the linear ramp functions with

$VPD_{max}$ ,  $VPD_{min}$ ,  $T_{min\_max}$  and  $T_{min\_min}$ , values prescribed in BPLUT for each biome category (Table 1).

Values of  $T_{min}$  and  $VPD$  are obtained from GMAO/NASA dataset, while the value of  $\epsilon_{max}$  is obtained from the BPLUT.

The GMAO/NASA daily meteorological data ([https://gmao.gsfc.nasa.gov/GMAO\\_products/](https://gmao.gsfc.nasa.gov/GMAO_products/)) is obtained with a spatial resolution: 0.5 Latitude degree by 0.625 Longitude degree (Gelaro et al., 2017).

The BPLUT provides the parametrization for individual biome types that is based on the land cover classification derived from MCD12Q1v006 (Friedl and Sulla-Menashe, 2019).

The net photosynthesis - PSNnet ( $\text{kg C day}^{-1}$ ) is calculated as:

$$PSN_{net} = GPP - Leaf\_MR - Froot\_MR \quad \text{Equation 10}$$

where:

$$Leaf\_MR = Leaf\_Mass * leaf\_mr\_base * Q10\_mr^{[(T_{avg} - 20.0) / 10.0]} \quad \text{Equation 11}$$

$$Froot\_MR = Fine\_Root\_Mass * froot\_mr\_base * Q10\_mr^{[(T_{avg} - 20.0) / 10.0]} \quad \text{Equation 12}$$

$$Leaf\_Mass = LAI \text{ (Leaf Area Index)} / SLA \text{ (projected leaf area)} \quad \text{Equation 13}$$

$$Fine\_Root\_Mass = Leaf\_Mass * froot\_leaf\_ratio \quad \text{Equation 14}$$

The other inputs include:

- LAI comes from the MOD15 product at 500 m pixel size; SLA, leaf\_mr\_base, froot\_mr\_base and froot\_leaf\_ratio are tabulated in the BPLUT table.
- $Q_{10\_mr} = 2$  for fine root and live wood calculation,  $Q_{10} = 3.22 - 0.046 * T_{avg}$  for maintenance respiration by leaf and  $T_{avg}$  is the average daily temperature from the GMAO/NASA dataset.

The annual maintenance respiration:

$$Livewood\_MR = livewood\_Mass * livewood\_mr\_base * annsum\_mrindex \quad \text{Equation 15}$$

where:

- $livewood\_Mass = ann\_leaf\_mass\_max * livewood\_leaf\_ratio$

- `ann_leaf_mass_max` = maximum of `Leaf_Mass` = `LAI / SLA`
- `livewood_leaf_ratio` and `livewood_mr_base` are tabulated in the BPLUT table
- `annsum_mrindex` is the annual sum of `Q10_mr` <sup>[(Tavg - 20.0) / 10.0]</sup>

## 3.2. High spatial resolution model input datasets

To generate high spatial resolution NPP estimates, MOD17 algorithm input parameters were replaced with high spatial resolution parameters which were derived from USGS Landsat, Copernicus Sentinel-2 (HLS data) and other Copernicus datasets (climate data).

### 3.2.1. Land cover map

Land cover (LC) map is used for extraction of biome-specific parameters from Look-Up Table (BPLUT). The Land Cover Map used for this model is a product of the S2GLC project acquired from the Sentinel-2 satellite, which consists of 13 land cover classes (deciduous and conifers for forest) at a spatial resolution of 10 m for the year 2017. Its overall accuracy, based on nearly 52,000 samples, was estimated to be 86 % (Malinowski et al., 2020).

### 3.2.2. Climate dataset

MOD17 uses global meteorological reanalysis data provided by GMAO/NASA with about half-degree spatial resolution (0.5 Latitude degree by 0.625 Longitude degree) (Running and Zhao, 2019).

High resolution NPP model uses ERA5-Land Copernicus Climate Change Service Product which runs at enhanced resolution of 0.1° (native resolution is 9 km) (Muñoz Sabater, 2019), from which hourly surface solar radiation downwards (incident shortwave radiation) is obtained. Daily incident shortwave radiation (SWRad) is accumulated for each day (joules per square meter per 1-hour time step).

E-OBS is another dataset from the Copernicus Climate Change Service (C3S) which contains series of daily observations at meteorological stations throughout Europe (Cornes et al., 2018). E-OBS v23.1e has 0.1° horizontal resolution which provides daily mean temperature, daily minimum temperature, and relative humidity, usually at 2-meter height.

### 3.2.3. Harmonized Landsat and Sentinel-2 dataset

The Harmonized Landsat/Sentinel-2 (HLS) project provides a surface reflectance product that combines observations from USGS/NASA's Landsat 8 and ESA/Copernicus's Sentinel-2 satellites at moderate spatial resolution (30 m) (Claverie et al., 2018). The combined measurement enables global observations of the land every 2–3 days. HLS has adopted the tiling system used by Sentinel-2 and includes 4090 MGRS (Military Grid Reference System) tiles.

For generating a harmonized, analysis-ready surface reflectance data the following algorithms are applied to the HLS data: atmospheric correction, cloud and cloud-shadow masking, spatial co-registration and common gridding, illumination and view angle normalization and spectral

bandpass adjustment (Claverie et al., 2018). In this study, the HLS dataset is used for estimation of LAI and FPAR.

With the land cover map obtained from the Sentinel-2 Global Land Cover (S2GLC) project, meteorological reanalysis data from ERA5 and E-OBS datasets and reflectance data from HLS, higher spatial resolution inputs for all parameters is achievable. Land cover map spatial resolution changed from 500 m to 10 m, climate data ( $T_{\min}$ ,  $T_{\text{mean}}$ , SWrad and RH) from 70 km to 11 km (0.625° to 0.1°) and vegetation indices (FPAR/LAI) from 500 m to 30 m (Figure 6).

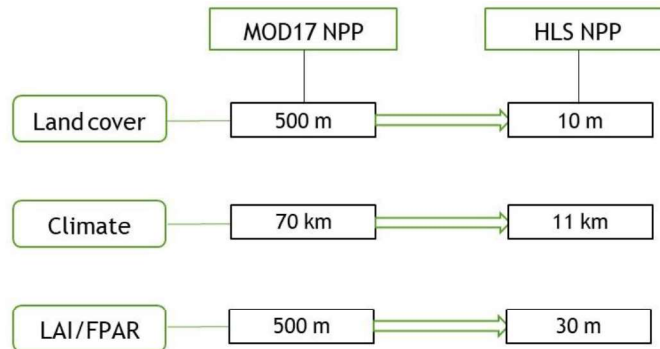


Figure 6: Increase of spatial resolution of model inputs when introducing new datasets.

### 3.3. Study area

Slovenia is geographically situated between 45°25'–46°53'N and 13°23'–16°37'E with the area of 20,273 km<sup>2</sup>. With the mountain ranges in the north, hilly central part with its numerous valleys and basins, and Pannonian plain in the northeast, Slovenia is a very diverse country. Average inclination of the terrain is 25% and the average altitude is 550 m (Kus et al., 2018).

The three main types of climates in Slovenia are (1) temperate humid climate with hot summers, (2) temperate continental climate and (3) mountain climate (Komac et al., 2020). Terrain diversity, climate and pedological variety, large forests and the preservation of traditional ways of managing parts of the cultural landscape are the reasons for the high biodiversity (Kus et al., 2018). Average temperatures of the coldest months do not drop below -3° C and at least four months have an average temperature of above 10° C (Komac et al., 2020).

According to the Slovenia's National Inventory Report (2020), forest land area in Slovenia in 2018 was 1,208,010 ha, which is 59.6% of the country. Beech, fir-beech and beech-oak sites cover most of the forest land (70%). The share of growing stock of coniferous trees in 2017 was 46.4% and 53.6% of deciduous trees. Main tree species are beech (*Fagus sylvatica*), spruce (*Picea abies*), fir (*Abies alba*), oak (*Quercus* sp.) and Scotch pine (*Pinus sylvestris*).

Five districts in the southern part of Austria (Spittal/Drau, Tamsweg, Murau, St. Veit/Glan, Feldkirchen) were selected for the second NPP validation. These districts are geographically situated between 46° 38'–47° 20'N and 12° 41'–14° 41'E with the area of 7224.34 km<sup>2</sup>. Most of

the study area is mountainous and elevation range from 456 m to 3449 m with the average altitude of 1449 m.

The climate is humid continental, with hot and moderately wet summers and long harsh winters with an average temperature of 7.4°C. Forest area covers approximately 45% of the selected area. Dominant tree species are Norway spruce (*Picea abies*) with share of more than 90%, pine (*Pinus sylvestris*), and European larch (*Larix decidua*). Broadleaf trees like European beech (*Fagus sylvatica*) or oak (*Quercus petraea*, *Quercus robur*) are only of local importance (Gutleb 1998).

### 3.4. Reference data

For the purpose of testing the high spatial resolution NPP model (hereafter called HLS NPP), data from Slovenian Forest Ecosystem Condition Survey (FECS) were used for evaluation of 10 m spatial resolution NPP. Slovenian FECS took place on the systematic grid of permanent sampling plots (4 km x 4 km) across the entire Slovenia in the years 2000, 2007, 2012, and 2018 (Skudnik et al., 2021). Figure 7 shows the distribution of the FECS plots. In the last inventory cycle, 759 out of the 1260 plots (60%) were categorized as forests and the NPP was modelled at the coordinates of these plots. The data available from the FECS: standing volume in 2012 and 2018, total periodic increment, share of deciduous and conifers, ID of the plots completely located in forest and ID of the plots where harvesting or mortality did not occur between the last two inventories. Plots are circular with the size of 500 m<sup>2</sup>. National forest inventory data was provided by the Slovenian Forestry Institute.

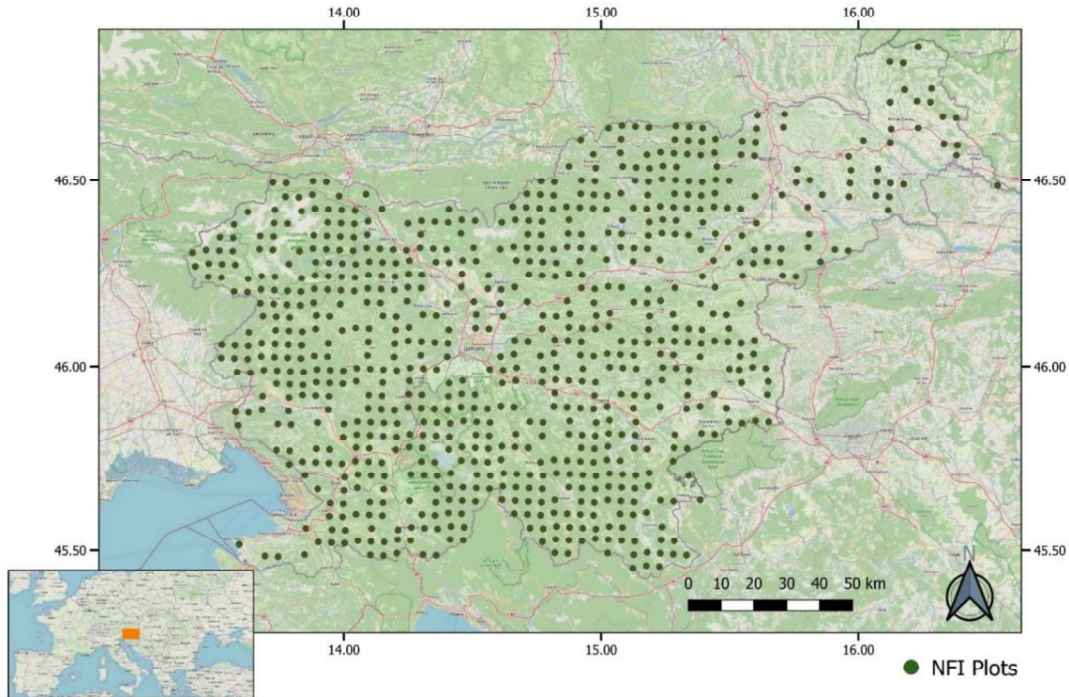


Figure 7: Sampling plots of the Slovenian National Forest Inventory. The green dots represent plots categorized as forests in 2018.

Due to the Slovenian Forestry Institute regulations only the degraded NFI plot coordinates were available which were rough approximations of the exact plot locations. As the real NFI plots are located in the area approximately up to 1 km distance from the degraded coordinates, square buffer polygons of 1.96 km<sup>2</sup> around the available NFI points were created for NPP modelling and analysis (Figure 8).

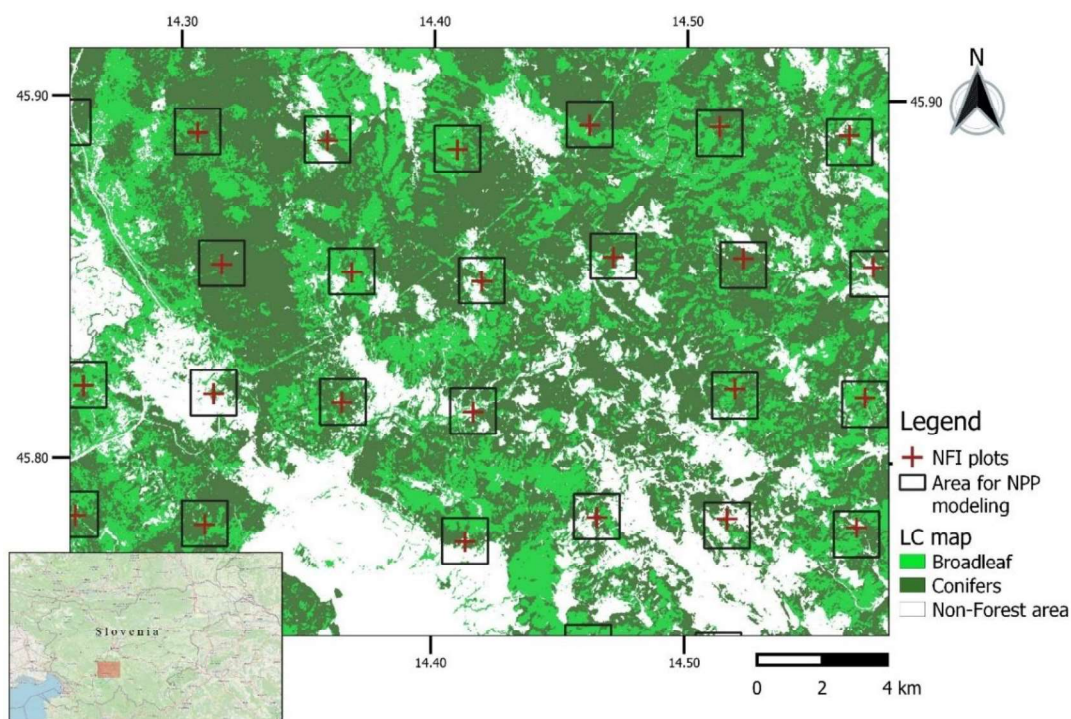


Figure 8: NFI plots and polygons in Slovenia for which the NPP is estimated. This map represents part of the NFI plots with the shapefile of polygons for NPP estimation and land cover classification.

As the HLS dataset is available from 2016, and the last inventory cycle was for period 2012-2018, correlation between the annual average NPP for the period 2016-2018 and annual average increment data for the period 2012-2018 was studied. However, HLS dataset is still not available for the entire globe and the eastern part of Slovenia is not being processed in the HLS dataset. Therefore, 557 NFI plots (73.4 %) are covered with the HLS dataset.

Out of 759 plots, 714 are completely in forest. On 104 plots harvesting or mortality did not occur between two inventory periods and 299 plots are comprised of either only broadleaf or conifer species. As there is no data available for the year of harvest, for reliable comparison it was only possible to analyse the correlation between the NPP and annual increment for plots for which harvesting was not reported between 2012 and 2018. It is assumed that the annual increment from 2012 to 2018 did not vary too much. Therefore, periodic annual volume increment (PAI) is considered for correlation analysis against the mean NPP for the period 2016-2018.

Due to limits on data sharing and actual lack of data, we could obtain only data for standing tree volume in years 2012 and 2018 and share of conifers/broadleaves for each plot. Individual tree data (dbh – diameter at breast height, age, height) and deadwood data were not available. As tree NPP is strongly influenced by age, volume of separate tree compartments and

individual taxation data (Thurnher et al., 2013), it was not reliable to calculate the terrestrial NPP only with the annual increment for entire plot. Thus, comparison between MODIS NPP and HLS NPP as well as correlation analysis between annual HLS NPP and the periodic annual increment were performed. For further research it is necessary to compare high spatial resolution NPP with the NPP obtained from forest growth observation including individual tree measurements, mortality and turnover of foliage.

For testing the HLS NPP model for five districts in the southern part of Austria (Figure 9) tree core samples from 30 plots were analysed. Annual data for growth ring size was provided and analysed by BFW within the H2020 Landsupport project and based on the contract for services concluded between the Umweltbundesamt and the Bundesforschungszentrum für Wald (BFW) (20.10.2021). Annual diameter increment values were measured from 1991 to 2019. For the period from 2016 to 2019 NPP is estimated for forest areas in these 5 districts with the HLS NPP model.

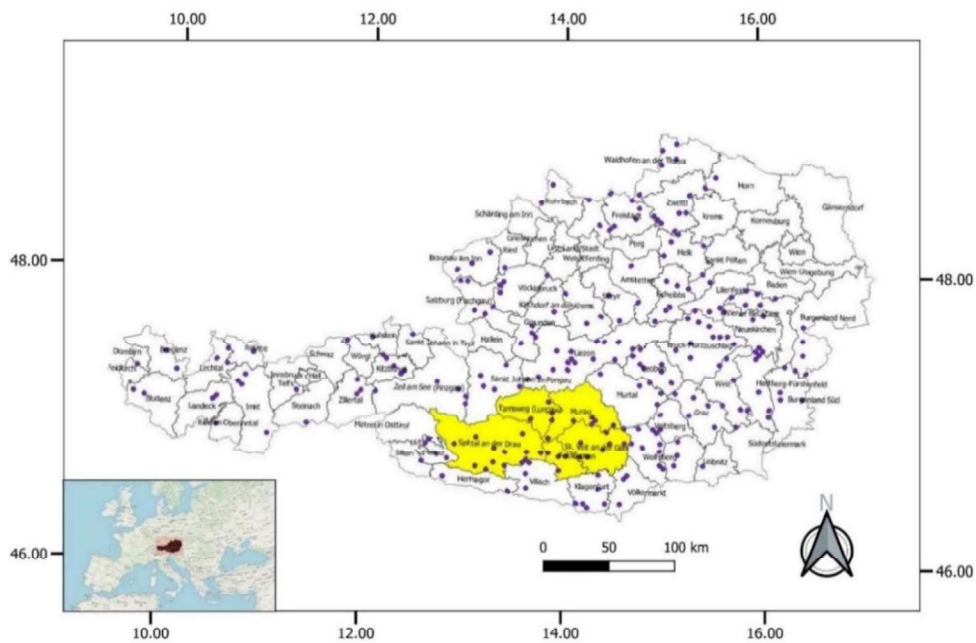


Figure 9: Selected area (marked in yellow) of the tree core samples taken in 2020.

Timber volume increment data was not provided by BFW. Therefore, it was not feasible to do a correlation analysis between timber volume/biomass growth and the NPP estimation. Nevertheless, connection between the annual NPP and annual growth ring size obtained from sampled cores was tested.

We also compared the modelled HLS NPP for study areas in Slovenia and Austria with MODIS NPP data. The Collection 6.1 yearly NPP data was downloaded from *The Land Processes Distributed Active Archive Center* (LP DAAC) and projected to the UTM coordinate system (UTM zone 33) using nearest neighbour sampling.

The MODIS NPP data used in this study were gridded at 0.5-km resolution at the global scale. To address an issue of scale differences, manually selected polygons of 1 km<sup>2</sup> area covering homogeneous forest areas were selected for NPP comparison and aggregated weighted mean NPP values from both datasets were extracted for the selected polygons. In addition, 1362

forest stands located on NFI points in Slovenia were selected for NPP comparison and the same method for NPP extraction was used.

### 3.5. Input data processing

The NPP calculation was described in the chapter 3.1. In the following text, more detailed explanation of the calculation of photosynthetic efficiency ( $\epsilon$ ) and vapor pressure deficit is presented, as well as how to obtain meteorological data and FPAR/LAI time series at a high spatial resolution.

For HLS NPP model, the MOD17 algorithm scripts were modified to run with HLS and other Copernicus data (weather and land cover) to achieve high spatial resolution NPP of 10 m. All the raster data were projected to the UTM projection system. The open-access R statistical software 4.1 version was used to process all the input data and to run the algorithm.

Inputs for NPP model are PAR (45% of SWrad), FPAR, LAI, BPLUT parameters (obtained from forest type), conversion efficiency ( $\epsilon_{\max}$ ) and weather data ( $T_{\min}$ ,  $T_{\text{mean}}$ , VPD).

Areas for NPP modelling were selected around Slovenian NFI coordinates. To cover the whole forest stands in which NFI plots are located, areas of 1.96 km<sup>2</sup> are selected for NPP estimation. Pixel values from the Sentinel-2 Global Land Cover (S2GLC) (Malinowski et al., 2020) map were extracted for the selected polygons. Pixels representing non-forest classes were masked out. For the study area in Austria, NPP was estimated for entire area classified as forest.

Based on the land cover map (S2GLC), set of biome-specific parameters were extracted from the Biome Properties Look-Up Table (BPLUT) for each pixel. Forest type is classified in two classes in S2GLC map (coniferous and broadleaf) and all BPLUT parameters were derived for these two classes. Biome-specific parameters are represented in Table 1.

Table 1. Biome-Property-Look-Up-Table (BPLUT) for MODIS GPP/NPP algorithm (Running and Zhao, 2019).

S2GLC	Evergreen Needleleaf Forest ( <i>coniferous</i> )	Deciduous Broadleaf Forest ( <i>broadleaf</i> )
LUEmax (KgC/m <sup>2</sup> /d/MJ)	0.000962	0.001165
Tmin_min (C)	-8.00	- 6.00
Tmin_max (C)	8.31	9.94
VPD_min (Pa)	650.0	650.0
VPD_max (Pa)	4600.0	1650.0
SLA (LAI/KgC)	14.1	21.8
Q10*	2.0	2.0
froot_leaf_ratio	1.2	1.1
livewood_leaf_ratio	0.182	0.203
leaf_mr_base	0.00604	0.00778
froot_mr_base	0.00519	0.00519
livewood_mr_base	0.00397	0.00371

\*: The constant Q10 = 2.0 is applied to fine roots and live wood, while for leaves, a temperature acclimation is: Q10 = 3.22 – 0.046 \* Tavg

MOD17 algorithm uses land cover map derived from MCD12Q1v006 which has 2 land cover types (needleleaf and broadleaf) for both, evergreen and deciduous forests and mixed forest type (5 in total). S2GLC map, which is used in adjusted, high resolution model (HLS NPP), differentiate only coniferous (needleleaf) and broadleaf land cover classes. However, evergreen broadleaf and deciduous needleleaf forest (except for larch stands) are negligible in the study areas. According to MODIS MCD12Q1v006 land cover map, area of deciduous needleleaf class is 0.12% of forest areas in selected polygons in Slovenia and 0.1% of forest areas in study area in Austria. Area of evergreen broadleaf class is 0.02% of forest areas in study area in Austria. Therefore, BPLUT values for coniferous land cover class pixels were obtained from parameters based on evergreen needleleaf forest class and for broadleaf class pixels from parameters based on deciduous broadleaf class.

All meteorological values ( $T_{min}$ ,  $T_{mean}$ ,  $SWrad$  and relative humidity) for each NFI plot in Slovenia were spatially interpolated using bilinear interpolation method. For the study area in Austria, entire area is gridded at 2 km resolution and 3240 polygons of 4 km<sup>2</sup> were created. All meteorological values for each polygon were also spatially interpolated with the same method because spatial interpolation for each 10 m resolution pixel demands high computing power and is unproductive.

Photosynthetic efficiency ( $\mathcal{E}$ ) is attenuated  $\mathcal{E}_{max}$  with scalars of daily  $T_{min}$  and VPD (Equation 9).  $T_{min\_scalar}$  and  $VPD\_scalar$  (Figure 10) are linear ramp functions of daily  $T_{min}$  and VPD and they convert  $T_{min}$  and VPD to scalars ranging from 1 (optimal conditions) to 0 (extremely stressed conditions).  $T_{min}$  is obtained from E-OBS dataset and VPD is calculated for daytime as the difference between saturated vapor pressure (SVP) and actual vapor pressure (AVP) (Equation 16). SVP is estimated with daytime average air temperature (Equation 17). Daytime is determined when hourly downward solar radiation is above zero. AVP is calculated with relative humidity (RH) (Equation 18) (He et al., 2018).

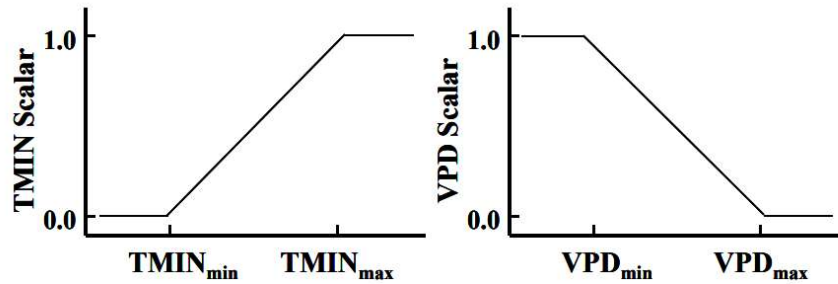


Figure 10: The TMIN and VPD attenuation scalars are simple linear ramp functions of daily TMIN and VPD (Running and Zhao, 2019).

Vapor pressure deficit (VPD) is calculated as follows:

$$VPD = SVP - AVP \quad \text{Equation 16}$$

where:

$$SVP = 6.1078 * \exp((17.269 * T_{daytime}) / (237.3 + T_{daytime})) \quad \text{Equation 17}$$

Daytime is determined when hourly downward solar radiation is above zero. Thus, only temperature for hours when radiation is above 0 is averaged.

Actual vapor pressure (AVP) is based on the following equation:

$$AVP = (RH * SVP) / 100 \quad \text{Equation 18}$$

RH – daily relative humidity obtained from E-OBS database, spatially interpolated for NFI points.

Finally, VPD scalar and  $T_{\min}$  scalar are linear ramp functions of daily VPD and  $T_{\min}$  (Figure 10). The following formulas show how  $T_{\min}$  and VPD scalars are calculated:

$$T_{\min\_scalar} = (T_{\min} - T_{\min\_min}) / (T_{\min\_max} - T_{\min\_min}) \quad \text{Equation 19}$$

$$VPD_{scalar} = 1 - (VPD - VPD_{\min\_min}) / (VPD_{\min\_max} - VPD_{\min\_min}) \quad \text{Equation 20}$$

Daily SWrad is accumulated hourly radiation for each day expressed with units in joules per square meter ( $J m^{-2}$ ) and converted into  $MJ m^{-2}$ .

All climate data ( $T_{\min}$ ,  $T_{\text{mean}}$ , SWrad and relative humidity) are spatially interpolated with the four nearest neighbour technique.

Daily respiration calculation is done in the same way as in MOD17 algorithm, but with high spatial resolution of LAI and BPLUT parameters.

### 3.6. FPAR/LAI estimation

Firstly, FPAR and LAI obtained from S2 (<https://github.com/IVFL-BOKU/sentinel2>) were tested. LAI and FPAR are derived using an Artificial Neural Network (ANN) approach implemented for the ESA S2ToolBox (Weiss and Baret, 2016). The ANN was trained with simulations from the radiative transfer model PROSPECT+SAIL. The model makes some assumptions, particularly regarding canopy architecture, which should be a turbid medium model. The algorithm is ‘generic’ and it should apply to any type of vegetation with reasonable performances. However, the algorithm handbook also advises about the possibility to apply simple correction for specific canopies that do not respond to the main assumption of the model (like forest).

For Sentinel-2 LAI raster cloud masks was applied to S2 LAI raster data in RStudio to eliminate pixels classified as Cirrus, Cloud and Cloud shadow pixels. Next, data was smoothed using the Whittaker smoother (Eilers, 2003) with a Lambda of 1000. Finally, smoothed and gap-filled images were compared with the MODIS LAI for the forest areas in the western part of Slovenia. In Figure 11 the results for the LAI comparison are illustrated and a bias was found in the relationship between the two LAI products, with S2 LAI data (range 1.0 to 2.5 LAI) constantly lower than MODIS LAI data (range 1.0 to 6.0 LAI). We assume that the problem is in the S2 LAI data and correction of this bias would be beneficial.

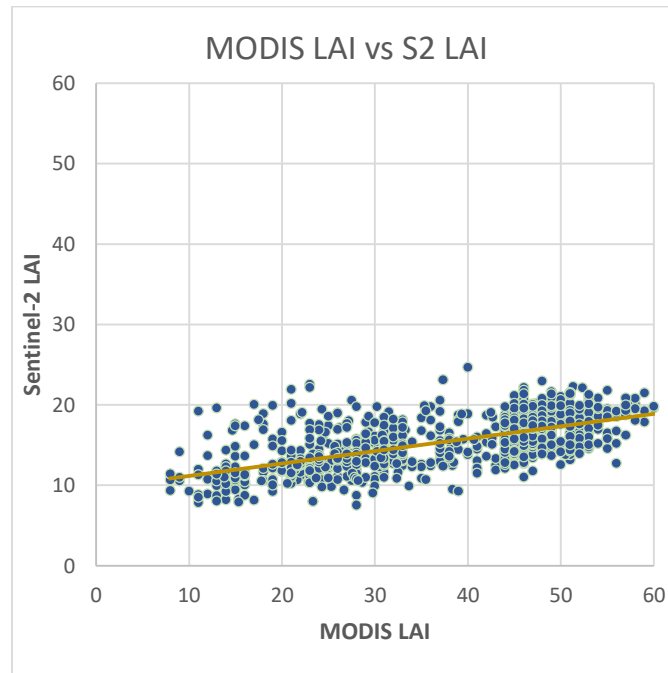


Figure 11: Sentinel-2 LAI vs. MODIS LAI for a large and uniform forest area obtained on 01.05.2019. Scale: 0.1

Nevertheless, knowing that there is still a linear relationship between the two datasets, we applied the modified MOD17 algorithm in which MODIS LAI was replaced with the Sentinel-2 LAI to estimate NPP and the results are presented in Figure 12 and Figure 13.

As respiration calculation is highly sensitive to LAI values and Sentinel-2 (S2) LAI has lower values than MODIS LAI, we expected the S2 NPP being higher. The results of the MOD17 algorithm implemented with the new S2 input parameters (LAI) was compared to the native MOD17 product for a large and uniform forest stands where we can assume that the spatial resolution has a minor impact. The calculation was applied to the entire year 2019 and we obtained a S2 NPP of 1.072 kg C/m<sup>2</sup> (NPP per hectare of 10.72 t C/ha). In comparison, the MOD17 NPP was 0.836 kg C/m<sup>2</sup> (NPP per hectare of 8.36 t C/ha).

Due to the negative bias in LAI, the NPP model using the 10 m spatial resolution S2 LAI gives 28.23% higher NPP than MOD17 NPP model. However, the two algorithms showed a linear relationship, with S2 NPP showing a much greater (spatial) variability and range of values (Figure 12). The next step was to apply a correction for S2 LAI data for the negative bias, probably related to the strong assumptions made in the application of the S2 LAI model.

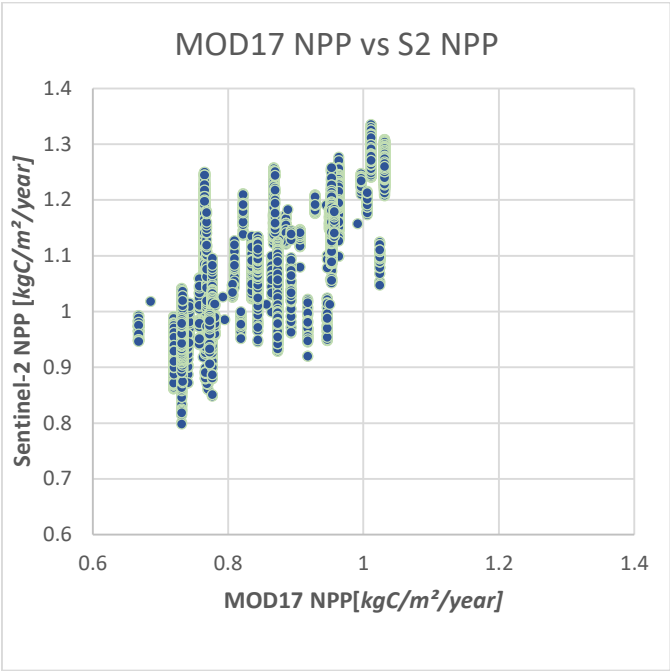


Figure 12: S2-derived NPP vs MODIS MOD17 NPP for a large and uniform forest area for 2019.

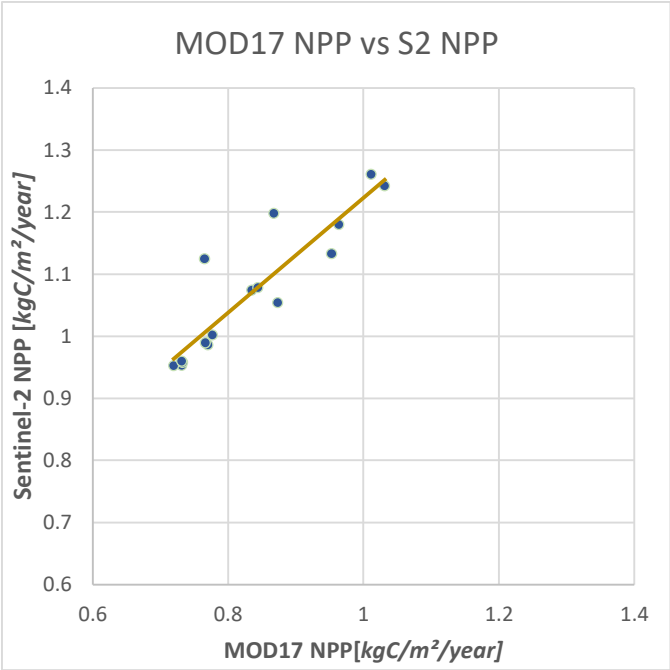


Figure 13: S2-derived NPP vs MODIS MOD17 NPP aggregated at the MODIS spatial resolution (500 m).

Considering the limitation in the Sentinel-2 LAI ANN model data and also to obtain better time series density, the Harmonized Landsat and Sentinel-2 dataset was used for LAI and FPAR estimation that provides better time series density. A simple correlation between the Normalized difference vegetation index (NDVI), which is one of the most used vegetation indices for estimating LAI and FPAR (Potithepa et al., 2010; Tan et al., 2018), was developed to obtain LAI and FPAR.

First, the NDVI is calculated from the HLS reflectance data and then applied to estimate LAI and FPAR. Satellite images for the area of Slovenia for the period of 2016 to 2018 and for the study region in Austria for the period of 2016 to 2020 were downloaded from the HLS dataset (Claverie et al., 2018), an NDVI band was calculated using the equation  $NDVI = \frac{NIR-Red}{NIR+Red}$  with band 8 for Sentinel-2 and band 5 for Landsat as the NIR and band 4 for both satellites as the red band. Cloud mask was applied to eliminate pixels of bad quality. Quality Assessment (QA) layer was used to create a cloud mask for elimination of pixels classified as Cirrus, Cloud and Cloud shadow pixels (Table 2).

Table 2: Description of the bits in the one-byte Quality Assessment layer. Bits are listed from the MSB (bit 7) to the LSB (bit 0)

Bit number	QA description	Bit combination	Description
7-6	Aerosol Quality	00	Climatology
		01	Low
		10	Average
		11	High
5	Water	1	Yes
		0	No
4	Snow/ice	1	Yes
		0	No
3	Cloud shadow	1	Yes
		0	No
2	Adjacent cloud	1	Yes
		0	No
1	Cloud	1	Yes
		0	No
0	Cirrus	1	Yes
		0	No

Whittaker smoother (Eilers, 2003) was used to smooth the NDVI time series for 7-days periods. The lambda value of 800 was set for this function. Total of 53 NDVI images per year were obtained for the study regions.

The FPAR–NDVI and LAI–NDVI relationships were examined to assign the appropriate FPAR and LAI estimation. FPAR and LAI were derived from the MODIS LAI/FPAR product (MOD15A2H Version 6).

Due to the coarse spatial resolution of MODIS (500 m), large and uniform forest stands were selected for analysis of the FPAR–NDVI and LAI–NDVI relationships. To determine which forest stands in Slovenia were appropriate for regression analysis, standard deviation of NDVI was calculated for all the forest stands in Slovenia. Shapefile of Slovenian forest stands is available from the open-source database of The Slovenia Forest Service (Zavod Za Gozdove Slovenije, 2021). Zonal statistic QGIS plugin was used for calculation of standard deviation (SD) of NDVI for each stand. For 22 stands which had the lowest SD of NDVI, in which conifers, broadleaves and mixed stands were equally selected, NDVI was extracted as a weighted arithmetic mean. Then, MODIS FPAR/LAI values were extracted on the same stands as a weighted arithmetic mean. Based on these forest stands, a linear and an exponential relationship (Figure 14) were developed showing a good correlation for both, FPAR and LAI ( $R^2=0.7707$  and  $R^2 = 0.7240$ , respectively).

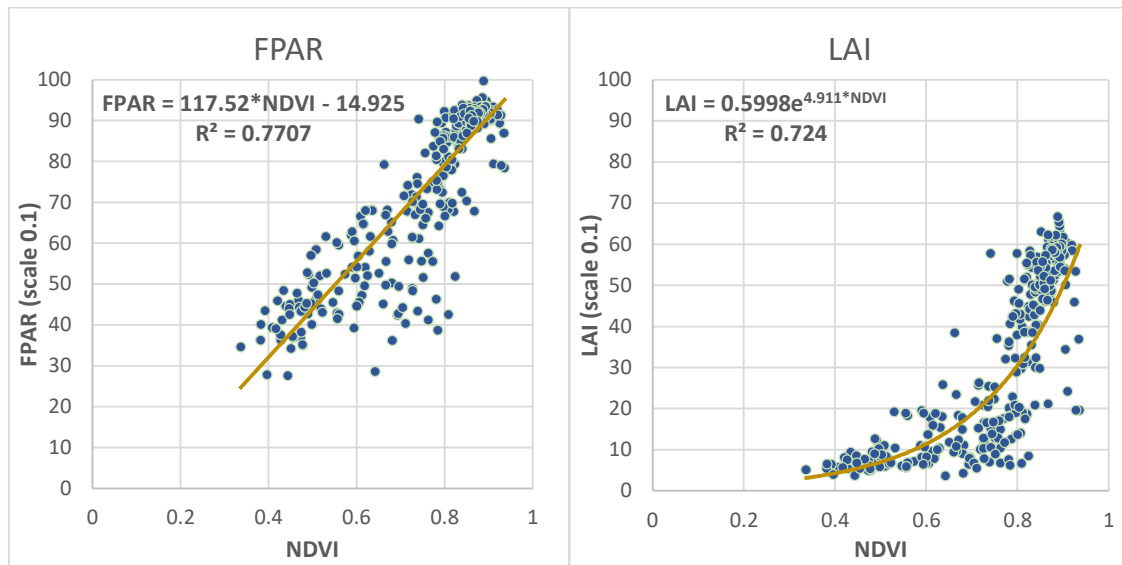


Figure 14: Regression of mean FPAR/LAI (MODIS) as a function of mean NDVI (HLS) for uniform forest stands. FPAR is logarithmic function, LAI is exponential function.

$$\text{FPAR} = (117.52 * \text{NDVI}) - 14.925 \quad \text{Equation 21}$$

$$\text{LAI} = 0.5998 * (e^{(4.911 * \text{NDVI})}) \quad \text{Equation 22}$$

Next, for estimation of FPAR and LAI for the NFI plots, NDVI annual stack raster data were cropped on 564, 1.4 km by 1.4 km polygons in Slovenia. 30 m cells were disaggregated to 10 m to fit with LC spatial resolution. Finally, regression formulas (Equation 21 and Equation 22) were used for estimation of 10 m spatial resolution FPAR and LAI for pixels classified as forest in the selected polygons.

### 3.7. HLS NPP estimation

New high-resolution inputs (FPAR, LAI,  $T_{\text{mean}}$ ,  $T_{\text{min}}$ , SWrad, VPD) replaced MOD17 inputs, and the model described in the chapter 3.1 was run. The 10 m spatial resolution NPP was estimated for the entire study area in the southern part of Austria (3295 km<sup>2</sup>) and for 564 NFI polygons of 1.96 km<sup>2</sup> area in Slovenia. Adapted 10 m spatial resolution model is referred to as HLS NPP in the following text.

For evaluation of the NPP and comparison with the NFI data in Slovenia and with the MOD17 NPP, two sets of data were extracted from the obtained NPP rasters from the modelled polygons. Firstly, aggregated weighted mean HLS NPP and MOD17 NPP were extracted for forest stands located within polygons selected for NPP estimation and then compared to each other. 1362 forest stands are located within these polygons, on NFI points or intersecting 70 m buffer zone around each NFI point (Figure 15). Then, to test the correlation between the HLS NPP and NFI data (timber increment), NPP was extracted as an annual mean value of a raster at the coordinates of the FECS plots. FECS plots are circular with the size of 500 m<sup>2</sup>. Therefore, to cover all the pixels which represent these plots weighted average extraction of pixels values from 30 m buffer zones (707 m<sup>2</sup>) was performed.

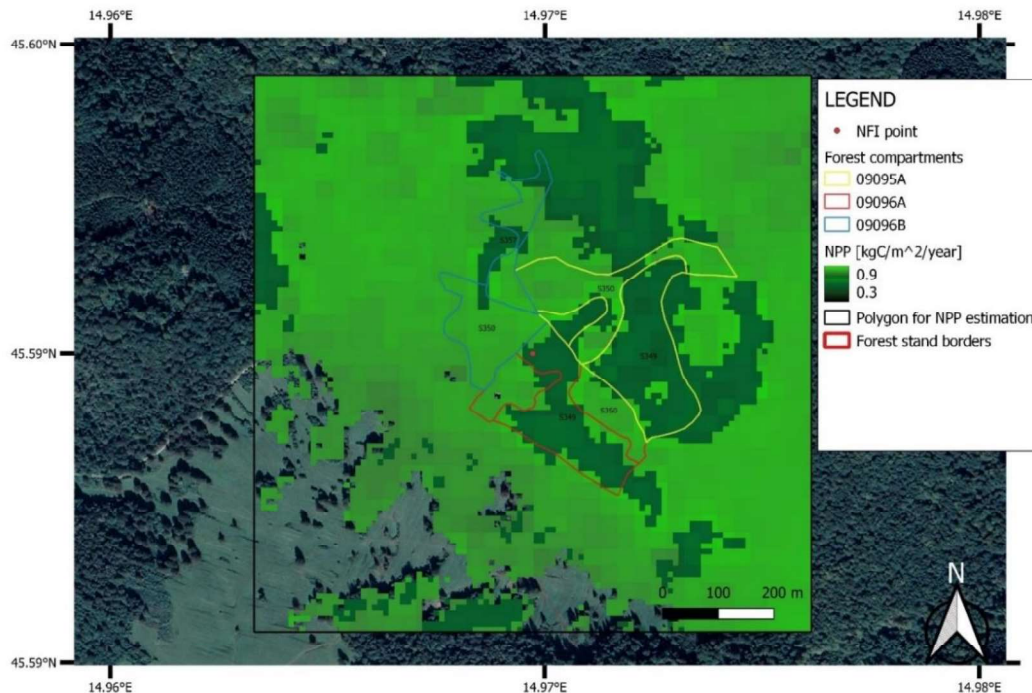


Figure 15: Example of one polygon for NPP estimation. Square polygon is a shapefile in which the NPP is calculated. Mean annual NPP was extracted for the forest stands which are located within this polygon (09095A, 09096A and 09096B). Pixels represent NPP values [kgC/m<sup>2</sup>/year]. The background RGB image was obtained from “Map data ©2021 Google”.

For the area in the southern part of Austria, the same model was run for the entire forest area of 3295 km<sup>2</sup> in 5 selected districts. The exact coordinates of the plots where tree core samples

were obtained were unknown (due to data policy). Therefore, the final rasters showing the annual NPP values for 4 years were delivered to BFW to do the extraction of the NPP values at the locations of the plots. After the NPP extraction, BFW also provided a dataset of the annual growth ring size, which is compared to the NPP dataset for the same plots.

## 4. Results

First, sensitivity analysis of NPP to model parameters was performed to quantify the impact and importance of individual input parameters. Then, for the study area in Slovenia, relationship between the HLS NPP and periodic annual volume increment (PAI) obtained from NFI data was studied. For the study area in Austria, relationship between the HLS NPP and the annual growth ring size was tested. Finally, HLS NPP was compared to the NPP derived from MODIS dataset.

### 4.1. Model parameters – sensitivity analysis

Correlation between the model parameters and the annual increment, as well as model sensitivity to various parameters were analysed. GPP and respiration were calculated daily and NPP on an annual basis. However, during the vegetation period values of GPP and respiration are much higher than in winter (Figure 16). Therefore, mean parameter values between 1st May and 31st August were considered for correlation analysis. This period, which is one third of a year, had 60% share in annual GPP and 66% in annual respiration value. This period had also high standard deviation (SD) for daily GPP between the plots. SD of daily GPP for period from 1st May to 31st August was 0.001295, which was twice as high as SD for the period before and after these dates (0.000654).

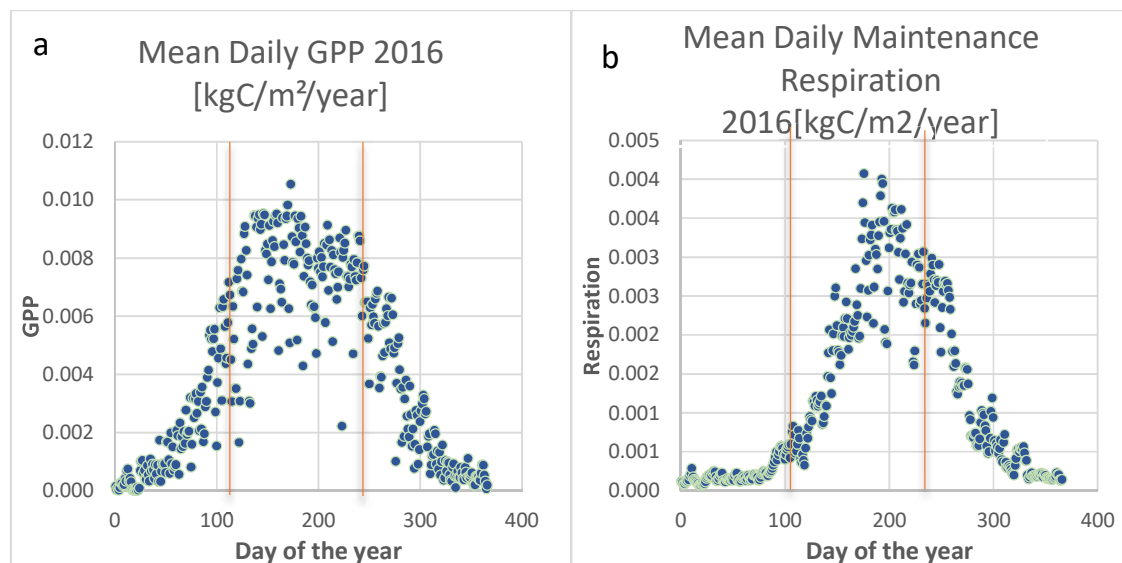


Figure 16: Daily GPP (a) and respiration (b) values. Orange vertical lines represent beginning and end of a period in which share of GPP and respiration is the highest, and for which mean parameter values are analysed.

All the inputs into the model could be divided into 3 main categories: Biome specific parameters, climate data and satellite data. Various parameters are products of more than one dataset. Hence, for sensitivity analysis parameters are categorized into 6 different groups:

- Biome specific parameters (BPLUT)
  - BPLUT and satellite parameters (Leaf mass, Annual leaf mass max)
  - BPLUT and climate (Leaf maintenance respiration)

- BPLUT and climate (Radiation use efficiency coefficient  $\epsilon$ )
- Climate parameters ( $T_{\min}$ ,  $SW_{\text{rad}}$ ,  $T_{\text{mean}}$ )
- Satellite parameters (FPAR, LAI)
  - Satellite and climate parameters (APAR)

Relationship between the periodic annual increment for NFI plots in Slovenia and individual parameters used in HLS NPP algorithm was tested to determine if there are model parameters which can individually represent spatial variability of timber growth. Model parameters did not show significant correlation with the NFI data. Only satellite derived data (FPAR and LAI) showed weak correlation with the periodic annual increment (PAI) with the highest  $R^2$  for 2018 (0.16 and 0.17,  $p < 0.01$  for FPAR and LAI, respectively) (Figure 17). Very weak relationship between the PAI and  $\epsilon$  ( $R^2 = 0.09$ ,  $p < 0.01$ ) was also detected.

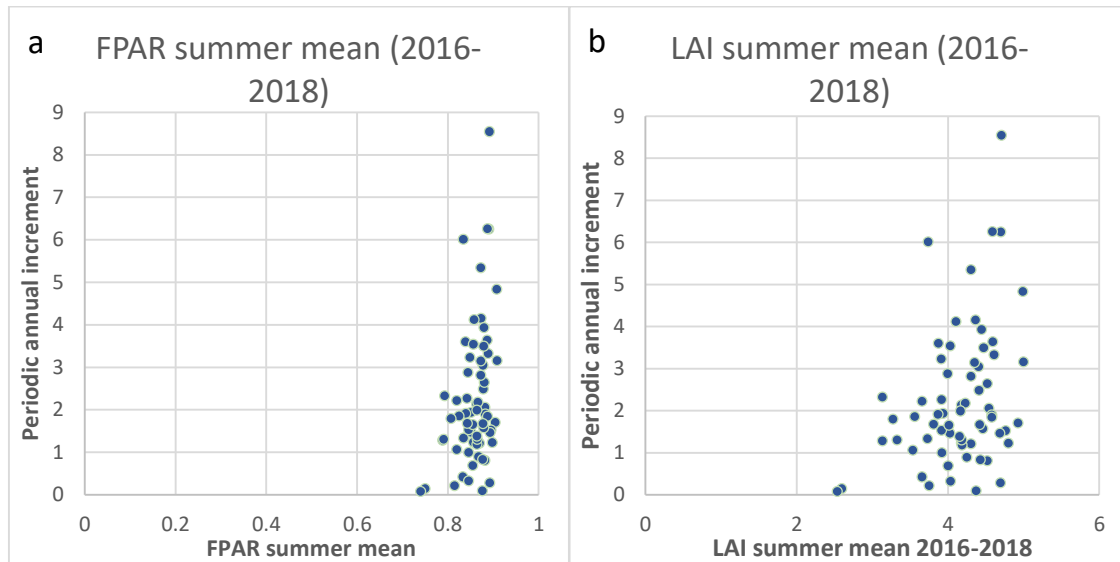


Figure 17: Correlation between FPAR(a)/LAI(b) and PAI (NFI data). Mean LAI/FPAR values between 1st May and 31st August are considered for correlation analysis.

Sensitivity analysis shows how individual model parameters affect the annual NPP. Sensitivity analysis is usually performed to examine which parameters have the largest impact on the model output (Matsushita et al., 2004). Individual parameters were increased and decreased by 1% to 25% from the current value and effects of these changes on the model output (annual NPP) were examined.

To quantify the impact of various parameters, two points located in coniferous and deciduous forest were selected and the HLS NPP algorithm was run with data representing these two points. Next, individual model parameter values were varied in a range of -25% to 25% and the modified NPP values were obtained. Then, change of NPP values were presented in percentage change relative to the original NPP values. Finally, percentage of change of individual model parameters was displayed on a horizontal axis while percentage of change of NPP values was shown on a vertical axis (Figure 18 and Figure 19).

The biggest error can be caused by wrong LC classification because all BPLUT parameters are completely based on LC class of a pixel. BPLUT parameters are also used for calculation of scalars of daily  $T_{\min}$  and VPD. Wrong LC classification leads to 25-33% error of NPP.

For sensitivity analysis, pixel representing coniferous LC (Figure 18) and pixel representing deciduous LC class (Figure 19) were chosen for analysis. Biggest impact on NPP change have changes of parameters used to calculate GPP (FPAR, Radiation use efficiency and shortwave radiation). These three parameters have all the same impact on the final NPP. NPP is increasing linearly with the increase of one of these three parameters. For example, change of radiation use efficiency ( $\epsilon$ ) of 15% results in a change of annual NPP of 21% for deciduous ( $NPP = 542g/m^2$ ) and 25% for coniferous forest type ( $NPP = 725g/m^2$ ). As for meteorological parameters, NPP is less sensitive to change in temperature than to change in radiation. Minimum daily temperature ( $T_{min}$ ) is a parameter used to calculate GPP while average daily temperature ( $T_{avg}$ ) is used to calculate respiration. Therefore, individual increase of  $T_{min}$  of 10% increases NPP by 2.7% on average, while increase of  $T_{avg}$  of 10% leads to a decrease of NPP by 4.8% and 8.3% for deciduous and conifers, respectively. LAI is part of the algorithm which estimates respiration. Hence, increase of LAI leads to decrease of NPP.

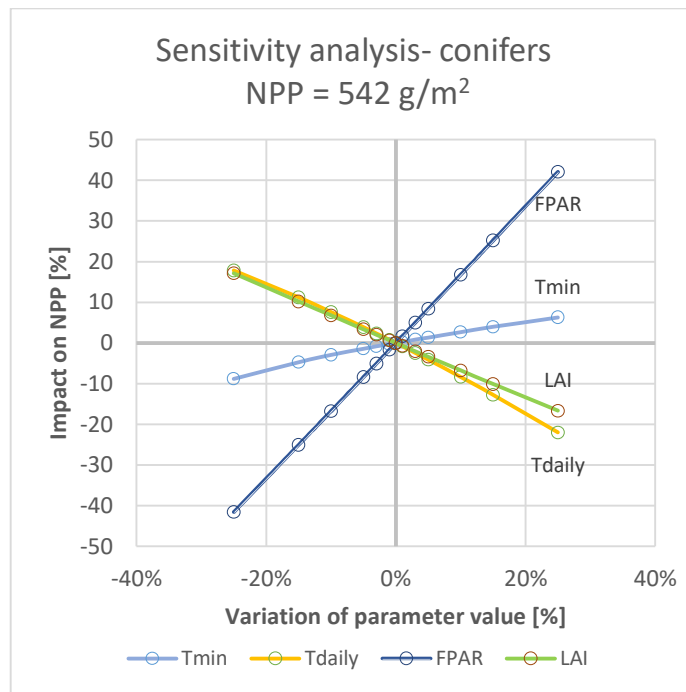


Figure 18: Sensitivity analysis of annual NPP to model parameters for conifers. Impact of change of parameters values in a range -25% to 25% on a change of NPP were calculated. Sensitivity of NPP to SWrad and  $\epsilon$  is the same as to FPAR. Therefore, FPAR is the only shown on the graphs.

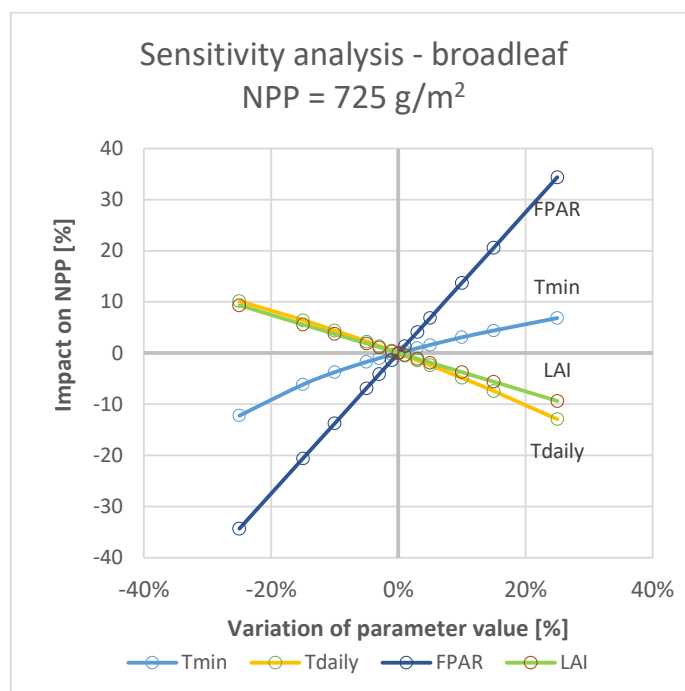


Figure 19: Sensitivity analysis of annual NPP to model parameters for broadleaf. Impact of change of parameters values in a range -25% to 25% on a change of NPP were calculated. Sensitivity of NPP to SWrad and  $\epsilon$  is the same as to FPAR. Therefore, FPAR is the only shown on the graphs.

## 4.2. Slovenia

Mean NPP for the years 2016, 2017 and 2018 obtained with HLS satellite dataset and European climate dataset for 71 NFI plot is 651.6 gC/m<sup>2</sup>/year (Table 3). Periodic annual increment for the period 2012 – 2018 is 7.6 m<sup>3</sup>/ha. NFI data showed much higher variation in PAI values than NPP with relative standard deviation of 70.7%. HLS NPP model estimated all the NPP values in a range 516.7 to 798 gC/m<sup>2</sup>/year with the relative standard deviation of 10.4%.

Table 3: Mean values of NPP estimation and forest inventory data. Relative standard deviation is used to show the difference of two sets of data with different units (gC/m<sup>2</sup>/year and m<sup>3</sup>/ha).

	Mean	Range	Relative standard deviation [%]
HLS NPP [gC/m <sup>2</sup> /year]	651.6	516.7 – 798.0	10.4
Periodic annual increment [m <sup>3</sup> /ha]	7.6	0.28 – 28.5	70.6
Timber volume 2012 [500 m <sup>2</sup> plot]	17.39	0.13 – 39.8	52.6
Timber volume 2018 [500 m <sup>2</sup> plot]	19.67	0.20 – 41.50	50.4

Relationship between the estimated 10 m spatial resolution HLS NPP and periodic annual increment of volume (PAI) of the NFI plots was analysed. With the assumption that the current annual increment (CAI) from 2012 to 2018 was consistent, correlation analysis between the PAI for this period and the mean NPP for the period 2016-2018 was conducted. For sampled

plots in Slovenian NFI, PAI represents timber annual increment of sampled trees which have diameter larger than 10 cm at height of 1.3 meters. NPP represents total carbon uptake by all vegetation, including below-ground production. Connection between the NPP and PAI was tested.

NFI plots (500 m<sup>2</sup>) on which harvesting or mortality between the two sampling periods were not detected were reliable for correlation analysis between the modelled NPP and periodic annual increment of timber volume. For 71 plots which met this criteria, 3-year annual average NPP (2016-2018) was not correlated to 6-years periodic annual increment (PAI) (2012-2018) (Figure 20).

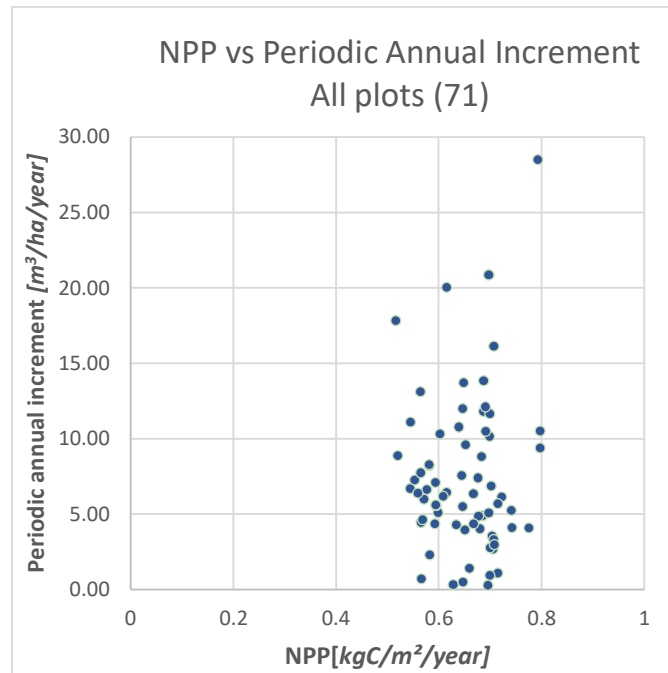


Figure 20: 6-years periodic annual increment (2012-2018) vs. 3-years annual average NPP (2016-2018).

After removing plots of low timber density and low timber volume (less than 18 m<sup>2</sup> in 2018) from analysis and keeping 60% of the plots with the highest timber volume, we obtained an R<sup>2</sup> of 0.1 (Figure 21).

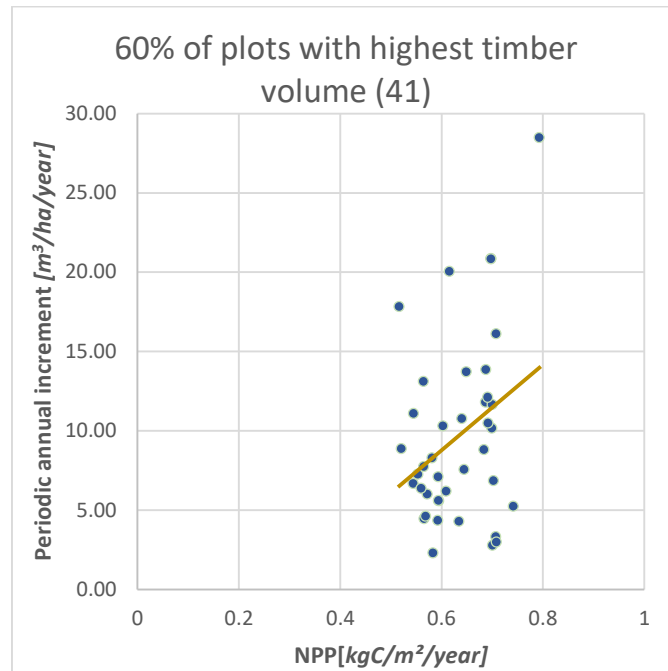


Figure 21: 6-years periodic annual increment (2012-2018) and 3-years annual average NPP (2016-2018) of 60% of the plots with highest timber volume.

Linear regression model showed weak correlation between the NPP and PAI for the plots which had average and above average timber volume. NFI plots which had very low timber volume in 2012 and 2018 NFI and low PAI, had average or above average NPP estimations. Figure 22a, Figure 22b and Figure 22c show examples of the plots which had only 1 - 2 trees for sampling (dbh larger than 10 cm) and therefore, have low PAI (0.08 – 0.22 m<sup>3</sup>/ha/year) compared to the mean PAI of 7.6 m<sup>3</sup>/ha/year. On the contrary, plots representing fully stocked forest shown on the Figure 22d, Figure 22e and Figure 22f had 14 - 19 trees for sampling. PAI on these plots was in a range 11.1 - 13.7 m<sup>3</sup>/ha/year. NPP for all the plots in the Figure 22 was in a range 550 to 700 and not correlated to PAI which suggests that NPP is not correlated to increment in stands with extreme low density and timber increment.

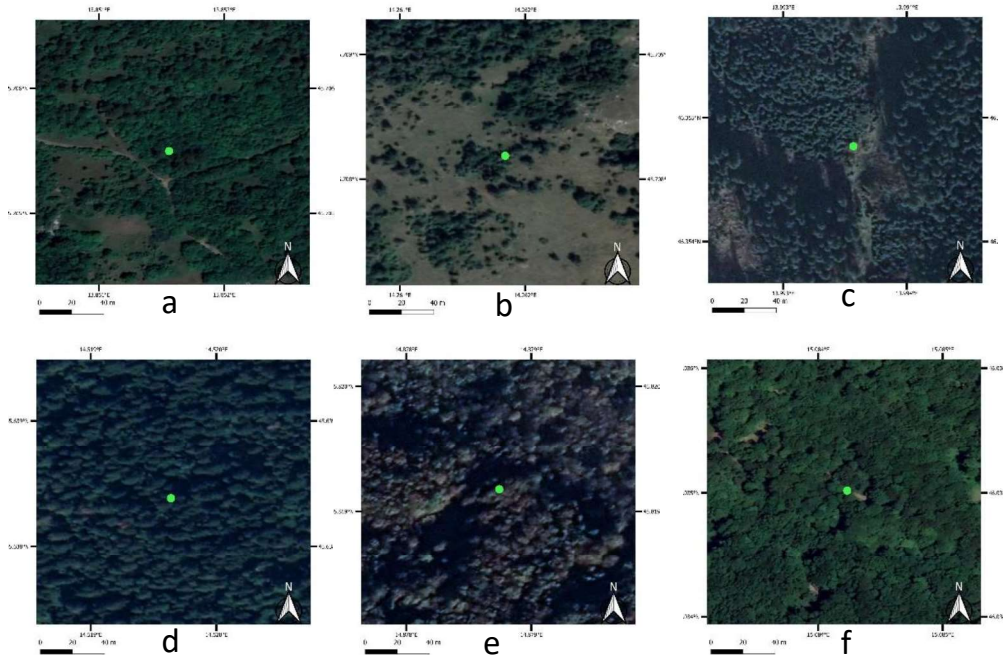


Figure 22: Examples of NFI plots with low stem density (a,b,c) and high stem density (d,e,f). The green point is the centre of a plot. Plots a, b and c have low PAI. Plots d, e and f have above average PAI. The background RGB imagery is obtained from “Map data ©2021 Google”.

### 4.3. Austria

NPP was estimated for the period 2016 - 2020 obtained with HLS satellite dataset and European climate dataset for five districts in the southern part of Austria for the 3295.6 km<sup>2</sup> area classified as a forest according to the LC map from Malinowski et al. (2020). Mean annual NPP for this area is 555.5 gC/m<sup>2</sup>/year. Table 4 gives the HLS NPP values for all the five districts for the analysed period. Figure 23 shows the variation of aggregated mean NPP for all the districts through the years. Estimated NPP showed an increase from 2016 peaking in 2018 for the entire study area, dropping in 2019 and high variety between the districts in 2020.

Table 4: HLS NPP for each region separately and for each year.

<b>District</b>	2016	2017	2018	2019	2020	Mean
Sankt Veit an der Glan	565.1	589.0	616.4	551.8	570.0	578.5
Spittal an der Drau	533.5	536.5	587.8	536.5	521.2	543.1
Feldkirchen	568.3	581.9	609.6	544.4	560.2	572.9
Tamsweg	500.5	517.4	571.7	533.1	508.0	526.1
Murau	533.9	556.7	601.6	549.2	542.8	556.8
<b>Mean NPP</b>	540.3	556.3	597.5	543.0	540.4	<b>555.5</b>

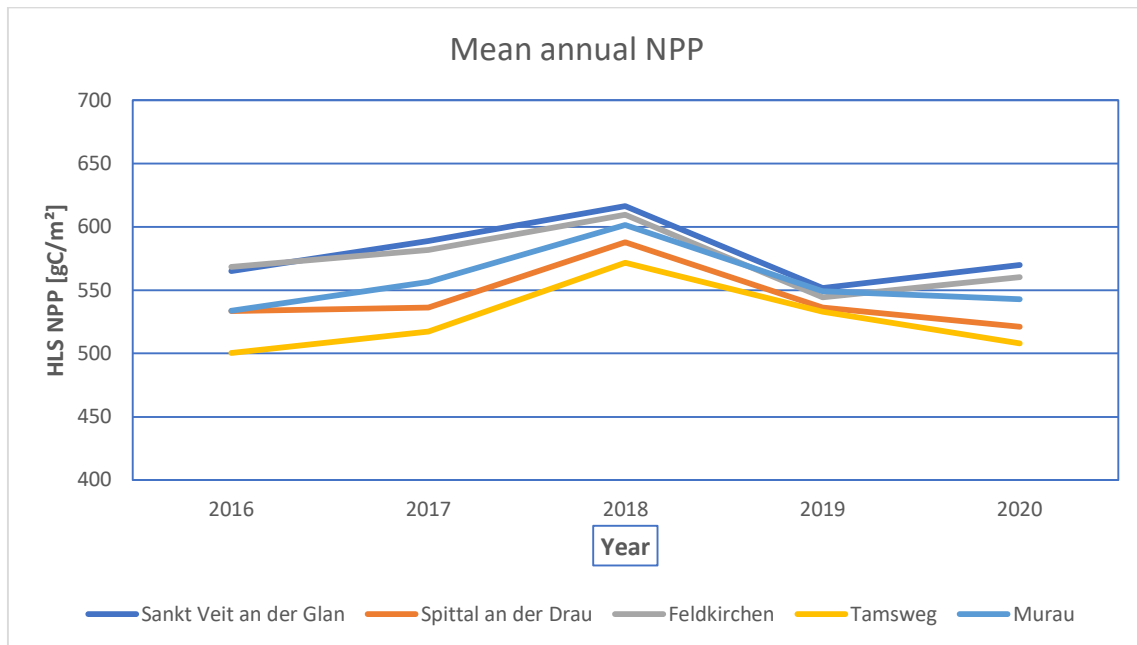


Figure 23: Annual HLS NPP for the period 2016-2020 for the 5 districts in the southern part of Austria.

For the study area in Austria connection between the annual NPP (net primary production) and annual growth ring size obtained from sampled cores was tested. Annual NPP is extracted from plot locations and a connection between the NPP and growth ring size obtained from sampled cores was analysed. Firstly, available data were plotted with one colour and symbol for each year (Figure 24).

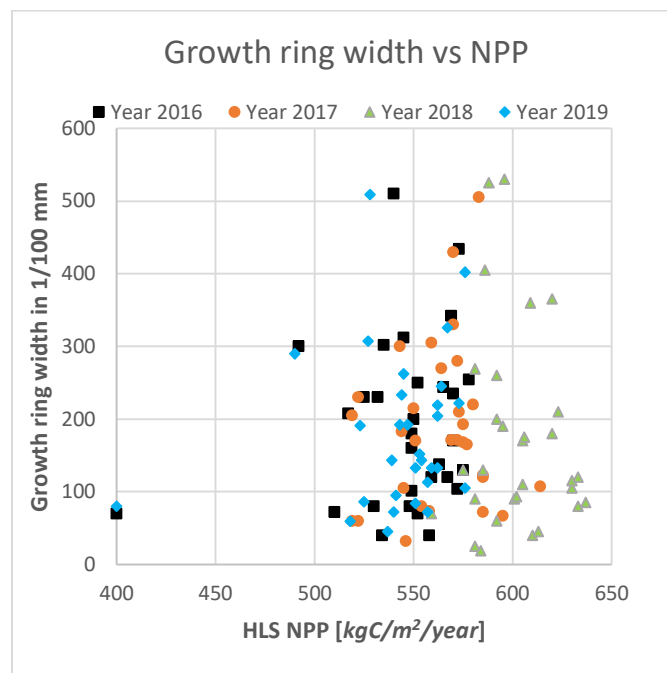


Figure 24: Growth ring width (1/100 mm) versus NPP

It is apparent that there is no clear dependency. The overall correlation is 0.07 and for the individual years it never exceeds 0.1, if the two outliers with NPP < 0.45 are omitted.

The same was carried out for the changes between the years (Figure 25). The highest found correlation is between the changes of the NPP and the changes of the year ring width from the year 2016 to 2017, again with the two outliers removed. However, it is only 0.26 (meaning that a linear model would have an  $R^2$  of only 0.07) and it is obvious from the second figure that there is no discernible trend.

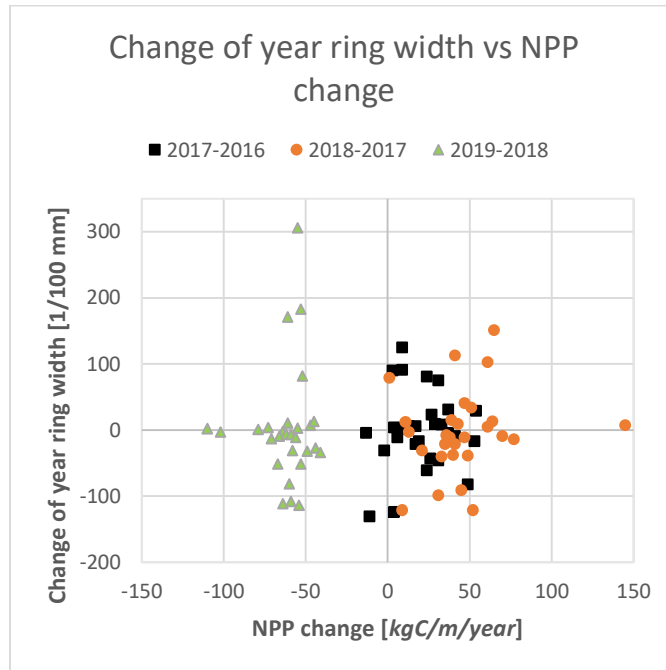


Figure 25: Change of year ring width versus NPP-change

Finally, boxplots for different years for NPP and growth ring width are presented (Figure 26) showing that estimated NPP has significant differences between the years while the sizes of the growth rings are very similar between the years.

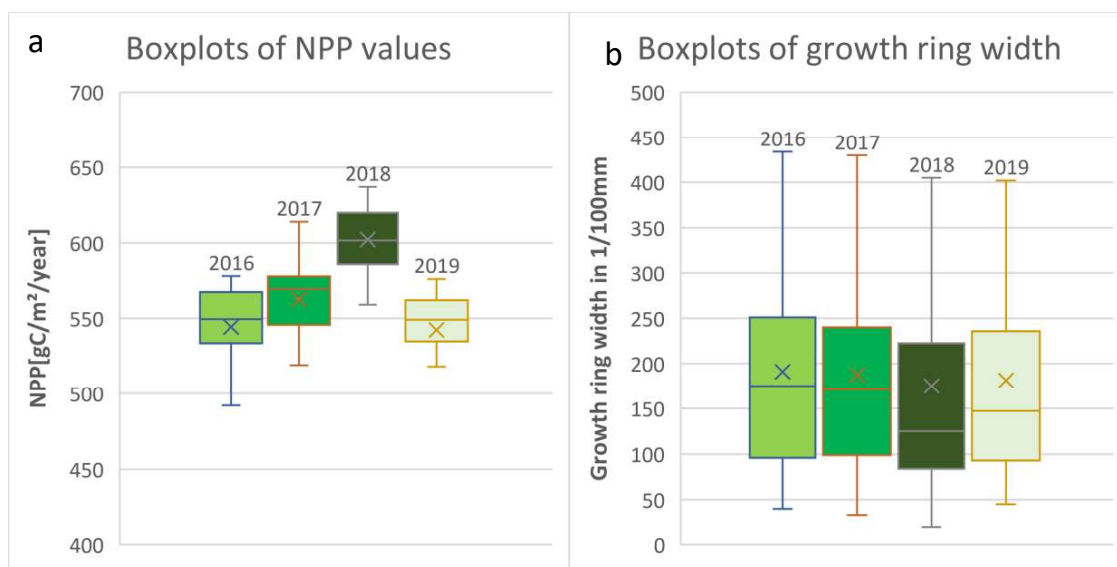


Figure 26: Boxplots of NPP (2016-2019) (a) and growth ring width (2016-2019) (b).

#### 4.4. HLS NPP and MODIS NPP comparison

NPP derived from MODIS dataset was compared to the NPP estimated with high spatial resolution inputs (HLS NPP) for the location of NFI plots in Slovenia. Firstly, both NPP datasets were compared for forest stands located in the polygons selected for the NPP analysis.

1362 forest stands for which NPP is estimated are located on 546 NFI points or intersecting 70 m buffer zone around each NFI point. NPP is estimated for years 2016, 2017 and 2018 (Table 5 Table 6 Table 7). NPP is expressed as a mean value in grams of carbon per square meter per year. HLS NPP has 17.93% lower net primary production than MOD17 NPP for year 2016, 14.47% for 2017 and 9.27% for 2018.

Table 5: Statistics for two modelled NPP for forest stands 2016. NPP [gC/m²/year]. RSD – relative standard deviation [%].

	HLS NPP [gC/m²/year]	MOD17 NPP [gC/m²/year]	Difference
Mean	659.3	803.3	144.1
Median	658.5	784.5	126.0
Standard deviation	76.1	90.4	
RSD [%]	11.5	11.3	

Table 6: Statistics for two modelled NPP for forest stands 2017. NPP [gC/m²/year]. RSD – relative standard deviation [%].

	HLS NPP [gC/m²/year]	MOD17 NPP [gC/m²/year]	Difference
Mean	633.1	740.2	107.1
Median	621.5	722.6	101.2
Standard deviation	64.6	97.6	
RSD [%]	10.2	13.2	

Table 7: Statistics for two modelled NPP for forest stands 2018. NPP [gC/m<sup>2</sup>/year]. RSD – relative standard deviation [%].

	<b>HLS NPP</b> [gC/m <sup>2</sup> /year]	<b>MOD17 NPP</b> [gC/m <sup>2</sup> /year]	<b>Difference</b>
Mean	707.1	779.3	72.2
Median	723.7	764.4	40.7
Standard deviation	79.1	92.1	
RSD [%]	11.2	11.8	

On average, NPP estimated with high spatial resolution inputs (HLS NPP) for years 2016, 2017 and 2018 is 13.02% (107.81 gC/m<sup>2</sup>/year) lower than MOD17 NPP (Table 8). Mean HLS NPP for years 2016, 2017 and 2018 for 1362 forest stands in Slovenia is 666.5 gC/m<sup>2</sup>/year (standard deviation 79.7 gC/m<sup>2</sup> /year). Final spatial resolution is 10m (HLS dataset spatial resolution is 30m, spatial resolution of S2GLC land cover and BPLUT values derived from LC is 10m and climate dataset has spatial resolution of 0.1°, which is spatially interpolated for every plot with the nearest neighbour interpolation). Mean MOD17 NPP for the same forest stands for the same period is 774.3 gC/m<sup>2</sup>/year (standard deviation 97.0 gC/m<sup>2</sup> /year). MOD17 NPP has spatial resolution of 500 m on average. For each forest stand, NPP is extracted as a weighted arithmetic mean.

Table 8: Statistics for two modelled NPP for forest stands for 2016-2018. NPP [gC/m<sup>2</sup>/year]

	<b>HLS NPP</b> [gC/m <sup>2</sup> /year]	<b>MOD17 NPP</b> [gC/m <sup>2</sup> /year]	<b>Difference</b>
2016	659.3	803.3	144.1
2017	633.1	740.2	107.1
2018	707.1	779.3	72.21
Average	666.5	774.3	107.8

For almost all forest stands, HLS NPP values are lower than MOD17 NPP (Figure 27), but there is no correlation between the two variables (Figure 28).

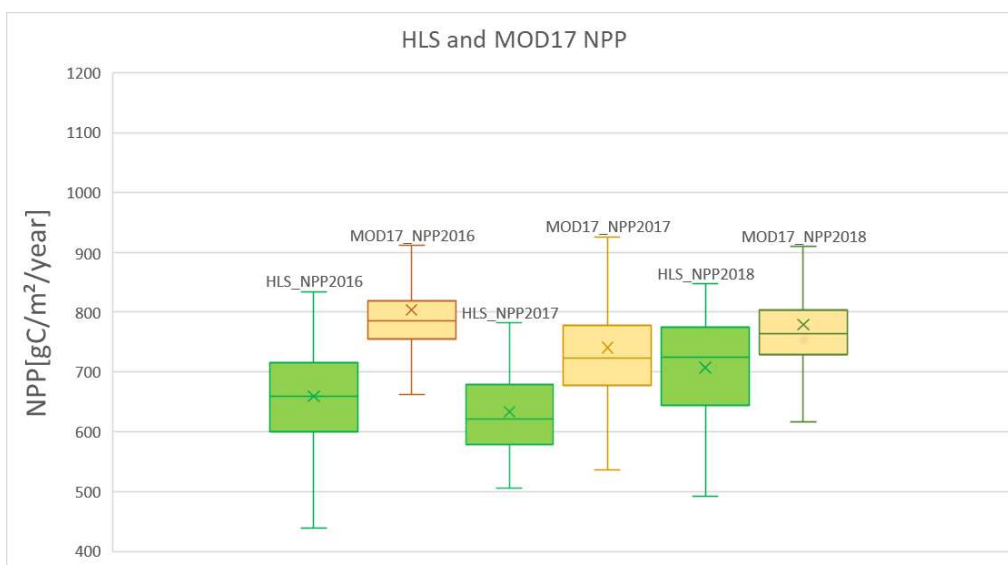


Figure 27: Comparison of HLS NPP and MOD17 NPP for forest stands in Slovenia: The boxes represent the median and the 25th and 75th percentile, the symbol x represents the arithmetic mean.

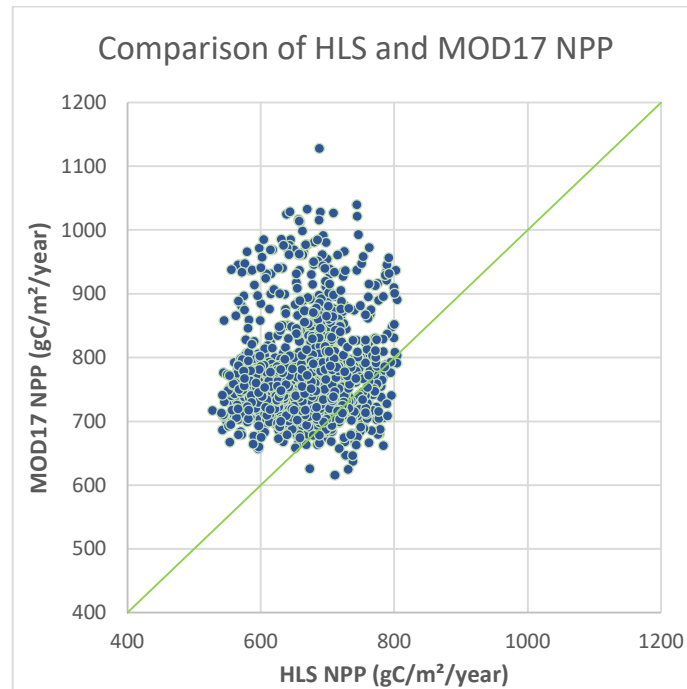


Figure 28: Scatter plot which shows the correlation between HLS NPP and MOD17 NPP. Solid line is identity line.

To avoid the effect of irregular shape of forest stands, which leads to disparity in spatial resolution with 500 m resolution MOD17 NPP, homogeneous and square-shaped forest polygons were selected to compare the NPP from the two datasets. For 50 polygons of 1 km<sup>2</sup> area covering homogeneous forest areas (29 broadleaves and 21 conifers) annual mean MOD17 NPP and HLS NPP were aggregated.

For the years 2016 and 2018 MOD17 NPP and HLS NPP datasets showed linear correlation with an  $R^2$  of 0.19 and 0.22, respectively (Figure 29a). There was no correlation for the year 2017. There was also a difference between the correlation for coniferous and broadleaf forests. For the year 2018 MOD17 NPP and HLS NPP had stronger correlation for coniferous forest type ( $R^2=0.37$ ) in comparison to broadleaf forest type ( $R^2=0.14$ ) while broadleaf forests also had a larger range of NPP values for both datasets (Figure 29).

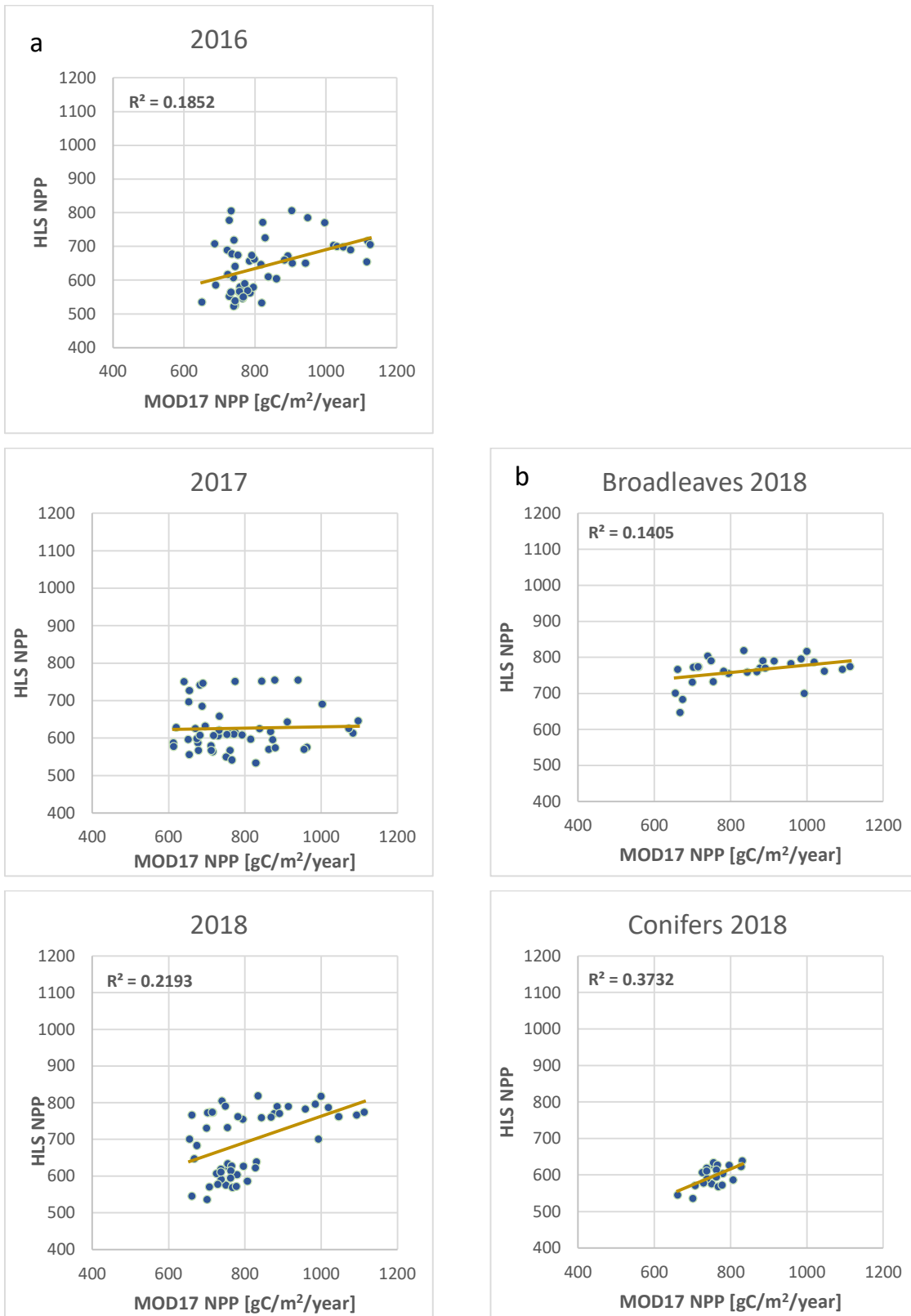


Figure 29: (a) Correlation between HLS NPP and MOD17 NPP for homogeneous 1 km<sup>2</sup> forest polygons of all forest types and (b) for coniferous and broadleaf forests separately in the year 2018

Mean NPP for the years 2016, 2017 and 2018 obtained with HLS satellite dataset and European climate data set for 50 forest polygons of 1 km<sup>2</sup> is 653.9 gC/m<sup>2</sup>/year (mean standard deviation is 89.3 gC/m<sup>2</sup> /year) (Table 9). Mean MOD17 NPP for the same polygons and for the same period is 804.0 gC/m<sup>2</sup>/year (standard deviation is 116.8 gC/m<sup>2</sup> /year). For each polygon NPP was extracted as a weighted arithmetic mean. HLS NPP values are lower than MOD17 NPP for all the years (Figure 30). On average, NPP estimated with high spatial resolution inputs for years 2016, 2017 and 2018 is 18.67% (150.1 gC/m<sup>2</sup>/year) lower than MOD17 NPP.

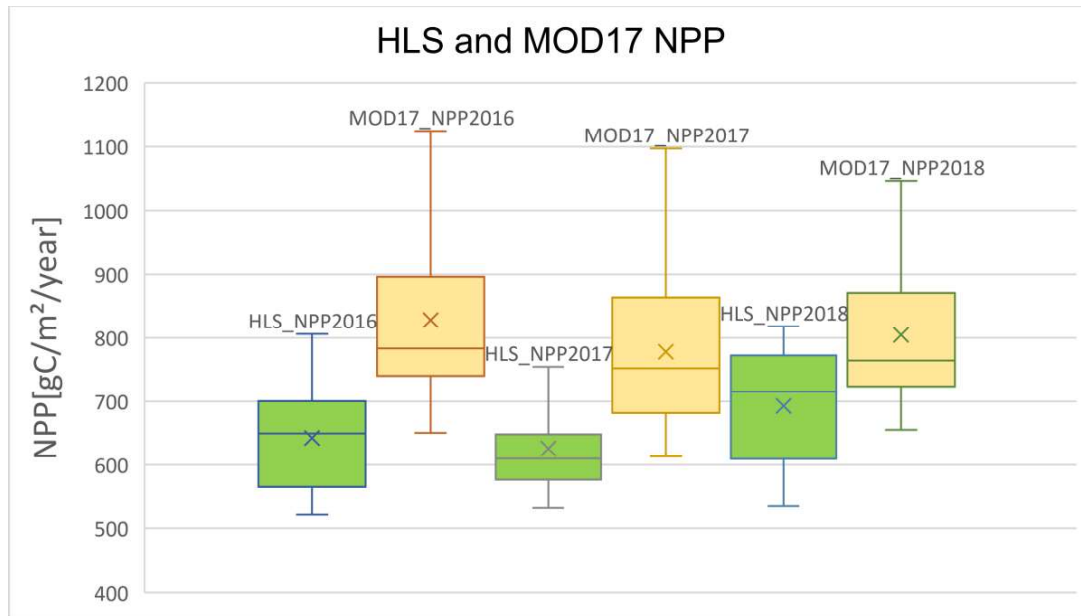


Figure 30: Comparison of HLS NPP and MOD17 NPP for homogeneous 1 km<sup>2</sup> forest polygons in Slovenia: The boxes represent the median and the 25th and 75th percentile, the symbol x represents the arithmetic mean.

Table 9: Statistics for two modelled NPP for 1 km<sup>2</sup> homogeneous polygons for 2016-2018. NPP [gC/m<sup>2</sup>/year]

	<b>HLS NPP</b> [gC/m <sup>2</sup> /year]	<b>MOD17 NPP</b> [gC/m <sup>2</sup> /year]	<b>Difference</b>
2016	642.8	828.6	185.8
2017	626.0	778.6	152.6
2018	692.9	804.7	111.9
Average	653.9	804.0	150.1

Comparison between the NPP estimations for coniferous and broadleaf forest types was calculated for the year 2018 (Table 10). Mean HLS NPP for broadleaf forests (762.1 gC/m<sup>2</sup>/year) was larger than for coniferous forests (597.2 gC/m<sup>2</sup>/year). The trend was the same for MOD17 NPP with 839.7 gC/m<sup>2</sup>/year for broadleaves forest type compared to 756.3 gC/m<sup>2</sup>/year for conifers. NPP values for broadleaves had larger standard deviation for both datasets with a lot larger variability for MOD17 NPP estimations. MOD17 NPP had standard deviation of 140.2 gC/m<sup>2</sup>/year (RSD = 16.7%) compared to 38.9 gC/m<sup>2</sup>/year for HLS NPP (RSD = 5.1%).

Table 10: Statistics for two modelled NPP for 1 km<sup>2</sup> homogeneous polygons for 2018. Data for conifers and broadleaves are given separately. NPP [gC/m<sup>2</sup>/year]. RSD – relative standard deviation [%].

	HLS NPP [gC/m <sup>2</sup> /year]	MOD17 NPP [gC/m <sup>2</sup> /year]	Difference
Broadleaves	762.1	839.7	159.1
Conifers	597.2	756.3	77.6
Average (total)	692.8	804.7	111.9
RSD Broadleaves [%]	5.1	16.7	
RSD Conifers [%]	4.9	5.4	

For the polygons in the study area in Slovenia, distribution of NPP values for the two datasets were compared in a histogram (Figure 31). Majority of the pixels for the selected polygons in the HLS NPP dataset have NPP values in a range of 500 - 850 kgC/m<sup>2</sup>/year. MOD17 dataset gives most of the pixel values in a range of 600 - 850 kgC/m<sup>2</sup>/year. For the HLS NPP dataset, pixels classified as conifers have clearly lower values than pixels representing broadleaf forest type.

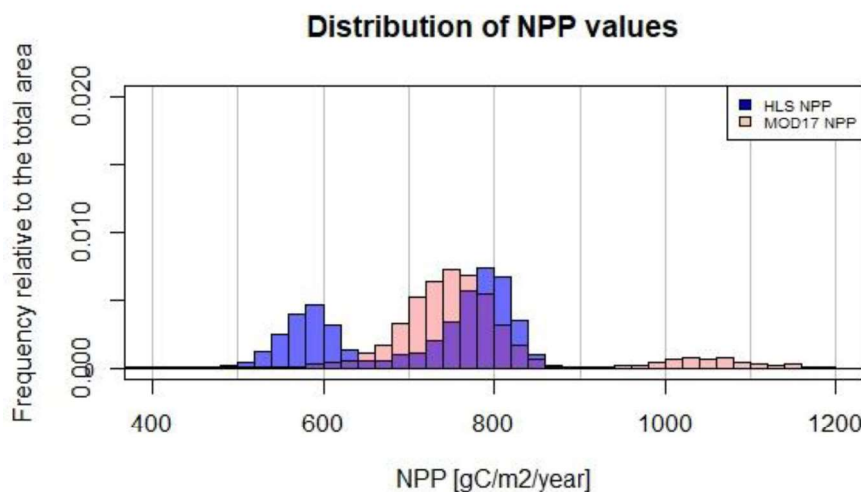


Figure 31: Distribution of aggregated NPP values for HLS NPP and MOD17 NPP products for the period 2016-2018 for the study areas in Slovenia. Two datasets differ in size and spatial resolution. Vertical axis shows frequency of the two NPP datasets relative to the total forest area of the analysed polygons. HLS NPP values for conifers and broadleaves have two peaks in distribution showing bimodal distribution.

For the region in the southern part of Austria, 10 m resolution HLS NPP was compared to 500 m resolution MOD17 NPP. Dominant land cover type for the study area in the southern part of Austria is coniferous tree cover (more than 90% of forest area).

To avoid the impact of non-forest areas within 500 m MODIS pixels and mismatch in scale of the two datasets, 64 polygons of 1 km<sup>2</sup> area covering homogeneous forest areas were selected for NPP comparison. For each polygon and for each year mean NPP was aggregated.

For every year MOD17 NPP and HLS NPP datasets showed linear correlation (32). 2018 has the lowest correlation ( $R^2=0.32$ ), while 2020 has an  $R^2$  of 0.54.

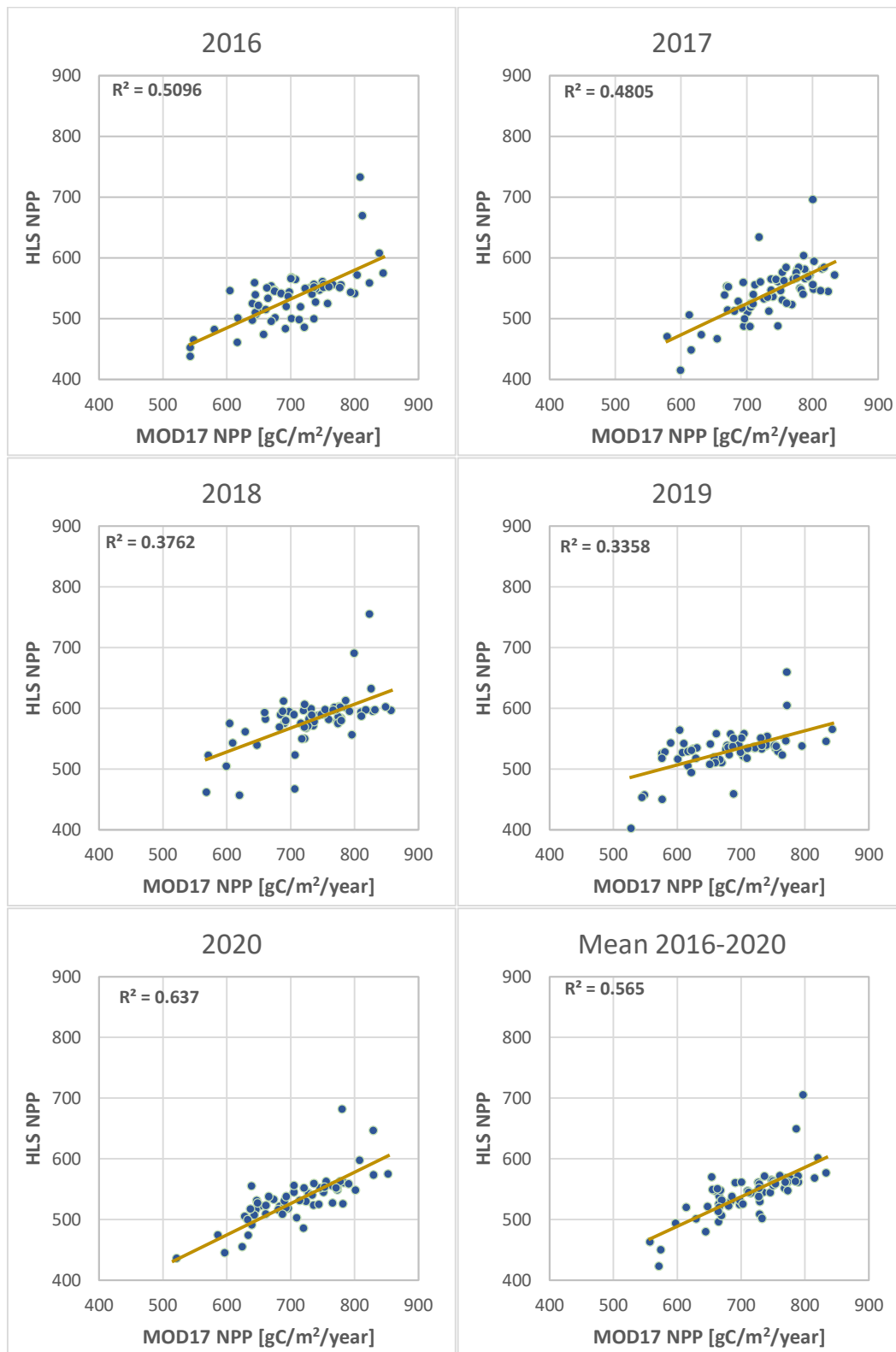


Figure 32: Correlation between HLS NPP and MOD17 NPP for homogeneous 1 km<sup>2</sup> forest polygons.

HLS NPP values are lower than MOD17 NPP for all the years (Figure 33). On average, NPP estimated with high spatial resolution inputs for years 2016 - 2020 is 23.24% (165.32 gC/m<sup>2</sup>/year) lower than MOD17 NPP.

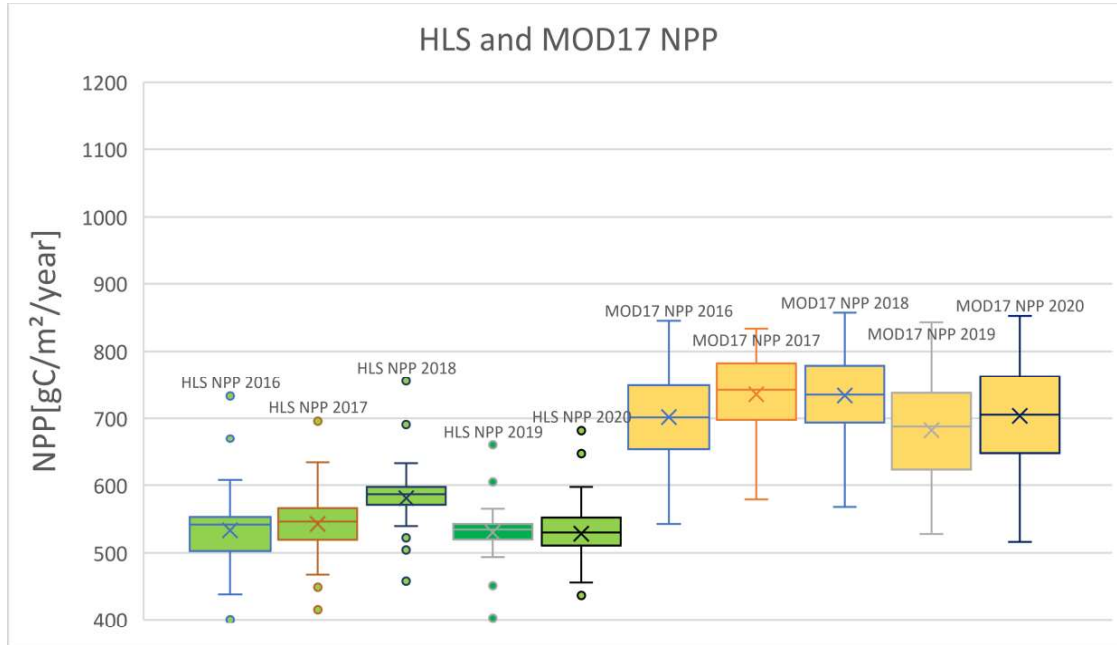


Figure 33: Comparison of HLS NPP and MOD17 NPP for homogeneous 1 km<sup>2</sup> forest polygons in Austria: The boxes represent the median and the 25th and 75th percentile, the symbol x represents the arithmetic mean.

Mean NPP for the years 2016 - 2020 obtained with the HLS satellite dataset and the European climate data set for 64 forest polygons of 1 km<sup>2</sup> is 543.0 gC/m<sup>2</sup>/year (mean standard deviation is 40.0 gC/m<sup>2</sup> /year) (Table 11). Mean MOD17 NPP for the same polygons and for the same period is 711.5 gC/m<sup>2</sup>/year (standard deviation is 61.9 gC/m<sup>2</sup> /year). For each polygon NPP is extracted as a weighted arithmetic mean.

Table 11: Statistics for two modelled NPP for 2016-2020 for 1 km<sup>2</sup> homogeneous polygons. NPP [gC/m<sup>2</sup>/year]

	HLS NPP [gC/m <sup>2</sup> /year]	MOD17 NPP [gC/m <sup>2</sup> /year]	Difference
2016	533.3	701.8	167.5
2017	542.6	735.3	190.1
2018	580.8	733.9	147.3
2019	530.0	682.6	151.7
2020	528.3	703.9	170.0
Average	543.0	711.5	168.5

Figure 34 gives the annual mean HLS NPP estimation for the period 2016-2020 at the spatial resolution of 10 m using high spatial resolution inputs for the forest area in the study region in Austria. Figure 35 shows the forest NPP map for the same area obtained from the MOD17A3H Version 6 product which has spatial resolution of 500 m on average. It is evident that for entire area HLS NPP estimation is producing lower values than MOD17 NPP, where 90% of the average NPP values were between 477 gC/m<sup>2</sup>/year and 711 gC/m<sup>2</sup>/year while MOD17 NPP had 90% of the average NPP values between 577 gC/m<sup>2</sup>/year and 815 gC/m<sup>2</sup>/year. MODIS land cover map derived from MCD12Q1v006

(AppEEARS, <https://lpdaacsvc.cr.usgs.gov/appeears/>) was used to mask out pixels which were not classified as forest. It resulted in the MOD17 NPP forest map which has forest area of 5374.0 km<sup>2</sup> while HLS NPP algorithm, which uses 10 m resolution S2GLC map, produced the map that has forest area is 3295.6 km<sup>2</sup>. In comparison, forest area based on dataset collected in National Forest Inventory in Austria (Die österreichische Waldinventur, 2007/09) in the study area is 4120±310 km<sup>2</sup> including non-productive forests. Therefore, LC map used in HLS NPP algorithm covers forest area which is 20% less than the area obtained in the forest inventory, and MODIS LC map (500 m resolution) used in MOD17 NPP algorithm overestimates forest area for 30.4% (Table 12). Considered that the area of non-productive forests (*Holzboden außer Ertrag* and *Schutzwald außer Ertrag*) is 550 km<sup>2</sup>, which two thirds of the area consists of shrubs and open areas (Hauk and Perzl, 2013), we can assume that the difference between S2GLC map and forest inventory data is lower than 20% and that the accuracy of S2GLC map is satisfactory and represents forest areas better than 500 m resolution MODIS LC map.

Table 12: Forest area according to two satellite-derived land cover maps (MODIS and Copernicus) and official Austrian forest inventory (BFW).  $\Delta$ Area and Rel.  $\Delta$ Area are the differences between the forest areas of satellite-derived LC maps (MCD12Q1 and S2GLC) and forest area obtained from NFI dataset.

	<b>MCD12Q1v006 LC [km<sup>2</sup>]</b>	<b>S2GLC [km<sup>2</sup>]</b>	<b>BFW total forest area [km<sup>2</sup>]</b>	<b>BFW non- productive forest area [km<sup>2</sup>]</b>
	5374	3295.6	4120±310	550
$\Delta$ Area [km <sup>2</sup> ]	1254	824.2		
Rel. $\Delta$ Area [%]	30.4	20.0		

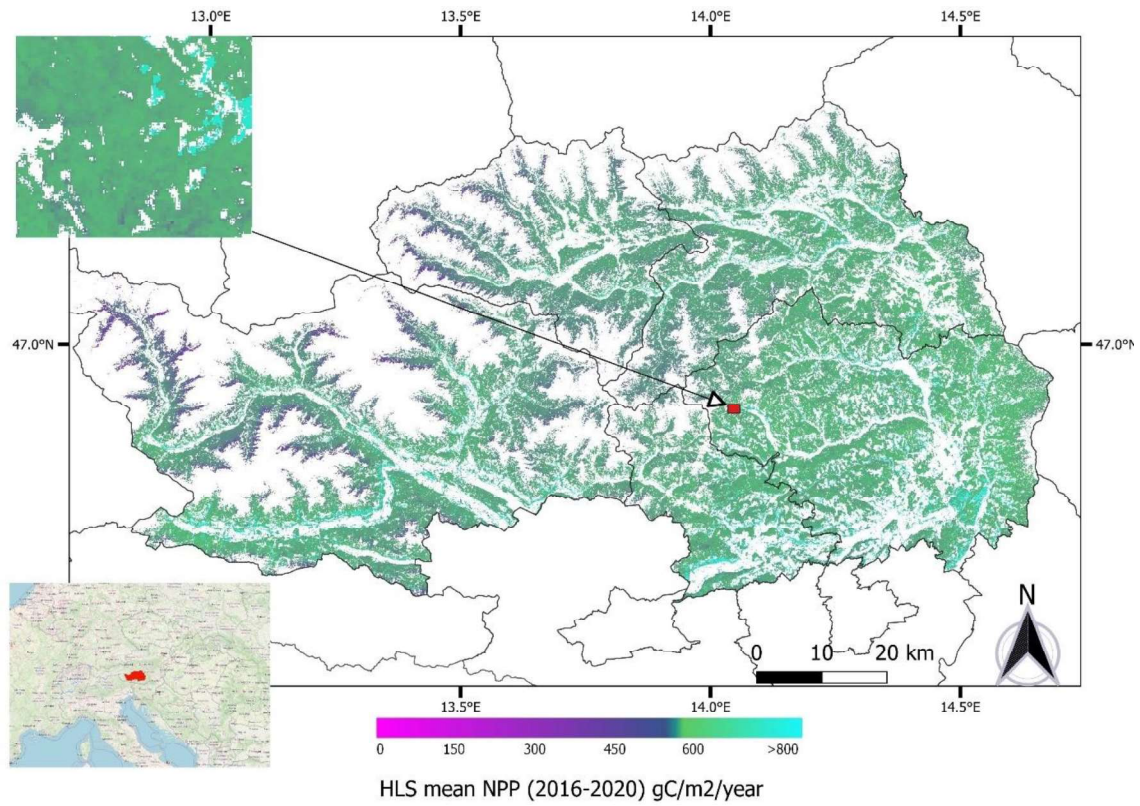


Figure 34: HLS NPP on 10-m resolution representing average NPP for the period 2016–2020 for the southern part of Austria. Estimated NPP was obtained with S2GLC map, meteorological reanalysis data from ERA5 and E-OBS datasets and reflectance data from HLS.

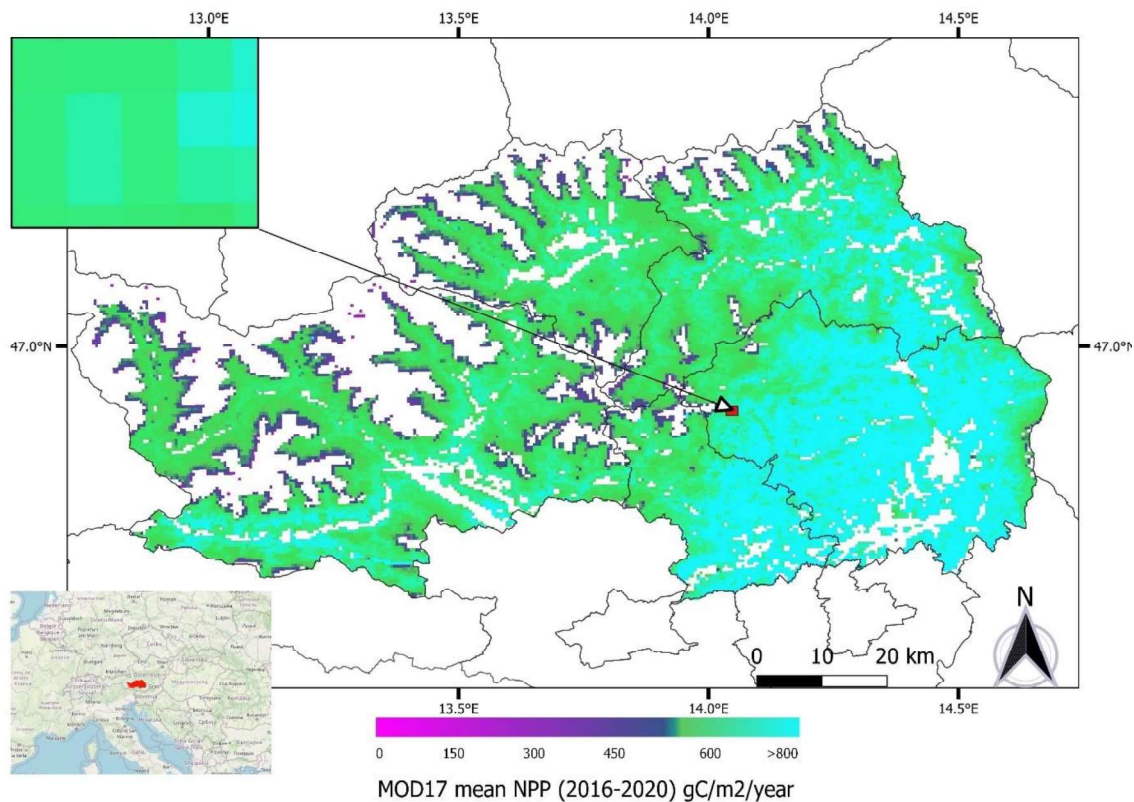


Figure 35: MOD17 NPP on 500-m resolution representing average NPP for the period 2016–2020 for the southern part of Austria. NPP data derived from the MOD17A3HGFv006 (AppEARS, <https://lpdaacsvc.cr.usgs.gov/appears/>)

Distribution of NPP values for the two datasets were compared (Figure 36). LC map used in MOD17 NPP algorithm has a lot larger area that was classified as forest compared to 10 m resolution LC used HLS NPP product. It resulted in 2078 km<sup>2</sup> larger forest area in MOD17 NPP. MOD17 NPP product has also NPP values which have larger range in comparison to the high spatial resolution NPP. HLS NPP values are mainly concentrated in a range of 500-600 kgC/m<sup>2</sup>/year for conifers and 700-800 kgC/m<sup>2</sup>/year for broadleaves, while the majority of the MOD17 NPP values were spread from 650 to 850 kgC/m<sup>2</sup>/year.

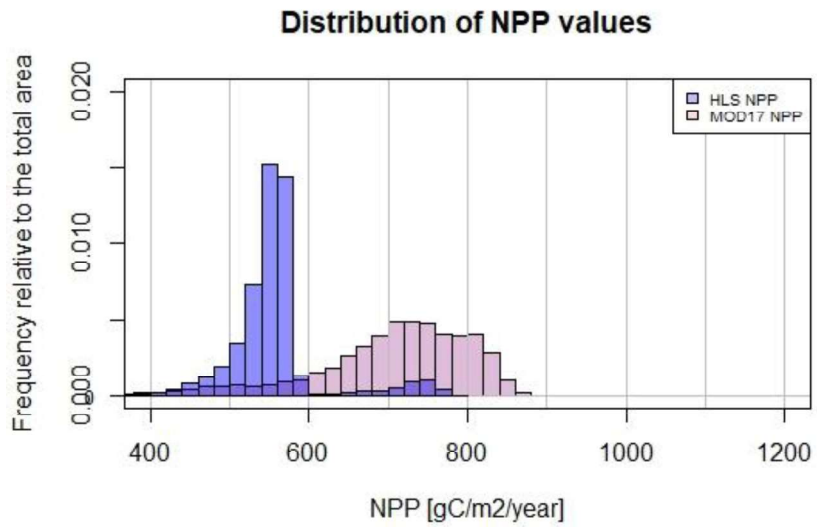


Figure 36: Distribution of aggregated NPP values for HLS NPP and MOD17 NPP products for the period 2016-2020 for the study region in the southern part of Austria. Two datasets differ in size and spatial resolution. Vertical axis shows frequency of the two NPP datasets relative to the total forest area.

## 5. Discussion and conclusion

MOD17 algorithm is adapted to run with the land cover map obtained from the Sentinel-2 Global Land Cover (S2GLC) project (10 m spatial resolution), meteorological reanalysis data from ERA5 and E-OBS datasets (0.1° spatial resolution, 9 km on average) and reflectance data from HLS (30m spatial resolution). Adapted algorithm (HLS NPP) produces final annual NPP data at the spatial resolution of 10 m. The structure of the algorithm remains the same as for MOD17 NPP product, while the source and spatial resolution of the input parameters are replaced. Another difference between the two products is FPAR and LAI dataset. As FPAR and LAI derived from S2 are not applicable for forest areas, NDVI derived from HLS was used to estimate FPAR and LAI at the spatial resolution of 30 m.

In this study, HLS NPP algorithm was applied to derive the 10 m resolution NPP and analyse its potentials and limitations. Firstly, sensitivity of the NPP to input parameters was quantified in a sensitivity analysis. Then, HLS NPP was compared to 500 m resolution MOD17 NPP for the study areas in Slovenia and Austria to test the consistency between the two products and to compare the results of the coarse and high spatial resolution NPP. To assess the potential of the NPP algorithm to represent and capture spatial heterogeneity of timber growth at the high spatial resolution, NPP results were compared to data obtained from forest inventory in Slovenia. Pixels of spatial resolution of 10-30 m can match the scales of forest inventory which plots usually have small area (500 m<sup>2</sup> in Slovenian NFI). This is particularly useful for validation of NPP results. Finally, potential improvements of the NPP model for estimating forest production was presented.

Sensitivity analysis showed that wrong LC classification is causing the biggest error in NPP estimation. S2GLC map of 10 m resolution, which was used for the HLS NPP algorithm, has two classes for forest areas (deciduous and conifers). All the biome specific parameters are derived from LC classification which generates the only distinction of vegetation types in this model. Biome specific (BPLUT) parameters are calibrated to global conditions for each LC type and as such, cannot capture local forest conditions. Among other parameters, FPAR, SWrad and radiation use efficiency have the biggest impact on the final NPP values. NPP is increasing linearly with the increase of one of these three parameters and at the same rate for all the parameters.

Individual model parameters were also compared to annual increment of timber volume obtained in NFI on a plot level (500 m<sup>2</sup>) to analyse which parameters can represent spatial variability of timber growth and local forest conditions. Radiation use efficiency, FPAR and LAI are all weakly correlated to timber increment and thus, can only to a small extent represent spatial variability of timber growth.

Comparison of PAI of NFI plots in Slovenia with the 10 m resolution HLS NPP showed weak correlation. Potential reasons for this are presented:

1. MOD17 algorithm parameters were created to represent average global conditions. Biome specific parameters are calibrated at the global conditions, and therefore, they cannot represent all the variations in local conditions because they do not distinguish diversity in vegetation apart from Land Cover types. Forest type is classified in two classes in S2GLC map (deciduous and conifers) and all BPLUT parameters are derived for these two classes. On the other hand, there is a high variability between various species within each of these classes. Factors such as humidity, nutrient availability,

- forest age (Govind and Kumari, 2014), physical and chemical characteristics of the soil, impact of animals, plant genetics (Field et al., 1995) are all important for the final quantity of captured carbon and biomass growth.
2. FPAR and LAI are the only parameters that can represent local conditions and impact of forest management at high spatial resolution. Copernicus climate parameters have 0.1° spatial resolution which is higher than GMAO/NASA dataset (0.5° by 0.625°) that is used by MOD17, but it still cannot capture microclimate and forest stand conditions. Therefore, climate data and FPAR/LAI cannot completely represent high variability of forest stand factors (stand density, age, site production, type of management).
  3. PAI obtained from Slovenian NFI represent timber annual increment of sampled trees which have diameter larger than 10 cm at height of 1.3 meters. NPP, on the other hand, represents total carbon uptake by all the vegetation, including below-ground production. In addition, NPP includes root exudates, carbon transfer to microbes that are symbiotically associated with roots, and biomass that dies or is removed by herbivores before it can be measured (Chapin and Eviner, 2007). Therefore, it is causing inconsistency between the estimated NPP and measured increment of timber volume for the NFI plots.

The greatest inconsistency between the NPP and PAI was for NFI plots which had very low timber volume and PAI. If a certain plot has low canopy cover and low stem density it is expected that the ground vegetation is dense during vegetation periods. As NPP algorithm quantifies total vegetation cover, it produces average NPP values (653.9 gC/m<sup>2</sup>/year for Slovenia) for such plots. On the other hand, inventory data represent trees with diameter larger than 10 cm, and therefore, do not consider growing stock of small trees and ground vegetation. Therefore, it is causing inconsistency between the estimated NPP and measured timber volume increment for the plots with low canopy cover.

Low correlation between the HLS NPP and PAI of NFI plots in Slovenia showed that this model cannot accurately represent heterogeneity and variability in forest stand conditions. Relative standard deviation (RSD) of 10.4 % for HLS NPP is much lower than RSD of periodic annual increment of timber volume for NFI plots (70.6 %). Variability of biomass growth is evidently much higher than the NPP model can capture. MOD17 algorithm and its parameters are created to estimate NPP on a large scale (region, country, globe) and BPLUT parameters represent only land cover class (deciduous and conifers) which leads to generally uniform NPP estimation for a given LC class.

Relationship analysis between the annual NPP and annual growth ring size obtained from sampled cores for the study area in Austria showed that at the current moment, it is not possible to make any predictions regarding growth ring width using NPP. Possible reasons for this are:

- 1- NPP estimation gives the annual carbon production for entire vegetation on the plots. On the other hand, growth ring size data does not provide us with the information on timber volume/biomass increment. It shows only tree ring growth, regardless of tree dbh, species, age, or stem density. Therefore, it is not possible to estimate the extent of biomass growth.
- 2- As mentioned previously, calibration of model parameters for the global conditions and variability of biomass growth that cannot be represented by NPP algorithm are causing inconsistency between the estimated NPP and tree growth data.

However, annual trend of NPP does not follow the yearly change in the size of the growth rings. Figure 26 (left side) showed that there are significant differences between the years, with 2018 having particularly high values. On the right side, the sizes of the growth rings are very similar between the years. This leads to the conclusion that either the NPP is not connected to growth ring size or that the variability and uncertainty in the measurement of NPP are too high so that the possibly existing connection is not discernible.

To have reliable comparison of time series, it would be necessary to compare data for periods longer than 4 years. As Sentinel-2 satellites have been in function from 2016, they cannot provide NPP data for a longer period. One way to address this issue is to use only Landsat satellite data.

Comparison between 10 m resolution HLS NPP and 500 m resolution MOD17 NPP showed good consistency between the two datasets for homogeneous coniferous forest areas. Dominant land cover type for the study area in the southern part of Austria is coniferous tree cover (more than 90% of forest area). Correlation between the two datasets was stronger for this area than for polygons in the study area in Slovenia where broadleaf tree cover type is dominant (29 polygons with broadleaf and 21 with coniferous LC class). This might be explained with the higher variability in NPP values for broadleaves than for conifers for both spatial resolutions.

Estimated HLS NPP of 10 m spatial resolution produce lower NPP estimates in comparison to MOD17 500 m resolution NPP. Lower NPP estimates using European climate dataset are expected considering previous research (Neuman et al., 2016). In this research, comparison of European national forest inventories datasets with MODIS EURO estimates (NPP with the European climate data on 1-km resolution) and with MOD17 algorithm (MODIS NPP) showed that the global MODIS NPP dataset differs from NFI NPP by 26%, while MODIS EURO only differs by 7%. For Austria, MOD17 NPP differs from NFI NPP by 17%. Both models produce larger NPP values than NPP calculated with the NFI data for Europe. Neuman et al. (2015) estimated forest NPP for Austria for the period 2000 - 2009 using National Austrian Forest Inventory data of 486.3 gC/m<sup>2</sup>/year. For the study region in the southern part of Austria for the years 2016 – 2020 our HLS NPP estimates give an average of 555 gC/m<sup>2</sup>/year, while MOD17 algorithm produces NPP of 711.5 gC/m<sup>2</sup>/year.

High spatial resolution HLS NPP for the forest areas at NFI plots in Slovenia also differ from MOD17 NPP, giving 18.67% lower values on average. For homogeneous forest polygons in Austria, which are mainly coniferous forest areas, HLS NPP for the period 2016-2020 is 23.24% lower than MOD17 NPP.

Therefore, HLS NPP model is producing lower NPP values than MOD17. Considering European average NPP values and previous research, NPP estimated with ground-based monitoring approach for the central Europe and the whole Europe is also lower than MOD17 NPP. Based on this data, we can state that the HLS NPP algorithm is producing NPP values closer to the NPP obtained from terrestrial forest inventory data in comparison to MOD17 NPP.

Another research (Park et al. 2021), which shows discrepancies between the global forest NPP estimates derived from MODIS and forest inventory data (Global Forest Resources Assessment FRA), claims that Slovenia is one of the countries for which absolute value of the difference between the two NPP estimates was less than 5% of their mean.

To precisely compare field data with both, MOD17 and HLS NPP, it is necessary to have bottom-up NPP estimates using terrestrial forest inventory data for the period from 2016 to present.

Comparison between HLS NPP and MOD17 NPP showed a linear correlation when homogeneous and square-shaped forest polygons were selected for comparison of the NPP from the two datasets. On the other hand, when weighted arithmetic mean NPP of forest stands was compared (Figure 28) there was no correlation.

MOD17 NPP 500 by 500 m pixels rarely fully fit into a forest stand and usually are highly affected by neighbouring areas of a different LC class or different forest stands. Additionally, forest stands usually have irregular shape and area less than 25 ha (area of an average MODIS pixel). Hence, coarse spatial resolution cannot represent NPP of forest stands because of mismatch in scale.

It leads to a conclusion that reliable comparison and estimation of NPP cannot be performed with MOD17 NPP for polygons of irregular shape and areas which have heterogeneous land cover and forest characteristics. HLS NPP has spatial resolution which can differentiate between the forest stands or different administrative units.

High spatial resolution NPP estimation is producing NPP that has values of lower range in comparison to 500 m resolution MOD17 model. This is particularly the case for forest areas classified as conifers.

Most important difference regarding methodology of NPP estimation between HLS and MOD17 NPP is FPAR/LAI estimation. For HLS FPAR/LAI estimation (Section 3.6), regression analysis with the HLS NDVI is applied and smoothing technique (Whittaker smoother) is used to get NDVI time series. Comparison of weekly time series of FPAR showed that MODIS FPAR has higher range of values and higher temporal variation than HLS-derived FPAR, especially for the summer period. FPAR and LAI are derived from regression formulas (Equation 21 and Equation 22) and majority of the values for the summer period have low range (FPAR = 0.8 - 0.9). On the other hand, MODIS-derived FPAR/LAI have much higher variation in this period (FPAR = 0.4 – 1).

Larger variability of FPAR/LAI dataset for MOD17 algorithm is the main reason for larger range and spatial variability of MOD17 NPP values in comparison to 10 m resolution HLS NPP.

In addition, even though the forest polygons with the homogeneous land cover are selected for comparison, impact of diversity of forest areas within 1 km<sup>2</sup> on MOD17 NPP pixels might still be an issue. Moreover, in the study area in Austria total area classified as forest in MOD17 dataset is 2078.4 km<sup>2</sup> larger than in HLS dataset. Larger area for NPP estimation, together with the impact of various LC classes on 500 m MODIS pixels, is another cause of high spatial variability of MOD17 NPP dataset.

We can conclude that high spatial resolution data (satellite reflectance data, climate, land cover map) are feasible to implement in MOD17 algorithm. With the increase in spatial resolution (from 500 m to 10 m) NPP values for the areas in Slovenia and southern part of Austria are lower and closer to the expected values. The 10 m resolution NPP raster data provide an opportunity to extract mean NPP for forest stands or forest compartments of irregular shape, which might be useful for forest management. Quantifying forest net primary production on a forest stand level could provide an opportunity to assess the impact of forest management practices on small areas (e.g. clear cuts, thinning operations) or forest disturbances (forest fires, bark beetle outbreak) and observe the change and recovery of annual NPP in the period after the change caused by abiotic or biotic factor. The 10 m spatial resolution S2GLC map can

capture small patches of land which are not classified as forest, and therefore, exclude them from NPP estimation.

HLS NPP model can easily be validated, provided that bottom-up estimation of NPP is available. NFI plots usually have size of less than 1 hectare. Therefore, it is not feasible to compare NPP of spatial resolution of 500 m to data of biomass growth collected at the plots of much smaller area. HLS NPP estimation gives possibility to match the scale for validation and direct comparison of results collected with different methodologies.

One of the shortcomings of this model is the fact that using high spatial resolution inputs is leading to longer processing time and for making NPP maps on a country or continental level it would be necessary to have high computing power. Another current drawback is inability of the HLS NPP to represent local forest conditions and high spatial variability of timber growth as discussed previously. Potential improvements and necessary validation are considered in the following section.

## 5.1. Future work

To precisely compare field data with both, MOD17 and HLS NPP, it is necessary to have bottom-up NPP estimates using terrestrial forest inventory data for the period from 2016 to present. After comparison of NPP obtained with MOD17 (and HLS NPP) algorithm with the ground truth NPP data, steps presented in the following paragraphs could be applied.

LAI and FPAR data were obtained from HLS NDVI data. This is considered not optimal and only a temporary solution for the study areas in Slovenia and Austria. For reliable and robust FPAR and LAI data that could be used for other areas in Europe and to better represent local forest conditions and improve the HLS NPP model it is necessary to develop LAI and FPAR product for forest at high spatial resolution.

Since there is high variability in growing conditions and tree characteristics, modification of the model with terrestrial (NFI) or remote sensing data could potentially improve the NPP estimations and increase the correlation between the NPP and NFI data. Stand density effect, which impacts growth variation and accumulation of carbon, is not fully detectable with satellite driven NPP estimates. Integrating stand density, stand age and site index into HLS NPP model might provide an opportunity to quantify changes of NPP which are attributed to stand conditions and forest management effects.

As consistent forest inventory data are rarely available for large-scale, it is not feasible to obtain spatio-temporally continuous NPP product using terrestrial forest growth data as inputs. However, forest inventory data would be useful for validation of HLS NPP. By grouping the differences ( $\Delta$ NPP) between the HLS NPP and ground based NPP estimates according to various stand parameters, impact of these parameters on deviation of estimated HLS NPP could be calculated. Addressing the effect of stand parameters (stand density, stand age, site index, elevation, dominant tree species) on NPP would decrease the differences between the two NPP estimates and lead to better correlation between the NPP and NFI data. In addition, it would contribute to better representation of variation in growing conditions which satellite driven NPP cannot reflect.

More remote sensing data, in addition to FPAR and LAI, would be practical to implement into the HLS NPP model and keep the possibility to implement the model at the large scale. These input data could include: digital elevation model (DEM), tree species classification maps,

global forest canopy height database from Potapov et al. (2021) or tree height estimation maps with lidar.

For model validation and for analysing the connection between HLS NPP and forest inventory data, it is essential to have reliable ground-based NPP estimates for forests of various type, production, stand characteristics and at different altitudes. Further research should be based on comparison of HLS NPP and ground-based NPP, on addressing the impact of forest stand parameters on NPP estimates and on integration of available remote sensing data into the HLS NPP model.

## References

- Alexandrov, G. A., Oikawa, T., & Yamagata, Y. (2003). Climate dependence of the CO<sub>2</sub> fertilization effect on terrestrial net primary production. *Tellus B: Chemical and Physical Meteorology*, 55(2), 669–675. <https://doi.org/10.3402/tellusb.v55i2.16698>
- Apps, M., Bhatti, J., & Bernier, P. (2005). Forests in the Global Carbon Cycle. *Climate Change and Managed Ecosystems*, 175–200. <https://doi.org/10.1201/9780849330971.ch9>
- Azhdari, Z., Rafeie Sardooi, E., Bazrafshan, O., Zamani, H., Singh, V. P., Mohseni Saravi, M., & Ramezani, M. (2020). Impact of climate change on net primary production (NPP) in south Iran. *Environmental Monitoring and Assessment*, 192(6), 409. <https://doi.org/10.1007/s10661-020-08389-w>
- Bacastow, R., & Keeling, C. K. (1973). Atmospheric carbon dioxide and radiocarbon in the natural carbon cycle: II. Changes from A. D. 1700 to 2070 as deduced from a geochemical model. *Brookhaven Symposia in Biology*, (30):86-135. PMID: 4807349.
- Baldocchi, D., Falge, E., Gu, L., Olson, R., Hollinger, D., Running, S., Anthoni, P., Bernhofer, C., Davis, K., Evans, R., Fuentes, J., Goldstein, A., Katul, G., Law, B., Lee, X., Malhi, Y., Meyers, T., Munger, W., Oechel, W., . . . Wofsy, S. (2001). FLUXNET: A New Tool to Study the Temporal and Spatial Variability of Ecosystem-Scale Carbon Dioxide, Water Vapor, and Energy Flux Densities. *Bulletin of the American Meteorological Society*, 82(11), 2415–2434. [https://doi.org/10.1175/1520-0477\(2001\)082](https://doi.org/10.1175/1520-0477(2001)082)
- Bar-On, Y. M., Phillips, R., & Milo, R. (2018). The biomass distribution on Earth. *Proceedings of the National Academy of Sciences*, 115(25), 6506–6511. <https://doi.org/10.1073/pnas.1711842115>
- Bundesforschungszentrum für Wald (BFW). (2011). *Die österreichische Waldinventur 2007/09*. Available online: <http://bfw.ac.at/rz/wi.home> (accessed on 15 Dec 2021)
- Cao, M., Prince, S. D., Small, J., & Goetz, S. J. (2004). Remotely Sensed Interannual Variations and Trends in Terrestrial Net Primary Productivity 1981-2000. *Ecosystems*, 7(3), 233–242. <https://doi.org/10.1007/s10021-003-0189-x>
- Chapin, F. S., & Eviner, V. T. (2007). Biogeochemistry of Terrestrial Net Primary Production. In *Treatise on Geochemistry* (pp. 1–35). *Elsevier*. <https://doi.org/10.1016/B0-08-043751-6/08130-5>
- Chave, J., Andalo, C., Brown, S., Cairns, M. A., Chambers, J. Q., Eamus, D., Fölster, H., Fromard, F., Higuchi, N., Kira, T., Lescure, J. P., Nelson, B. W., Ogawa, H., Puig, H., Riéra, B., & Yamakura, T. (2005). Tree allometry and improved estimation of carbon stocks and balance in tropical forests. *Oecologia*, 145(1), 87–99. <https://doi.org/10.1007/s00442-005-0100-x>
- Claverie, M., Ju, J., Masek, J. G., Dungan, J. L., Vermote, E. F., Roger, J.-C., Skakun, S. v., & Justice, C. (2018). The Harmonized Landsat and Sentinel-2 surface reflectance data set. *Remote Sensing of Environment*, 219, 145–161. <https://doi.org/10.1016/j.rse.2018.09.002>
- Cornes, R. C., van der Schrier, G., van den Besselaar, E. J. M., & Jones, P. D. (2018). An Ensemble Version of the E-OBS Temperature and Precipitation Data Sets. *Journal of Geophysical Research: Atmospheres*, 123(17), 9391–9409. <https://doi.org/10.1029/2017JD028200>
- Cramer, W., Kicklighter, D. W., Bondeau, A., Iii, B. M., Churkina, G., Nemry, B., Ruimy, A., Schloss, A. L., & Intercomparison, T. P. O. T. P. (1999). Comparing global models of terrestrial net primary productivity (NPP): overview and key results. *Global Change Biology*, 5(S1), 1–15. <https://doi.org/10.1046/j.1365-2486.1999.00009.x>
- Dixon, R. K., Solomon, A. M., Brown, S., Houghton, R. A., Trexler, M. C., & Wisniewski, J. (1994). Carbon Pools and Flux of Global Forest Ecosystems. *Science*, 263(5144), 185–190. <https://doi.org/10.1126/science.263.5144.185>
- FAO and UNEP. (2020). *The State of the World's Forests 2020*. Forests, biodiversity and people. <https://doi.org/10.4060/ca8642en>
- Field, C. B., Randerson, J. T., & Malmström, C. M. (1995). Global net primary production: Combining ecology and remote sensing. *Remote Sensing of Environment*, 51(1), 74–88. [https://doi.org/10.1016/0034-4257\(94\)00066-v](https://doi.org/10.1016/0034-4257(94)00066-v)

- Friedl, M., Sulla-Menashe, D. (2019). *MCD12Q1 MODIS/Terra+Aqua Land Cover Type Yearly L3 Global 500m SIN Grid V006* [Data set]. NASA EOSDIS Land Processes DAAC. Accessed 2021-10-27 from <https://doi.org/10.5067/MODIS/MCD12Q1.006>
- Friedlingstein, P., O'Sullivan, M., Jones, M. W., Andrew, R. M., Hauck, J., Olsen, A., Peters, G. P., Peters, W., Pongratz, J., Sitch, S., Le Quéré, C., Canadell, J. G., Ciais, P., Jackson, R. B., Alin, S., Aragão, L. E. O. C., Arneeth, A., Arora, V., Bates, N. R., . . . Zaehle, S. (2020). Global Carbon Budget 2020. *Earth System Science Data*, 12(4), 3269–3340. <https://doi.org/10.5194/essd-12-3269-2020>
- Gelaro, R., McCarty, W., Suárez, M. J., Todling, R., Molod, A., Takacs, L., Randles, C. A., Darmenov, A., Bosilovich, M. G., Reichle, R., Wargan, K., Coy, L., Cullather, R., Draper, C., Akella, S., Buchard, V., Conaty, A., da Silva, A. M., Gu, W., . . . Zhao, B. (2017). The Modern-Era Retrospective Analysis for Research and Applications, Version 2 (MERRA-2). *Journal of Climate*, 30(14), 5419–5454. <https://doi.org/10.1175/JCLI-D-16-0758.1>
- Goel, S., & Agarwal, D. (2014). Carbon Dioxide. *Encyclopedia of Toxicology*, 675–677. <https://doi.org/10.1016/b978-0-12-386454-3.00269-4>
- Govind, A., & Kumari, J. (2014). Understanding the Terrestrial Carbon Cycle: An Ecohydrological Perspective. *International Journal of Ecology*, 2014, 1–18. <https://doi.org/10.1155/2014/712537>
- Gower, S. T. (2003). Patterns and Mechanisms of the Forest Carbon Cycle. *Annual Review of Environment and Resources*, 28(1), 169–204. <https://doi.org/10.1146/annurev.energy.28.050302.105515>
- Gutleb, B. (1998). The Brown Bear in Carinthia: History and Status in Southern Austria. *Ursus*, 10, 75–79. <http://www.jstor.org/stable/3873113>
- Hasenauer, H., Petritsch, R., Zhao, M., Boisvenue, C., & Running, S. W. (2012). Reconciling satellite with ground data to estimate forest productivity at national scales. *Forest Ecology and Management*, 276, 196–208. <https://doi.org/10.1016/j.foreco.2012.03.022>
- Hauk, E., & Perzl, F. (2013) Freiflächen in Österreichs Wald-Viehweiden und Gefahrenquellen? *BFW Praxisinfor*, 32, 24–31. Retrieved from: [https://bfw.ac.at/050/pdf/BFWPraxisinfo32\\_oewispezial.pdf](https://bfw.ac.at/050/pdf/BFWPraxisinfo32_oewispezial.pdf)
- Hilker, T., Coops, N. C., Wulder, M. A., Black, T. A., & Guy, R. D. (2008). The use of remote sensing in light use efficiency based models of gross primary production: A review of current status and future requirements. *Science of The Total Environment*, 404(2–3), 411–423. <https://doi.org/10.1016/j.scitotenv.2007.11.007>
- Ito, A. (2011). A historical meta-analysis of global terrestrial net primary productivity: are estimates converging? *Global Change Biology*, 17(10), 3161–3175. <https://doi.org/10.1111/j.1365-2486.2011.02450.x>
- Jay, S., Potter, C., Crabtree, R., Genovese, V., Weiss, D. J., & Kraft, M. (2016). Evaluation of modelled net primary production using MODIS and landsat satellite data fusion. *Carbon Balance and Management*, 11(1), 8. <https://doi.org/10.1186/s13021-016-0049-6>
- Keenan, T., & Williams, C. (2018). The Terrestrial Carbon Sink. *Annual Review of Environment and Resources*, 43(1), 219–243. <https://doi.org/10.1146/annurev-environ-102017-030204>
- Kimball, H. L., Selmants, P. C., Moreno, A., Running, S. W., & Giardina, C. P. (2017). Evaluating the role of land cover and climate uncertainties in computing gross primary production in Hawaiian Island ecosystems. *PLOS ONE*, 12(9), e0184466. <https://doi.org/10.1371/journal.pone.0184466>
- Komac, B., Pavšek, M., & Topole, M. (2020). Climate and Weather of Slovenia. Pages 71–89 in: Perko D., Ciglič R., & Zorn M. (eds) *The Geography of Slovenia*. World Regional Geography Book Series. Springer, Cham. [https://doi.org/10.1007/978-3-030-14066-3\\_5](https://doi.org/10.1007/978-3-030-14066-3_5)
- Kus, Z., Česen, M., Majaron, T. M., Piciga, D., & Dolinar, M. (2018). 7th National Communication & 3rd Biennial Report from Slovenia under the United Nations Framework Convention on Climate Change. Republic of Slovenia, Ministry of the Environment and Spatial Planning. [https://unfccc.int/sites/default/files/resource/453201\\_Slovenia-BR3-NC7-1-7NC3BR-EN\\_v0b%20F.pdf](https://unfccc.int/sites/default/files/resource/453201_Slovenia-BR3-NC7-1-7NC3BR-EN_v0b%20F.pdf)
- Kwon, Y., & Baker, B. W. (2016). Area-based fuzzy membership forest cover comparison between MODIS NPP and Forest Inventory and Analysis (FIA) across eastern U.S. forest. *Environmental Monitoring and Assessment*, 189(1), 19. <https://doi.org/10.1007/s10661-016-5745-x>
- Lang, M., Kölli, R., Nikopensius, M., Nilson, T., Neumann, M., & Moreno, A. (2017). Assessment of MODIS NPP algorithm-based estimates using soil fertility and forest inventory data in mixed hemiboreal forests. *Forestry Studies*, 66(1), 49–64. <https://doi.org/10.1515/fsmu-2017-0006>

- Lang, M., Traškovs, A., & Gulbe, L. (2013). Assessment of NTSG MODIS NPP product for forests in Kurzeme region, Latvia. *Forestry Studies*, 58(1), 26–36. <https://doi.org/10.2478/fsmu-2013-0003>
- Lewis, S. L., Lopez-Gonzalez, G., Sonké, B., Affum-Baffoe, K., Baker, T. R., Ojo, L. O., Phillips, O. L., Reitsma, J. M., White, L., Comiskey, J. A., K. M. N. D., Ewango, C. E. N., Feldpausch, T. R., Hamilton, A. C., Gloor, M., Hart, T., Hladik, A., Lloyd, J., Lovett, J. C., . . . Wöll, H. (2009). Increasing carbon storage in intact African tropical forests. *Nature*, 457(7232), 1003–1006. <https://doi.org/10.1038/nature07771>
- Li, P., Peng, C., Wang, M., Li, W., Zhao, P., Wang, K., Yang, Y., & Zhu, Q. (2017). Quantification of the response of global terrestrial net primary production to multifactor global change. *Ecological Indicators*, 76, 245–255. <https://doi.org/10.1016/j.ecolind.2017.01.021>
- Lieth, H. (1975). Primary productivity in ecosystems: comparative analysis of global patterns. *Unifying Concepts in Ecology*, 67–88. [https://doi.org/10.1007/978-94-010-1954-5\\_7](https://doi.org/10.1007/978-94-010-1954-5_7)
- Liu, C., Dong, X., & Liu, Y. (2015). Changes of NPP and their relationship to climate factors based on the transformation of different scales in Gansu, China. *CATENA*, 125, 190–199. <https://doi.org/10.1016/j.catena.2014.10.027>
- Liu, J. (1997). A process-based boreal ecosystem productivity simulator using remote sensing inputs. *Remote Sensing of Environment*, 62(2), 158–175. [https://doi.org/10.1016/s0034-4257\(97\)00089-8](https://doi.org/10.1016/s0034-4257(97)00089-8)
- Maisongrande, P., Ruimy, A., Dedieu, G., & Saugier, B. (1995). Monitoring seasonal and interannual variations of gross primary productivity, net primary productivity and net ecosystem productivity using a diagnostic model and remotely-sensed data. *Tellus B: Chemical and Physical Meteorology*, 47(1–2), 178–190. <https://doi.org/10.3402/tellusb.v47i1-2.16039>
- Malinowski, R., Lewiński, S., Rybicki, M., Gromny, E., Jenerowicz, M., Krupiński, M., Nowakowski, A., Wojtkowski, C., Krupiński, M., Krätzschmar, E., Schauer, P. (2020). Automated Production of a Land Cover/Use Map of Europe Based on Sentinel-2 Imagery doi:10.3390/rs12213523
- Matsushita, B., Xu, M., Chen, J., Kameyama, S., & Tamura, M. (2004). Estimation of regional net primary productivity (NPP) using a process-based ecosystem model: How important is the accuracy of climate data? *Ecological Modelling*, 178(3–4), 371–388. <https://doi.org/10.1016/j.ecolmodel.2004.03.012>
- Monteith, J. L. (1972). Solar Radiation and Productivity in Tropical Ecosystems. *The Journal of Applied Ecology*, 9(3), 747. <https://doi.org/10.2307/2401901>
- Monteith, J. L. (1977). Climate and the efficiency of crop production in Britain. *Philosophical Transactions of the Royal Society of London. B, Biological Sciences*, 281(980), 277–294. <https://doi.org/10.1098/rstb.1977.0140>
- Muñoz Sabater, J., (2019). ERA5-Land hourly data from 1981 to present. Copernicus Climate Change Service (C3S) Climate Data Store (CDS). (Accessed on 15-05-2021). <https://doi.org/10.24381/cds.e2161bac>
- Myneni, R., Knyazikhin, Y., Park, T. (2015). *MODIS Collection 6 (C6) LAI/FPAR Product User's Guide*. NASA EOSDIS Land Processes DAAC. Accessed 2021-05-02 from <https://doi.org/10.5067/MODIS/MCD15A2H.006>
- Nemani, R. R. (2003). Climate-Driven Increases in Global Terrestrial Net Primary Production from 1982 to 1999. *Science*, 300(5625), 1560–1563. <https://doi.org/10.1126/science.1082750>
- Neumann, M., Zhao, M., Kindermann, G., & Hasenauer, H. (2015). Comparing MODIS Net Primary Production Estimates with Terrestrial National Forest Inventory Data in Austria. *Remote Sensing*, 7(4), 3878–3906. <https://doi.org/10.3390/rs70403878>
- Neumann, M., Moreno, A., Thurnher, C., Mues, V., Härkönen, S., Mura, M., Bouriaud, O., Lang, M., Cardellini, G., Thivolle-Cazat, A., Bronisz, K., Merganic, J., Alberdi, I., Astrup, R., Mohren, F., Zhao, M., & Hasenauer, H. (2016). Creating a Regional MODIS Satellite-Driven Net Primary Production Dataset for European Forests. *Remote Sensing*, 8(7), 554. <https://doi.org/10.3390/rs8070554>
- Nilson, T., Rennel, M., Luhamaa, A., Hordo, M., Olesk, A., & Lang, M. (2012). MERIS GPP/NPP product for Estonia: I. Algorithm and preliminary results of simulation. *Forestry Studies*, 56(1), 56–78. <https://doi.org/10.2478/v10132-012-0005-5>
- Pan, S., Tian, H., Dangal, S. R. S., Ouyang, Z., Tao, B., Ren, W., Lu, C., & Running, S. (2014). Modeling and Monitoring Terrestrial Primary Production in a Changing Global Environment: Toward a Multiscale Synthesis of Observation and Simulation. *Advances in Meteorology*, 2014, 1–17. <https://doi.org/10.1155/2014/965936>

- Pan, Y., Birdsey, R. A., Fang, J., Houghton, R., Kauppi, P. E., Kurz, W. A., Phillips, O. L., Shvidenko, A., Lewis, S. L., Canadell, J. G., Ciais, P., Jackson, R. B., Pacala, S. W., McGuire, A. D., Piao, S., Rautiainen, A., Sitch, S., & Hayes, D. (2011). A Large and Persistent Carbon Sink in the World's Forests. *Science*, 333(6045), 988–993. <https://doi.org/10.1126/science.1201609>
- Pan, Y., Birdsey, R., Hom, J., McCullough, K., & Clark, K. (2006). Improved Estimates Of Net Primary Productivity From MODIS Satellite Data At Regional And Local Scales. *Ecological Applications*, 16(1), 125–132. <https://doi.org/10.1890/05-0247>
- Park, J. H., Gan, J., & Park, C. (2021). Discrepancies between Global Forest Net Primary Productivity Estimates Derived from MODIS and Forest Inventory Data and Underlying Factors. *Remote Sensing*, 13(8), 1441. <https://doi.org/10.3390/rs13081441>
- Potapov, P., Li, X., Hernandez-Serna, A., Tyukavina, A., Hansen, M. C., Kommareddy, A., Pickens, A., Turubanova, S., Tang, H., Silva, C. E., Armston, J., Dubayah, R., Blair, J. B., & Hofton, M. (2021). Mapping global forest canopy height through integration of GEDI and Landsat data. *Remote Sensing of Environment*, 253, 112165. <https://doi.org/10.1016/j.rse.2020.112165>
- Potitthep, S.; Nasahara, K.N.; Muraoka, H.; Nagai, S.; Suzuki, R.; Science, E. (2010). What Is the Actual Relationship Between LAI and VI in a Deciduous Broadleaf Forest? *International Archives of the Photogrammetry, Remote Sensing and Spatial Information Science*. 38, 609–614.
- Potter, C. S., Randerson, J. T., Field, C. B., Matson, P. A., Vitousek, P. M., Mooney, H. A., & Klooster, S. A. (1993). Terrestrial ecosystem production: A process model based on global satellite and surface data. *Global Biogeochemical Cycles*, 7(4), 811–841. <https://doi.org/10.1029/93gb02725>
- Prince, S. D. (1991). A model of regional primary production for use with coarse resolution satellite data. *International Journal of Remote Sensing*, 12(6), 1313–1330. <https://doi.org/10.1080/01431169108929728>
- Pugh, T. A. M., Lindeskog, M., Smith, B., Poulter, B., Arneeth, A., Haverd, V., & Calle, L. (2019). Role of forest regrowth in global carbon sink dynamics. *Proceedings of the National Academy of Sciences*, 116(10), 4382–4387. <https://doi.org/10.1073/pnas.1810512116>
- Pulselli, F., & Marchi, M. (2015). Global Warming Potential and the Net Carbon Balance. *Reference Module in Earth Systems and Environmental Sciences*, 1741–1746. <https://doi.org/10.1016/b978-0-12-409548-9.09526-9>
- Quaife, T., Quegan, S., Disney, M., Lewis, P., Lomas, M., & Woodward, F. I. (2008). Impact of land cover uncertainties on estimates of biospheric carbon fluxes. *Global Biogeochemical Cycles*, 22(4), n/a. <https://doi.org/10.1029/2007gb003097>
- Ruimy, A., Saugier, B., & Dedieu, G. (1994). Methodology for the estimation of terrestrial net primary production from remotely sensed data. *Journal of Geophysical Research*, 99(D3), 5263-5283. <https://doi.org/10.1029/93jd03221>
- Running, S. W., & Zhao, M. (2019). Daily GPP and Annual NPP (MOD17A2H/A3H) and Year-end Gap-Filled (MOD17A2HGF/A3HGF) Products NASA Earth Observing System MODIS Land Algorithm (For Collection 6). Missoula, Montana, USA: NASA LP DAAC. [https://lpdaac.usgs.gov/documents/495/MOD17\\_User\\_Guide\\_V6.pdf](https://lpdaac.usgs.gov/documents/495/MOD17_User_Guide_V6.pdf)
- Running, S. W., Nemani, R. R., Heinsch, F. A., Zhao, M., Reeves, M., & Hashimoto, H. (2004). A Continuous Satellite-Derived Measure of Global Terrestrial Primary Production. *BioScience*, 54(6), 547. [https://doi.org/10.1641/0006-3568\(2004\)054\[0547:ACSMOG\]2.0.CO;2](https://doi.org/10.1641/0006-3568(2004)054[0547:ACSMOG]2.0.CO;2)
- Running, S. W., Thornton, P. E., Nemani, R., & Glassy, J. M. (2000). Global Terrestrial Gross and Net Primary Productivity from the Earth Observing System. *Methods in Ecosystem Science*, 44–57. [https://doi.org/10.1007/978-1-4612-1224-9\\_4](https://doi.org/10.1007/978-1-4612-1224-9_4)
- Running, S., Zhao, M. (2019). MOD17A3HGF MODIS/Terra Net Primary Production Gap-Filled Yearly L4 Global 500 m SIN Grid V006 [Data set]. NASA EOSDIS Land Processes DAAC. Accessed 2021-10-27 from <https://doi.org/10.5067/MODIS/MOD17A3HGF.006>
- Scurlock, J. M. O., Cramer, W., Olson, R. J., Parton, W. J., & Prince, S. D. (1999). Terrestrial NPP: Toward a Consistent Data Set for Global Model Evaluation. *Ecological Applications*, 9(3), 913. <https://doi.org/10.2307/2641338>
- Skudnik, M., Jevšenak, J., Poljanec, A., & Kušar, G. (2021). Condition and changes of Slovenian forests in the last two decades – results of the State and changes large-scale spatial forest monitoring. *Gozdarski vestnik*, 4(79), 151–170. Retrieved from: <http://dirros.openscience.si/IzpisGradiva.php?lang=slv&id=14174>

- Slovenian Environment Agency (2020). Slovenia's National Inventory Report 2020. Republic of Slovenia Ministry of the Environment and Spatial Planning. Retrieved from: <https://unfccc.int/documents/226320>
- Tan, C., Wang, D., Zhou, J., Du, Y., Luo, M., Zhang, Y., & Guo, W. (2018). Remotely Assessing Fraction of Photosynthetically Active Radiation (FPAR) for Wheat Canopies Based on Hyperspectral Vegetation Indexes. *Frontiers in Plant Science*, 9. <https://doi.org/10.3389/fpls.2018.00776>
- Thurnher, C., Gerritzen, T., Maroschek, M., Lexer, M.J., & Hasenauer, H. (2013). Analysing different carbon estimation methods for Austrian forests. *Austrian Journal of Forest Science*, 130(3), 141-166.
- Tum, M., Zeidler, J., Günther, K., & Esch, T. (2016). Global NPP and straw bioenergy trends for 2000–2014. *Biomass and Bioenergy*, 90, 230–236. <https://doi.org/10.1016/j.biombioe.2016.03.040>
- Turner, D. P., Ritts, W. D., Cohen, W. B., Gower, S. T., Running, S. W., Zhao, M., Costa, M. H., Kirschbaum, A. A., Ham, J. M., Saleska, S. R., & Ahl, D. E. (2006). Evaluation of MODIS NPP and GPP products across multiple biomes. *Remote Sensing of Environment*, 102(3–4), 282–292. <https://doi.org/10.1016/j.rse.2006.02.017>
- Turner, D. P., Ritts, W. D., Cohen, W. B., Maieringer, T. K., Gower, S. T., Kirschbaum, A. A., Running, S. W., Zhao, M., Wofsy, S. C., Dunn, A. L., Law, B. E., Campbell, J. L., Oechel, W. C., Kwon, H. J., Meyers, T. P., Small, E. E., Kurc, S. A., & Gamon, J. A. (2005). Site-level evaluation of satellite-based global terrestrial gross primary production and net primary production monitoring. *Global Change Biology*, 11(4), 666–684. <https://doi.org/10.1111/j.1365-2486.2005.00936.x>
- Turner, D. P., Urbanski, S., Bremer, D., Wofsy STEVEN C., Meyers, T., Gower, S. T., & Gregory, M. (2003). A cross-biome comparison of daily light use efficiency for gross primary production. *Global Change Biology*, 9(3), 383–395. <https://doi.org/10.1046/j.1365-2486.2003.00573.x>
- Veroustraete, F. (1994). On the use of a simple deciduous forest model for the interpretation of climate change effects at the level of carbon dynamics. *Ecological Modelling*, 75–76, 221–237. [https://doi.org/10.1016/0304-3800\(94\)90021-3](https://doi.org/10.1016/0304-3800(94)90021-3)
- Veroustraete, F., Sabbe, H., & Eerens, H. (2002). Estimation of carbon mass fluxes over Europe using the C-Fix model and Euroflux data. *Remote Sensing of Environment*, 83(3), 376–399. [https://doi.org/10.1016/s0034-4257\(02\)00043-3](https://doi.org/10.1016/s0034-4257(02)00043-3)
- Wang, L., Gong, W., Ma, Y., & Zhang, M. (2013). Modeling Regional Vegetation NPP Variations and Their Relationships with Climatic Parameters in Wuhan, China. *Earth Interactions*, 17(4), 1–20. <https://doi.org/10.1175/2012ei000478.1>
- Weiss, M., & Baret, F. (2016). S2 ToolBox Level 2 Products: LAI, FAPAR, FCOVER, Version 1.1. *ESA. S2 Toolbox Level 2 Product Algorithms v1.1. Issued 05*. Available online: [https://step.esa.int/docs/extra/ATBD\\_S2ToolBox\\_L2B\\_V1.1.pdf](https://step.esa.int/docs/extra/ATBD_S2ToolBox_L2B_V1.1.pdf) (accessed on 14 May 2021)
- Woodwell, G., & Whittaker, R. (1968). Primary Production in Terrestrial Ecosystems. *American Zoologist*, 8(1), 19–30. <https://doi.org/10.1093/icb/8.1.19>
- Xu, Z., Smyth, C. E., Lemprière, T. C., Rampley, G. J., & Kurz, W. A. (2017). Climate change mitigation strategies in the forest sector: biophysical impacts and economic implications in British Columbia, Canada. *Mitigation and Adaptation Strategies for Global Change*, 23(2), 257–290. <https://doi.org/10.1007/s11027-016-9735-7>
- Yu, T., Sun, R., Xiao, Z., Zhang, Q., Liu, G., Cui, T., & Wang, J. (2018). Estimation of Global Vegetation Productivity from Global LAnd Surface Satellite Data. *Remote Sensing*, 10(2), 327. <https://doi.org/10.3390/rs10020327>
- Yu, T., Sun, R., Xiao, Z., Zhang, Q., Wang, J., & Liu, G. (2018). Generation of High Resolution Vegetation Productivity from a Downscaling Method. *Remote Sensing*, 10(11), 1748. <https://doi.org/10.3390/rs10111748>
- Yuan, J., Niu, Z., & Wang, C. (2006). Vegetation NPP distribution based on MODIS data and CASA model—A case study of northern Hebei Province. *Chinese Geographical Science*, 16(4), 334–341. <https://doi.org/10.1007/s11769-006-0334-5>
- Zavod Za Gozdove Slovenije. (2021). *Forest data viewer* [Data set]. Accessed 2021-05-15 from [https://prostor.zgs.gov.si/pregledovalnik/?locale=en&layers=gg\\_obmocja%252Cgg\\_enote%252CDOF25&bbox=424180.8245%252C118688.3407%252C439776.816%252C125422.3371](https://prostor.zgs.gov.si/pregledovalnik/?locale=en&layers=gg_obmocja%252Cgg_enote%252CDOF25&bbox=424180.8245%252C118688.3407%252C439776.816%252C125422.3371)
- Zhang, C., Wu, S., & Leng, G. (2020). Possible NPP changes and risky ecosystem region identification in China during the 21st century based on BCC-CSM2. *Journal of Geographical Sciences*, 30(8), 1219–1232. <https://doi.org/10.1007/s11442-020-1778-8>

- Zhao, M., & Running, S. W. (2010). Drought-Induced Reduction in Global Terrestrial Net Primary Production from 2000 Through 2009. *Science*, 329(5994), 940–943. <https://doi.org/10.1126/science.1192666>
- Zhao, M., Heinsch, F. A., Nemani, R. R., & Running, S. W. (2005). Improvements of the MODIS terrestrial gross and net primary production global data set. *Remote Sensing of Environment*, 95(2), 164–176. <https://doi.org/10.1016/j.rse.2004.12.011>
- Zhao, M., Running, S. W., & Nemani, R. R. (2006). Sensitivity of Moderate Resolution Imaging Spectroradiometer (MODIS) terrestrial primary production to the accuracy of meteorological reanalyses. *Journal of Geophysical Research*, 111(G1), G01002. <https://doi.org/10.1029/2004jg000004>
- Zheng, Y., Zhang, L., Xiao, J., Yuan, W., Yan, M., Li, T., & Zhang, Z. (2018). Sources of uncertainty in gross primary productivity simulated by light use efficiency models: Model structure, parameters, input data, and spatial resolution. *Agricultural and Forest Meteorology*, 263, 242–257. <https://doi.org/10.1016/j.agrformet.2018.08.003>